Symmetric Neural Progenitor Divisions Require Chromatin-Mediated Homology-Directed DNA Repair

by

Jason Keil

A dissertation submitted in partial fulfillment
of the requirements for the degree of
Doctor of Philosophy
(Human Genetics)
in the University of Michigan
2019

Doctoral Committee

Assistant Professor Kenneth Y. Kwan, Chair
Assistant Professor Jacob O. Kitzman
Professor Donna M. Martin
Professor John V. Moran
Professor Jack M. Parent

Jason Keil

jmkeil@umich.edu

ORCID iD: 0000-0002-3431-5540

Acknowledgements

Christie Carlson has been my wonderful partner for seven and a half years. She has been my constant supporter and an inspiration in many ways. Along with our current (Franklin and Elle) and past (Dexter) four-legged companions, this has been a great adventure.

I have a wonderful family that has supported me throughout this work. My parents, Ralph and Leslyn, have provided my sisters and I with a supportive environment and taught us to maintain a 'big picture' view of the world from a young age. It has been incredible to watch Lauren and Natalie grow into adults and for you both to bring wonderful husbands, Hareth and Joe, and baby Tala into our loving family.

My 'Michigan Family' includes Zach Huttinger and Katie Brown, Danny and Liz Triner, Tyler Menge and Katie Wataha, and Matt, Chelsea, Camille, and Nolan Tafoya. All are very accomplished people with bright futures and have been a joy for Christie and I during our time in Ann Arbor.

I would like to thank my mentor, Ken Kwan. Ken has an infectious enthusiasm for understanding mechanisms of cortex development. Even when science is perplexing, his passion and creativity have made my work interesting and meaningful. Being the first graduate student in a lab can feel daunting, as the student and mentor are learning for the first time, often from one another. Through this process, Ken and I have

developed a rigorous, collaborative mentor-mentee relationship centered on a mutual curiosity to understand the development of cortical neurons and uncover new biology.

Ken has crafted a lab culture that often feels like the whole lab is part of the Kwan family, so thanks to Ken, Mandy, Ally, and Brendan for ‘adopting’ all of us. I would like to thank all current and former members of the Kwan Lab, for many hours spent at snack time, in the mouse room, solving escape rooms, and bowling. The fun, collaborative, and curious nature of each of you has made science fun and rewarding.

My committee has been instrumental in helping me to drive this project forward. Dr. Jacob Kitzman, Dr. Donna Martin, Dr. John Moran, and Dr. Jack Parent each contribute specific knowledge that has elevated individual components of this story. And, collectively, they are rigorous and thoughtful scientists, and kind people.

Mentorship has been critical in my desire to pursue research and my development as a scientist. My first scientific mentor was my father, Dr. Ralph Keil, a yeast geneticist who has driven me to understand systems, biological or not. My biochemistry professor at Franklin & Marshall College, Dr. Ryan Mehl, instilled in me a simultaneous sense of seriousness and fun around scientific investigation. After college, I joined a research group headed by Dr. David Antonetti and Dr. Thomas Gardner. Their synergistic relationship as a basic biologist and a physician-scientist, respectively, demonstrated the powers of collaboration. I am grateful to have learned from both of them and proud to consider them friends and mentors to this day. In addition to former mentors, I have been educated and inspired by numerous colleagues during my training, notably Dr. Paul Titchenell and Dr. Xuwen Liu.

Table of Contents

List of Figures

List of Tables

List of Abbreviations

Alt-EJ	Alternative-end joining (also called MMEJ)
aRG	Apical radial glia
bRG	Basal radial glia
c-NHEJ	Classical non-homologous end joining
cKO	Conditional knockout
cKO-E	Conditional knockout via *Emx1*^{Cre}
cKO-N	Conditional knockout via *Neurod6* ^{Cre}
cKO-F	Conditional knockout via *Foxg1* ^{Cre}
cKO-hG	Conditional knockout via Tg(*hGFAP-Cre)*
cKO-L	Conditional knockout via Tg(*Lmx1a-Cre)*
CNV	Copy number variants
DDR	DNA damage response
dKO	Double conditional knockout
dKO-E	Double conditional knockout via *Emx1*^{Cre}
DSB	Double strand break
dsDNA	Double-stranded DNA
E*n*	Embryonic day *n*
HR	Homologous recombination
HDR	Homology-directed repair
IKNM	Interkinetic nuclear migration
INO80-C	INO80 complex
IPC	Intermediate progenitor cell
MMEJ	Microhomology-mediated end joining (also called Alt-EJ)
NHEJ	Non-homologous end joining
NPC	Neural progenitor cell
NSC	Neural stem cell
OSVZ	Outer subventricular Zone
P*n*	Postnatal day *n*
SNV	Single nucleotide variants
SSA	Single strand annealing
ssDNA	Single-stranded DNA
SV	Structural variants
SVZ	Subventricular zone
VZ	Ventricular zone

Abstract

The cerebral cortex is generated by a highly coordinated series of cellular proliferations, beginning with symmetric neural progenitor cell (NPC) divisions to expand the pool of progenitors, and subsequent asymmetric NPC divisions that give rise to molecularly-distinct subtypes of excitatory post-mitotic neurons. Recent analyses have convergently implicated chromatin-regulating enzymes in a broad range of disordered cortex development. Regulation of chromatin coordinates spatiotemporal gene expression during neurodevelopment, but is also necessary for other processes including DNA damage repair crucial to proliferating NPCs. *INO80*, which encodes the catalytic subunit of the INO80 chromatin remodeling complex, is a candidate gene for human microcephaly. However, *Ino80* function in the developing brain has not been empirically studied.

Here, leveraging a conditional allele of *Ino80*, I created *Ino80* cKO models using multiple Cre-driver lines to dissect the spatial and temporal specificity with which *Ino80* functions in cortex development. I uncovered molecularly dissociable roles for *Ino80* in chromatin-mediated transcriptional regulation and genome maintenance in corticogenesis. Conditional deletion of *Ino80* led to apoptosis of early NPCs and postnatal microcephaly, consistent with the microcephaly reported in individuals who carry recessive *INO80* mutations. Cortical NPCs deficient in INO80 demonstrated impaired DNA double strand break (DSB) repair, which led to p53 activation, massive

apoptosis, and microcephaly. Using a novel *in vivo* DSB repair assay, I found that *Ino80* deletion selectively impaired homology-directed repair (HDR) of DSBs, implicating chromatin-mediated DSB repair as essential to proper cortex development. Consistent with impaired DSB repair and downstream p53-dependent apoptosis as the cause of microcephaly, co-deletion of *Trp53* and *Ino80* led to a remarkable reversal of all *Ino80* phenotypes. Notably, the role of INO80 in DNA repair was mechanistically distinct from previously described function in mediating gene transcription with the transcription factor YY1. Therefore, INO80 plays molecularly dissociable roles in transcriptome and genome maintenance during cortical development.

Unexpectedly, sensitivity to loss of INO80-mediated HDR differed starkly based on the mode of NPC division. *Ino80* deletion caused extensive DNA damage and apoptosis in symmetric NPC-NPC divisions, but not in asymmetric NPC-neuron divisions. These observations were confirmed using conditional deletion of the HR gene *Brca2*, demonstrating that the sensitivity of symmetric divisions to impaired HR was generalizable to multiple members of the HR pathway and not specific to chromatin-mediated HR.

Together, these experiments revealed a critical role for *Ino80* in chromatin-mediated HR DNA repair in the embryonic cortex. This role is molecularly distinct from previously identified gene regulatory functions, the disruption of which did not contribute to NPC apoptosis or the microcephaly phenotype. Furthermore, symmetric NPC divisions were exquisitely sensitive to impaired HDR, whereas asymmetric divisions were largely unaffected. This dichotomy suggested that distinct modes of division may employ distinct strategies for genome fidelity. Insights from this work have important

implications for the genetics of microcephaly, understanding of chromatin-mediated DSB repair, and the acquisition of brain somatic mutations during expansive NPC-NPC and neurogenic NPC-neuron divisions.

Chapter 1: DNA damage repair in the developing cortex

Thesis Overview

This thesis aims to understand the role of *Ino80,* encoding the catalytic subunit of the INO80 chromatin remodeling complex, in the development of the cerebral cortex. In the first chapter, I present the current understanding of how the cortex develops with a particular focus on how DNA damage repair pathways and chromatin remodeling play critical roles in this process. In the second chapter, I describe my work characterizing the function of the chromatin remodeler *Ino80*, which participates in multiple pathways via nucleosome remodeling, and how I have demonstrated the importance of *Ino80* in homologous recombination (HR), a type of DSB repair crucial for genome fidelity in cortical development. Chapter 3 describes the novel finding that early, symmetrically dividing NPCs are exquisitely sensitive to impaired HR whereas asymmetric, neurogenic divisions are largely unaffected. This is demonstrated by genetic deletion of *Ino80* at different developmental timepoints, as well as deletion of a *bona fide* HR gene, *Brca2*. Chapter 4 provides a summary of my findings and discusses implications of this work for development, function, and disorders of the brain, with exploration of possible future investigations.

Organization and function of the cerebral cortex

The cerebral cortex is responsible for our species' most complicated and remarkable thoughts and actions. A paragon of complexity, the cortex has more than 20

billion neurons, 25 billion glial cells (Pelvig et al., 2008) and many trillions of synaptic connections. The mammalian cortex is composed of the evolutionarily ancient archicortex and paleocortex, in addition to the more recently evolved neocortex. The neocortex, in particular, has greatly expanded in the primate lineage, with notable enlargement in *Homo sapiens*. The dramatic increase in size and functional connectivity is thought to underlie many of the cognitive, sensory, and motor abilities of our species. As a result of the complexity underlying the organization and function of the brain, disordered cortical development results in a number of pathological states including microcephaly, intellectual disability, epilepsy, schizophrenia, and autism spectrum disorder, among others. Understanding basic mechanisms of development and genetic causes of pathological development can inform successful screening, diagnostic, and therapeutic approaches.

Organization of the cortex

The cell bodies of the neocortex are contained in the most superficial aspect of the cerebral hemispheres, a thin layer of gray matter over the large telencephalic surface area. These cells are organized into six horizontal layers, which are cytoarchitectonically distinct, and make stereotypical connections to other structures within the central nervous system (**Figure 1.1**). Further organization occurs tangentially throughout the cortex, where regions of the cortex are divided broadly into sensory, motor, or associative types of cortex. Finer resolution was provided by Brodmann in 1909 and has been continually refined over the past century, and are now referred to as Brodmann regions. These smaller regions of cortex have stereotypical cellular laminae structure and participate in similarity connectivity and functionality between individuals.

Brodmann described cortical structure purely from cytoarchitectural analyses, though these distinct regions were, in fact, later found to correspond with functionally parcellated regions of the cortex responsible for specific functionality (Glasser et al., 2016).

Neurons and glia of the cortex

The six-layered cortex is phylogenetically conserved among mammals. Layers 2-6 are composed of glutamatergic, excitatory neurons that project to subcortical structures and also within the cortex. Excitatory neurons in different layers maintain stereotypical patterns of gene expression, axonal and dendritic projections, electrophysiological properties, and circuitry. For an excitatory neural circuit to function appropriately, it must also have modulatory inhibitory input that is provided by GABA-ergic inhibitory neurons. These interneurons reside and function in the cortex, but are born in ventral structures like the medial and caudal ganglionic eminences, and then migrate tangentially into the cortex to incorporate into circuits. Many subtypes of inhibitory neurons are present in the cortex with differing gene expression, localization, morphology, and patterns of connectivity (Butt et al., 2005; DeFelipe et al., 2013; Hendry et al., 1987).

Additional support and maintenance for proper neuronal function is supplied by glial cells, including oligodendrocytes, microglia, and astrocytes. Oligodendrocytes provide myelination for efficient communication whereas microglia are the resident macrophages of the brain, with roles in synaptic pruning (Hong et al., 2016) and disposal of cellular debris during development (Ashwell, 1990; Neumann et al., 2009) (Shi L, Qalieh A, Lam MM, Keil JM and Kwan KY, In press, Nature Communications).

There are roughly as many astrocytes in the brain as neurons and they participate in multiple processes including support of synapse function, protection from oxidative damage, and support of the blood-brain barrier (Blackburn et al., 2009). The entire central nervous system is maintained in a very specific milieu dictated and controlled by the blood-brain barrier. Astrocytes function as part of the neurovascular unit to induce specialized cell-cell connections called tight junctions that regulate the flow of macromolecules into the brain parenchyma (Harhaj and Antonetti, 2004).

Circuitry of cortical projection neurons informs function

Each layer of the cortex contains specific subtypes of neurons that have stereotyped connectivities to provide the necessary functionality. Layers 2-4 are upper layer neurons and largely make connections within the cortex, termed cortico-cortical or intracortical. The largest and most anatomically obvious group of intracortical axons is the corpus callosum, which is a large bundle of axons from each cortical hemisphere that projects across the midline and connects to homotypic areas of the contralateral hemisphere. Intracortical connections, as a whole, provide the ability for associative and integrative functionality. In contrast, layers 5 and 6 mostly send corticofugal axons to subcortical structures, allowing the cortex to communicate with the rest of the nervous system and body. Layer 6 projects to the thalamus through the cortico-thalamic tract. Layer 5 sends axons to multiple subcortical structures, notably the brainstem and the spinal cord, comprising the axons of the corticospinal tract, which controls voluntary movement throughout the body (**Figure 1.1**). The process of axon pathfinding is controlled by guidance cues that direct axons to appropriate targets. These cues include attractive and repulsive signals like morphogen gradients (Stoeckli, 2018) and cellular

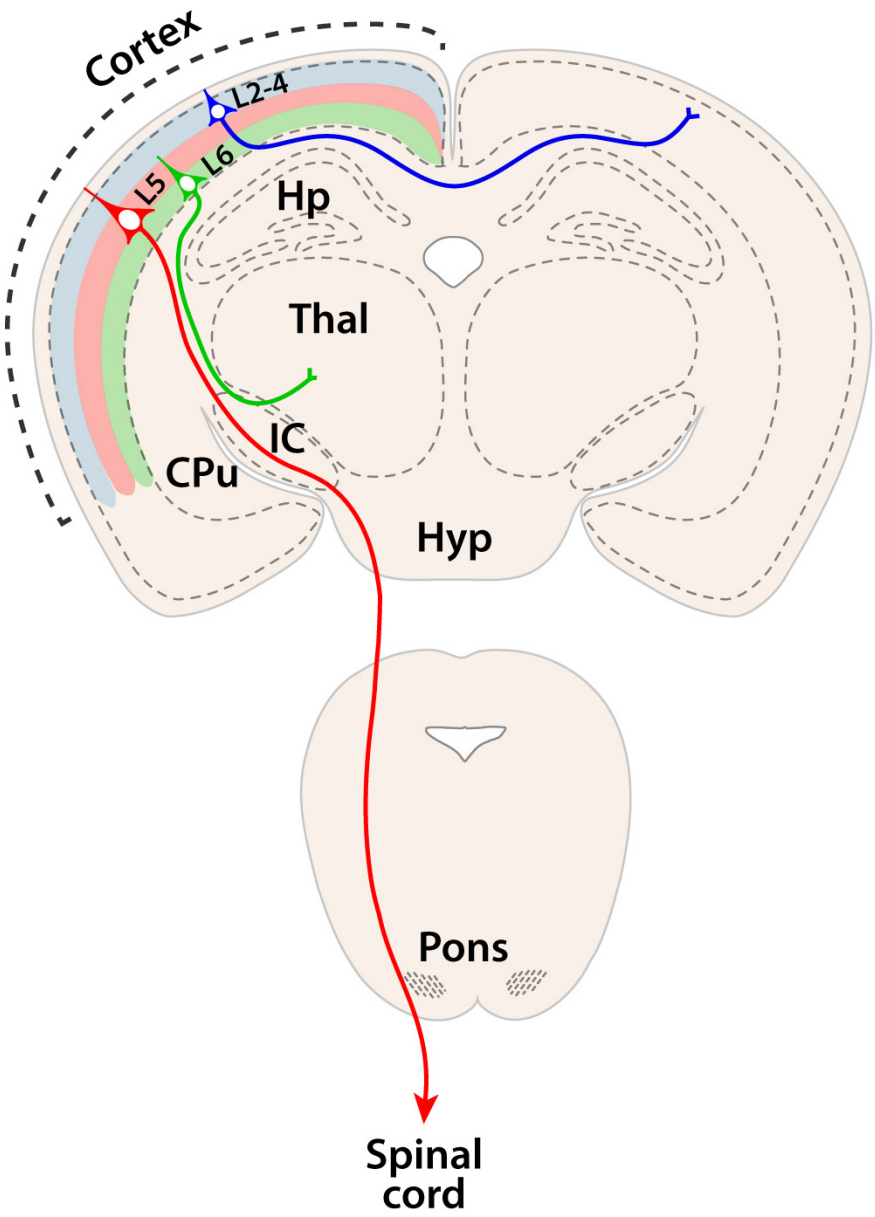

Figure 1.1: The six-layered neocortex enables complex connectivity

The cortex is the most dorsal structure of the mammalian brain (mouse schematized here), composed of six horizontal laminae, with stereotypical connectivity. Upper layers (L2-4) primarily make intracortical connections, including interhemispheric projection across the corpus callosum (blue axon). Deep layers (L5 and L6) send corticofugal projections to sub-cortical structures, allowing the cortex to communicate with the rest of the nervous system.

Hp: hippocampus, Thal: thalamus, IC: internal capsule, CPu: caudate putamen, Hyp: hypothalamus, L2-4: layer 2-4, L5: layer 5, L6: layer 6

populations like the indusium griseum, glial wedge, subcallosal sling and midline zipper glia that facilitate corpus callosum axonal crossing (Paul et al., 2007).

Cortical neurogenesis and development

Generation of neurons

In mice, the first cortical neurons are born around embryonic day (E) 11, and neurogenesis continues until ~E17 (**Figure 1.2**). Neurons arise from NPCs present in the germinal zones lining the fluid-filled lateral ventricles. In mice, the germinal zones are composed of the ventricular zone (VZ) and the subventricular zone (SVZ). NPCs called apical radial glia (aRG) reside in the VZ and form a pseudostratified epithelium, maintaining membrane contact with cerebrospinal fluid of the lateral ventricle. These aRG send their basal process to the pial surface, thereby extending a scaffold through the entire thickness of the developing cortex in the radial direction. aRG are the stem cells that will give rise to neurons of the cortex (Anthony et al., 2004; Mallamaci et al., 2000). Early cortical development (before E11) consists of symmetric aRG divisions, where one aRG divides and both daughter cells maintain contact with the ventricle and are maintained as stem cells. This symmetric division process exponentially increases the number of NPCs. Starting at ~E11, aRG begin to transition to asymmetric divisions that produce neurons, called neurogenic divisions. These asymmetric divisions result in two daughter cells with different fates. One daughter maintains stem-ness and its connection with the ventricular membrane and regenerates an aRG, which can undergo further neurogenic divisions. The other daughter is destined to become a post-mitotic neuron of the cortex, migrating radially away from the VZ into the cortical plate. aRG additionally have another function in this process. The pial-extending process of an aRG

forms a continuous scaffold for the newly post-mitotic daughter neuron to use as a guidance structure during migration to the cortical plate.

The first born neurons generate transient structures called the preplate and subplate (Kwan et al., 2012) that perform specialized functions to allow for post-mitotic neurons of L2-6 to subsequently populate the cortical plate. Neurons born after subplate and preplate neurons migrate along the aRG scaffold into the nascent cortical plate, becoming the deep layer neurons of L6. Subsequent divisions of the aRG generates new neurons that also travel along the radial scaffold, and migrate past the previously born neurons to the superficial portion of the cortex, stopping when they encounter the marginal zone at the extreme dorsal aspect. This continues, generating L6 → L5 → L4 → L3 → L2 neurons in an inside-out fashion, building the excitatory cells of the cortex from E11 - E17, in a process called sequential neurogenesis (**Figure 1.2**). After generating upper layer neurons, aRG switch to generating astrocytes through gliogenic divisions. An additional source of neurons in the cortex are intermediate progenitor cells (IPCs). IPCs are born from aRG and migrate into the SVZ, where they can undergo divisions to generate two IPCs or undergo terminal division to generate two daughter neurons without the regeneration of an NPC (Pontious et al., 2008).

Mouse brain development is simpler than that of gyrencephalic mammals, including the primate lineage. With the development of larger brains and increasing numbers of neurons, new strategies emerged to generate those neurons. Chief among these is the abundance in primates of basal radial glia (bRG) that populate the inner subventricular zone (ISVZ) and outer subventricular zone (OSVZ). As a type of radial

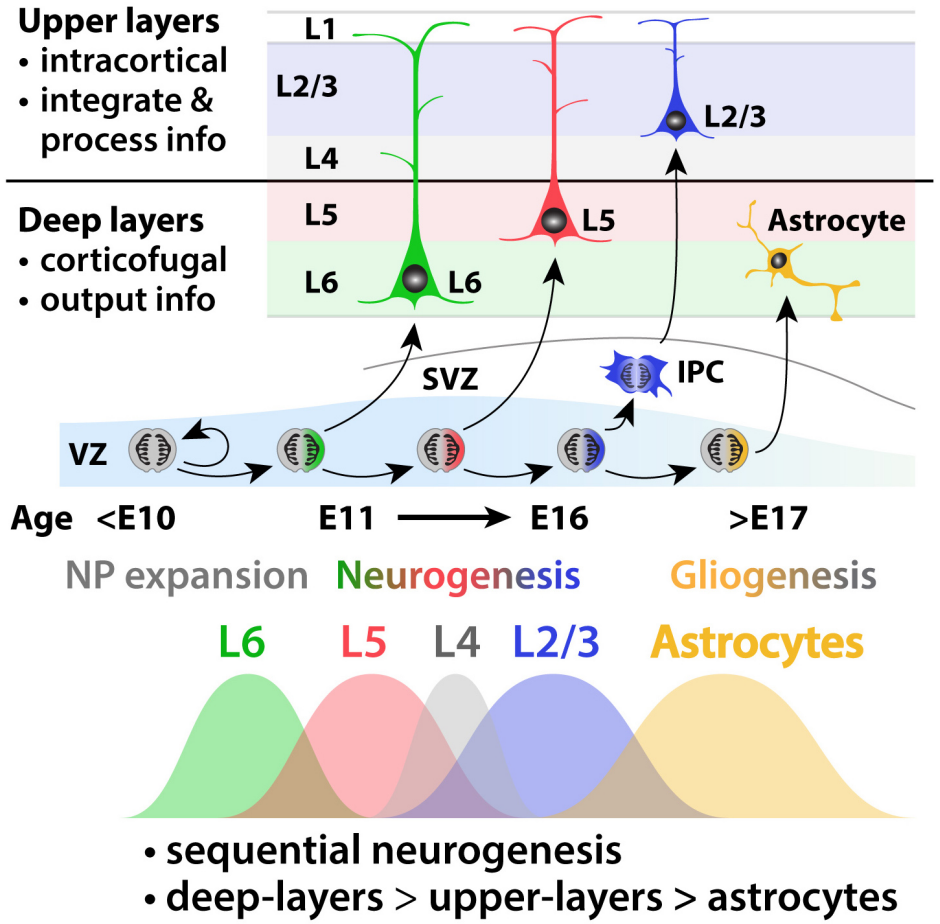

Figure 1.2: The neocortex develops by sequential neurogenesis

Neurons are generated by NPCs that first divide symmetrically (<E11) to expand the pool of NPCs. These NPCs then transition to asymmetric division, and generate neurons in a process called sequential neurogenesis. Deep layer neurons (L6) are born first and migrate into the cortical plate, with subsequent divisions giving rise to L5, then L4 neurons and so on. These neurons migrate dorsally and pass the deeper, established layers to form more superficial layers. After L2 neurons are born, NPCs transition to gliogenesis and give rise to astrocytes.

L1: layer 1, L2/3: layer 2/3, L4: layer 4, L5: layer 5, L6: layer 6, VZ: ventricular zone, SVZ: subventricular zone, IPC: intermediate progenitor cell

glial cell, they divide to give rise to post-mitotic neurons, which migrate along the bRG scaffold into the cortical plate. However, their cell bodies do not have a physical connection to the ventricle, differentiating them from the aRG population. This additional population of progenitors, present at low numbers in mice but highly prevalent in primates, may have played a prime role in the extraordinary expansion of the human neocortex (Hansen et al., 2010). Recent work has demonstrated that the evolution of a larger brain in mammals as compared to avian or reptilian cortex has coincided with increasing function of 'indirect' neurogenesis utilizing bRG and IPCs as opposed to solely relying on aRG for neuron generation (Cárdenas et al., 2018).

Migration and specification of neurons

Neurons are born in the germinal zones that are closely apposed to the ventricles, but must migrate to the most superficial region of the cortical plate to find their permanent location within the cortex. Newly post-mitotic neurons utilize the glial scaffold of their progenitor to guide their migration into the cortex, passing previously born neurons along the way. Due to the fact that a neuron follows the process of its progenitor into the cortex, neuronal tangential position within the cortex is fixed to the place where the scaffold of the progenitor ends (Rakic, 1972). Radial position within this region of the cortex is determined by birthdate, defining which layer and potentially which subtype of neuron it is destined to be. These discoveries form the basis of the radial unit hypothesis that pictures the cortex as a collection of columns (Mountcastle, 1997). Each column represents a clonal group of cells that originated from a single progenitor, and therefore, neurons within a column are related spatially as well as genetically (**Figure 1.3**). These ontogenetic columns form what may be called the

fundamental unit of the cortex, which is repeated many times over the surface of the cortical hemispheres. Each column contains neurons of each horizontal layer and molecular subtype and is wired together vertically, as evidenced by elicited responses to a single stimulus throughout the full cortical thickness of a column (Hubel and Wiesel, 1969; Mountcastle et al., 1957).

This columnar framework for understanding the developmental anatomy of the cortex also provides insight into the developmental function of early, symmetric NPC divisions and subsequent asymmetric, neurogenic divisions. Symmetric, expansive divisions exponentially increase the number of NPCs present, therefore increasing the number of columns within the VZ and the resultant cortex. Increasing the number of symmetric divisions functions mainly to increase the surface area of the VZ and eventual neocortex. Neurogenic divisions, in contrast, serve to increase the thickness of the cortex with no effect on cortical surface area (Dwyer et al., 2016; Rakic, 1995). Each additional neurogenic division of an NPC adds another post-mitotic neuron to an individual column and can contribute to the thickness of the cortex. Understanding this developmental anatomy illuminates the necessity for proper cellular proliferation in the generation of the vast numbers of cells of the cortex. During these cellular divisions, which form the NPCs and neurons of the cortex, DNA must be accurately replicated and DNA damage that occurs must be repaired. Unrepaired DNA damage during NPC proliferation has key implications for somatic mutations that occur during cortical development, as illustrated by the columnar architecture of the radial unit hypothesis.

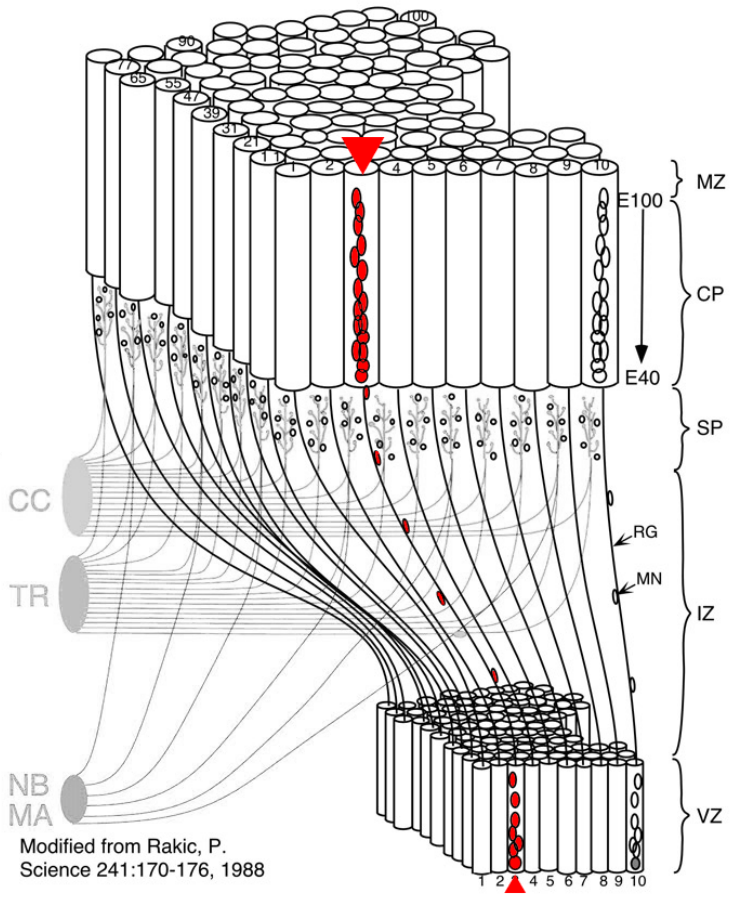

Figure 1.3: Radial units generate neurons in spatially and genetically related columns

A schematic of neocortex development in the rhesus macaque. NPCs reside in the VZ where divisions produce neurons that migrate along the radial glial scaffold into the cortical plate. The earliest born neurons are deep layer neurons (E40) with later born neurons migrating to more superficial areas (E100). Neurons born in the VZ use the radial glia scaffold to migrate into the cortex, dictating that a spatial relationship is maintained between the NPCs and the post-mitotic neurons that it generates. The radial unit hypothesis states that the cortex is composed of repeating collections of genetically and spatially related post-mitotic neurons called ontogenetic columns (red neurons in cortical plate).

VZ: ventricular zone, IZ: intermediate zone, SP: subplate, CP: cortical plate, MZ: marginal zone, MN: migrating neuron, RG: radial glia, CC: cortico-cortical connections, TR: thalamic radiation, NB: nucleus basalis, MA: monoamine

Image modified from (Rakic, 1988)

DNA damage and repair during corticogenesis

In order for a cell to proliferate, it must replicate the billions of nucleotides composing its genome. And for development of an organism, cell divisions occur countless times to generate the cells that comprise each organ. Genome replication, however, is a complex process with potential for significant damage. Furthermore, genome replication is not the only way that DNA may be damaged. In fact, the genome of any cell is constantly under threat from mutations, ranging from single strand breaks, interstrand crosslinks, DSBs, damaged bases, and mismatched bases. DSBs are considered one of the potentially most dangerous types of damage due to the possibility for loss of genetic information, activation of apoptotic pathways, or improper repair, which can bring negative downstream effects such as tumorigenesis. As a result of these potentially dire consequences, multiple pathways have evolved to repair DSBs, the most widely used being non-homologous end joining (NHEJ) and HR. These pathways are complementary in function, as they predominate during different parts of the cell cycle. They are characterized by differing kinetics and levels of fidelity as a result of the independent molecular mechanisms employed. Despite their differences, both pathways are important in DSB repair during organismal development, illustrated by decreased survival and exquisite sensitivity to genotoxic agents of double-mutant mice, deficient in both pathways (Couëdel et al., 2004).

Resection-independent mechanisms of DSB repair

An important mechanism of DSB repair is NHEJ, which is sometimes referred to as classical NHEJ (c-NHEJ). Mechanistically, NHEJ functions by rapidly recruiting factors to the DSB in an effort to protect and preserve the free ends from further

degradation, which would lead to loss of sequence information. In eukaryotic cells, this function is performed by the KU70/KU80 heterodimer that forms a ring and physically encircles the free DNA end. Crystallography has demonstrated that the KU heterodimer has high affinity for the sugar backbone of dsDNA ends and therefore binds in a sequence-independent fashion (Walker et al., 2001), a hallmark of NHEJ-mediated repair (**Figure 1.4A**). After the KU heterodimer has bound, a host of other components (DNA-PKcs, XRCC4, LIG4, XLF, APLF, and others) are recruited and participate in processing and ligation (Davis and Chen, 2013; Lieber, 2010). This includes resection of overhangs generated when the DSB was formed, filling in gaps via polymerase activity, and eventual ligation of the broken ends.

As a result of the homology- and sequence-independent nature of NHEJ and the end-processing that occurs, the mechanism has the potential to be mutagenic. These mutations can have several outcomes. If the two initial ends of a DSB are successfully ligated, there is the possibility of small indels or SNVs being introduced during the processing of the free ends in preparation for ligation. These mutations may be significant if they are present in a region of the genome that is dependent on high sequence conservation, such as protein-coding regions or enhancer elements. Potentially more problematic, however, is when free DNA ends that did not originate from the same DSB event are ligated. This type of repair will lead to structural variation (SV) like copy number variation (CNVs) or translocations, where different chromosomes are ligated together. Examples of the mutagenic properties of NHEJ-mediated DSB repair can now be readily examined using genome-editing techniques including CRISPR-Cas9. Targeting of coding sequence often leads to imperfect repair including

indels, which can function to inactivate genes for use in an investigative (Ran et al., 2013) or therapeutic strategy. Recent work used CRISPR to induce DSBs in NPCs, identifying aberrant repair that led to CNVs and translocations. This work not only illustrated the potential for SV following DSB repair by NHEJ, but also identified long genes expressed in NPCs as especially susceptible to DNA breaks and mutation via improper repair (Wei et al., 2016). This follows work detailing replication-transcription conflict as a mechanism of damage that preferentially effects large gene units (Arlt et al., 2011; Arlt et al., 2012; Wilson et al., 2015).

Although NHEJ can introduce indels as well as larger structural variants, it is difficult to determine how prevalent this outcome is since many of these repair events can happen ‘silently’ without leaving a mark of mutation. Recent studies using I-SceI and CRISPR-Cas9 have estimated that up to 75% of induced DSBs are repaired in an accurate fashion by c-NHEJ (Guo et al., 2018). Accuracy in this context means that no bases were added, deleted, or mutated, but instead were repaired by perfect apposition of initially disparate cut sites. In addition, these rates are a likely underestimate since they rely on two DNA ends that originated from two distinct DSB events. Also complicating the question is whether DSBs that arise physiologically, as opposed to being enzymatically induced, are more complex and therefore may be more prone to indels as a result of end processing.

Since the NHEJ process does not utilize a template for repair, it is the preferred mechanism during times in the cell cycle when no appropriate template is present. The G1 phase is when cells are metabolically active and DNA is decompacted and made available for gene transcription, which means that homologous chromosomes are likely

far away from one another in the nucleus and difficult to access. Post-mitotic neurons live in a terminal G0 state where the cell cycle has been deactivated. In both of these cell phases, NHEJ is the preferred DSB repair mechanism (**Figure 1.4B**). Additionally, NHEJ is utilized during M phase, as the organization and compaction of chromosomes makes any type of homology search difficult (Ceccaldi et al., 2016).

DSB repair in post-mitotic neurons

To determine the necessity of NHEJ repair in the nervous system, multiple groups have deleted essential components of the NHEJ system in mice. Both *Lig4* and *Xrcc4*-deficient mice die in mid or late-embryogenesis (Frank et al., 2000; Gao et al., 1998; Orii et al., 2006; Sekiguchi et al., 2001), with high levels of neuronal apoptosis. Of note, this apoptosis is initially recognized around E12.5, coinciding with the developmental age when neurons start to become post-mitotic and are therefore dependent on NHEJ-mediated DSB repair as permanently G0-phase cells. As may be expected, at E14.5 apoptosis is confined to the post-mitotic neurons of the developing cortical plate and is not present in cycling NPCs (Orii et al., 2006). Whereas these severe defects led to embryonic lethality, deficiency in other components of the pathway illustrate how NHEJ is important throughout the lifetime of a post-mitotic neuron. Deletion of *Atm*, a kinase important in NHEJ signaling, does not lead to embryonic lethality or microcephaly in mice, but rather has a neurodegenerative phenotype that leads to ataxia as a result of post-mitotic neuron cell death (Barlow et al., 1996) and phenocopies important aspects of human ataxia-telangiectasia syndrome.

An important aspect of all of these mouse models is the dependence on the tumor suppressor protein p53 for apoptotic cell death. Indeed, even the most severe

neurodevelopmental and neurodegenerative defects are rescued by concomitant deletion of p53 in these NHEJ-deficient animals (Frank et al., 2000; Gao et al., 2000). Though the embryological developmental defects were rescued, these mice were subject to high levels of tumorigenesis as a result of the combination of impaired DSB repair and deficient apoptotic induction.

Resection-dependent mechanisms of DSB repair

More complex than the re-ligation of blunt ends in NHEJ are a collection of resection-dependent processes. These processes all rely on a homology-searching mechanism and share an early step where the free DSB ends are resected by CtIP and the MRN complex in a 5' to 3' direction to liberate 3' ssDNA (**Figure 1.4A**). There are three resection-dependent processes: homologous recombination (HR), single-strand annealing (SSA), and alternative end-joining (called alt-EJ or MMEJ). HR is the most well-studied and understood. The most important consequential difference between NHEJ and HR is that HR can conceptually function as a perfect, seamless repair mechanism. This is because HR relies on a template for repair, often the sister chromatid, that shares the same sequence and can therefore provide a perfect model for repair.

HR can take place when a DSB occurs at a time in the cell cycle when a sister chromatid is present to be used as a repair template, primarily during S- or G2-phase. The DSB is recognized by kinases like ATM and ATR that phosphorylate a host of proteins including the histone H2AX (termed γH2AX after phosphorylation on Ser139), tumor suppressor proteins like p53 and CHEK2, and the HR protein BRCA1. Although BRCA1 functions in multiple pathways, it plays a critical role as a scaffold for a number

of HR proteins. It is known to facilitate the 5' to 3' resection process via CtIP and the MRN complex and also binds with critical partners like BARD1 (Zhao et al., 2017) and PALB2. Following this end resection, which generates hundreds to thousands of base pairs of ssDNA, the single-stranded binding protein RPA coats these strands to allow for further processing and prevents degradation of the vulnerable ssDNA. Multiple components including BRCA1, PALB2 (Sy et al., 2009), and critically, BRCA2 (Pellegrini et al., 2002), then facilitate the switch from bound RPA to RAD51. At this point, the RAD51-coated ssDNA is termed a presynaptic filament, which can invade dsDNA to perform a homology search to find a suitable template to repair the DSB. Following the identification of the appropriate homology, multiple pathways are available to synthesize the necessary DNA and resolve the DSB. It is worth noting that as HR is generally thought to be a highly accurate repair mechanism with seamless repair, recent evidence has shown that, in fact, HR can also be mutagenic via the introduction of SNVs, indels, or large SVs (Keil and McWilliams, 1993; Rodgers and McVey, 2016). The frequency of these mutations is dependent on how the HR process is resolved with certain mechanisms being more mutagenic than others. For instance, break-induced replication results in higher mutagenicity than Holliday junction resolution or synthesis-dependent strand annealing.

In addition to HR, another mechanism of DSB repair that is increasingly appreciated in multiple contexts is the process termed Alt-EJ or MMEJ. Similarly to HR, Alt-EJ occurs after resection has generated a 3' single-stranded overhang (**Figure 1.4A**). These ssDNA strands then bind to other regions of ssDNA, but crucially, only rely on short stretches of homology in the range of 5-25 base pairs. These binding events

occur in cooperation with a protein called PARP-1, with DNA synthesis by POLQ and ligation by DNA ligase III. These molecular players make the pathway and mechanism distinct from HR, once the resection decision has been made. In stark contrast to HR, Alt-EJ does not have the capability to be a perfect mechanism of repair. Alt-EJ relies on only short stretches of homology and is therefore rather permissive about the level of shared sequence. Perhaps even more consequentially, free 3' ends in Alt-EJ anneal other ssDNA to form a contiguous repair of the DSB. This is critically different because the resected DNA end is not able to utilize the unbroken sister chromatid as a template for repair and therefore will never be able to make a seamless repair. In fact, DSBs repaired by Alt-EJ have been demonstrated to be highly mutagenic, forming many types of structural variation including CNVs and translocations (Wei et al., 2016).

Initial studies viewed Alt-EJ as a backup mechanism for failed c-NHEJ, though more recent understanding has demonstrated that Alt-EJ is in competition with HR after a DSB occurs. End resection is the decision point that differentiates between whether a break will be repaired by c-NHEJ or via a homology-dependent mechanism, including HR or Alt-EJ. Evidence for this can be seen in the fact that PARP-1 inhibitors exhibit synthetic lethality with genetic or pharmacologic inhibition of HR factors (Bryant et al., 2005). Although these findings were initially attributed to a mechanism involving deficiency of single strand break repair, more recent interpretations focus on the role of PARP-1 in Alt-EJ, and the resultant inability of resected DSBs to be repaired due to loss of HR as well as Alt-EJ (Ceccaldi et al., 2015).

DSB repair in cycling NPCs

In embryonic development, NPCs rapidly divide to give rise to the tremendous number of cells that make up the cortex. As in any dividing cell, DSBs can occur through multiple mechanisms and throughout the cell cycle. One of the cellular activities that has the highest risk for DSBs is the replication of the genome that occurs in S-phase, as a result of replication stress, replication fork collapse, R-loops and other mechanisms. NPCs therefore need robust responses for these DSBs as a way to ensure proper progression through the cell cycle and to maintain genomic integrity. This burden generally falls to the HR process, which is especially suited to DSBs that happen in S- or G2-phase, due to the presence of sister chromatids for use as repair templates (**Figure 1.4B**). Indeed, deletion of critical HR factors including *Brca1*, *Brca2*, and *Xrcc2* demonstrate robust apoptosis in the developing forebrain (Frappart et al., 2007; Orii et al., 2006; Pulvers and Huttner, 2009). The cells that are sensitive to HR impairment are actively cycling cells within the VZ and SVZ germinal zones, once again highlighting the importance of DSB repair via HR to repair DSBs that occur during S- and G2-phase. Similar to other models of impaired DNA damage response (DDR), HR-deficient cell death occurs in a p53-dependent fashion.

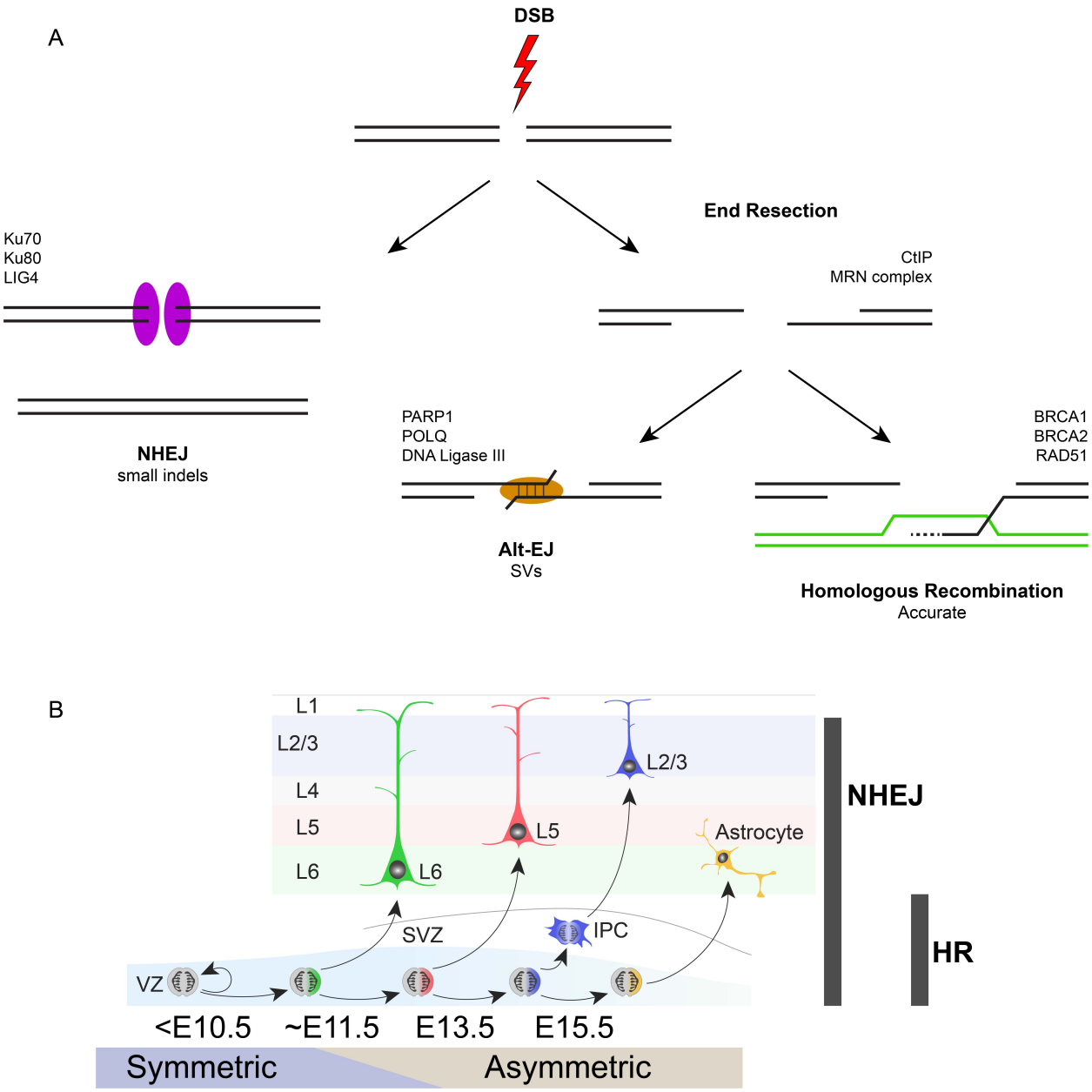

Figure 1.4: DSBs are repaired by multiple methods during corticogenesis

(A) DSBs can be repaired by multiple mechanisms. Initial decisions after the DSB occurs, dictated by cell cycle and repair factor binding, determine whether the break is end resected or repaired by NHEJ. If end resection occurs, pathways like HR and Alt-EJ, which rely on homologous sequence, can be used. NHEJ and Alt-EJ often produce mutations like indels or structural variants. HR can theoretically be seamless repair, using the sister chromatid as a template. Modified from (Ceccaldi et al., 2016).

(B) NHEJ can be used in cells throughout cortical development. HR is restricted to cycling cells in the VZ and SVZ due to need for an appropriate template for repair.

p53 mediates the response to improper DSB repair

The tumor suppressor protein p53 responds to many forms of cellular stress including DNA damage, hypoxia, and activation of oncogenes. Cells constantly express p53, though it is quickly degraded via interaction with MDM2. Upon a cellular stress stimulus, the interaction of p53 with MDM2 is disrupted by post-translational modifications on p53. This stabilizes p53 so it can effect changes in cellular processes that appropriately match the original stimulus. Among the repertoire of downstream functions are the abilities to induce cell cycle arrest at critical checkpoints, promote autophagy, or induce apoptosis, either through transcriptional activation of p53 targets or by mitochondrial activation of apoptosis (Zilfou and Lowe, 2009). DSBs, which can alter the genome in potentially tumorigenic fashion, are a potent activator of p53 function. p53 stabilization and downstream function is present in cells where NHEJ (Lim et al., 2000) or HR (Lim and Hasty, 1996) has been compromised, due to inability to repair DSBs in the appropriate way. p53 expression and function is important through development and the lifespan, and can contribute to neurodevelopmental disorders. Consistent with p53 signaling involvement in neurodevelopmental disorders, rare cases have been reported of germline mutations in p53 that produce a hyperactive form of the protein, resulting in developmental defects including microcephaly and co-occurring with bone marrow failure (Toki et al., 2018). Importantly, these cases demonstrate the effects of aberrantly active p53 signaling only, in the absence of additional genomic insults. More often, however, p53 is the mediator of cellular stress that leads to downstream proliferation defects or apoptosis of progenitors (Mao et al., 2016).

Microcephaly resulting from defective DNA damage repair

Microcephaly is clinically defined as small head circumference. A head circumference smaller than 2 - 3 standard deviations below the mean of an age- and gender-matched population meets the clinical criteria for a microcephaly diagnosis. Microencephaly is the clinical term for a small brain, and is generally a diagnosis based on neuroimaging. Though microcephaly technically refers to head size, it generally implies microencephaly, and the terms are used rather interchangeably in the literature. For the purposes of this work, microcephaly and microencephaly will both refer to pathologically small development of the brain, as cases where the skull restricts proper growth of the brain are not relevant to these discussions.

Microcephaly can occur in a congenital fashion, where pathological development is clinically apparent *in utero* or by birth, indicating a failure of proper brain growth during gestation. This is clinically distinct from postnatal microcephaly where a baby has a normal-sized head at birth, but fails to keep pace with expected growth in head circumference. Further characterization describes whether the microcephaly occurs in isolation, referred to as isolated or pure, or is present in a syndromic form where other anomalies are present. A common syndromic microcephaly presentation would be a somatic growth defect, which manifests in all tissues of the body, and the microcephaly is clinically notable in the context of intellectual disability of the patient.

The root cause of congenital microcephaly is the production of fewer neurons than would be present in a neurotypical individual. Microcephaly is associated with disrupted neuron production through a number of etiologies including CNS infections, teratogen exposure, hypoxic events, or trauma. Pertinent to this discussion, however,

are genetic causes of microcephaly. Microcephaly in humans has been linked to a number of genes, with certain recurring themes in gene functionality that inform the most vulnerable cellular processes during cortical development. Chief among these is the class of disorders arising from mutations in genes that function at the centrosome. The inaugural member of this class, microcephalin (*MCPH1*) (Jackson et al., 2002), functions at the centrosome and has a critical role in cell division. Since identification of *MCPH1*, multiple genes with functions at the centrosome have been identified as microcephaly genes, including *ASPM*, *CENPJ*, and *WDR62*. This also includes *CASC5 (*also called *KNL1*), a gene that mediates the spindle assembly checkpoint to ensure proper chromosome segregation. Recent work in our group has dissected the mechanism by which *Casc5*-deficiency leads to DNA damage and massive loss of NPCs to p53-dependent apoptosis (Shi L, Qalieh A, Lam MM, Keil JM and Kwan KY, In press, Nature Communications).

Impaired DSB repair is a cause of microcephaly

Another potential cause of microcephaly is mutations in genes involved in DSB repair. As previously described, DSBs can be repaired by by multiple mechanisms and these independent pathways predominate in different cellular settings during cortical development. Despite differences in mechanisms of repair and predisposition to occur in distinct cell populations, disruption of NHEJ and HR genes have both been identified as causative mutations in microcephalic patients (**Table 1.1**).

Table 1.1: Microcephaly caused by mutations in DSB repair genes

Gene	Associated symptoms*	Disrupted process	Citation
LIG4	Immunodeficiency, cancer	NHEJ, ligation	(O'Driscoll et al., 2001)
XLF	Immunodeficiency, cancer	NHEJ	(Buck et al., 2006)
NBS1	Immunodeficiency, cancer	NHEJ, HR	(Komatsu, 2016)
ATR	Somatic growth defect	HR, signaling in response to ssDNA/RPA	(Mokrani-Benhelli et al., 2013)
BRCA2	Somatic growth defect, aplastic anemia	HR, Fanconi anemia pathway, RPA to RAD51 switch	(Alter et al., 2007)
BRCA1	Early ovarian cancer, short stature, chemotherapy toxicity	HR, Fanconi anemia pathway, scaffold for resection and homology search factors	(Domchek et al., 2013)
RAD51	ID	HR, homology search	(Ameziane et al., 2015)
CtIP	Short stature	HR, end resection	(Qvist et al., 2011)

*Associated symptoms are not intended to be inclusive. Many of these genetic mutations have also been associated with cancer, growth deficiency, immune defects, as well as other developmental pathologies in individual cases.

Underscoring the importance of high-fidelity genome repair in brain development is the number of neurodevelopmental disorders associated with mutation of genes involved in HR, including *BRCA1, BRCA2, NBS1, ATR* and multiple members of the Fanconi Anemia pathway. In addition to microcephaly and intellectual disability reported in these patients, deficient HR is often accompanied by predispositions to malignancy, hematologic failure, and somatic growth defects, indicating the importance of genome fidelity in multiple tissues and throughout the lifespan.

Chromatin remodeling in cortex development

Chromatin and regulators of chromatin have become topics of intense study in brain development. The brain requires exquisite precision in gene expression programs to drive the complex processes necessary for proper development including cellular proliferation, neuronal migration and specification, maturation, as well as development

of appropriate connectivity. Many of these transcriptional programs rely on chromatin remodeling, in addition to specific transcription factor expression, to alter or finely tune the expression of critical genes. Indeed, emerging human genetic findings have convergently implicated dysregulation of chromatin as a key contributor to disorders of brain development (De Rubeis et al., 2014; Gabriele et al., 2018; Iwase and Martin, 2018). Recent studies have shown that altered chromatin function can perturb neural cell fates, circuit function, or neuronal plasticity via defective transcriptional regulation (Gallegos et al., 2018). Mutations in chromatin remodelers and chromatin regulators cause monogenic neurodevelopmental diseases (Sokpor et al., 2017; Vallianatos and Iwase, 2015), and have also been implicated in genetically complex disorders such as autism spectrum disorder (Sanders et al., 2015). Often, chromatin remodeling complexes are expressed broadly and constitutively, though phenotypes are often most severe or confined to neurodevelopment or neurologic function, suggesting that the developing brain is particularly sensitive to altered chromatin regulation. This observation warrants further investigation to better understand the full suite of functionality these molecules perform.

Functions of chromatin remodeling complexes in the cortex

Chromatin remodeling complexes alter the organization of the genome through a number of different mechanisms. They regulate the assembly and spacing of nucleosomes, which must occur each time replication occurs to protect naked DNA and provide organizational structure to the genetic information (**Figure 1.5A**)**.** Remodeling complexes can also regulate access of other factors, including transcription factors and RNA Polymerase II, via eviction or sliding of individual nucleosomes (**Figure 1.5B**)**.**

Lastly, remodeling complexes alter the nucleosome composition by substitution or incorporation of specific histone variants (**Figure 1.5C**) (Sokpor et al., 2018). Each of these functional modalities participate in chromatin regulation and contribute to complex cellular processes like genome replication, repair, and gene expression. Whereas chromatin remodelers have been demonstrated to function in many gene regulatory paradigms in the developing brain, their roles in genome replication and DNA repair remain understudied. Whether impaired chromatin-mediated DNA repair can contribute to developmental brain disorders is not well understood.

Chromatin remodeling enzymes participate in the DDR

DNA repair occurs in the context of chromatin as chromatin regulation is necessary to facilitate DNA repair, but few examples are present that implicate this functionality in human disease and organogenesis. Despite a lack of direct evidence, multiple remodeling complexes localize to damaged DNA, including DSBs, and participate in necessary aspects of repair. Multiple dramatic changes occur in chromatin structure and post-translational modifications in the immediate aftermath of a DSB and during repair (Clouaire et al., 2018). This includes the deposition or removal of histone post-translational modifications, selective enrichment or depletion of histone variants, and changes in DNA accessibility.

DNA accessibility is important for both NHEJ and HR. NHEJ generally needs minimal end-processing, though nucleosomes must be physically moved to allow for binding of necessary factors. The SWI/SNF family member BAF complex, specifically the complementary members ARID1A and ARID1B, bind near DSBs and help to recruit KU70/80 for NHEJ repair (Watanabe et al., 2014). HR, however, needs much more

chromatin processing to proceed. Not only must nucleosomes be liberated from the immediate region surrounding the DSB, but CtIP and the MRN complex also need access to hundreds or thousands of base pairs on each side of the break to allow for ssDNA production and subsequent presynaptic filament formation. Additionally, the presynaptic filament must conduct a homology search of the sister chromatid to find the proper repair template. All these steps are inhibited by tightly packed chromatin and therefore, chromatin undergoes dramatic changes after a DSB occurs (**Figure 1.5D**). Multiple remodeling complexes have been implicated in these functions. Indeed, the RSC complex (Chambers and Downs, 2012) and SMARCAD1 complex (Costelloe et al., 2012) both have roles in DNA end resection. Additionally, a chromatin remodeling complex termed the INO80 complex (INO80-C) has been implicated in DSB repair via the HR pathway. INO80-C functions by sliding nucleosomes and also catalyzes the removal of the histone variant H2AZ from nucleosomes for replacement with canonical H2A/H2B dimers. In yeast and mammalian cells, the INO80-C is recruited to DSB sites and is necessary for proper HR-mediated repair. *INO80*, however, has multiple functions and also plays important roles in gene regulation.

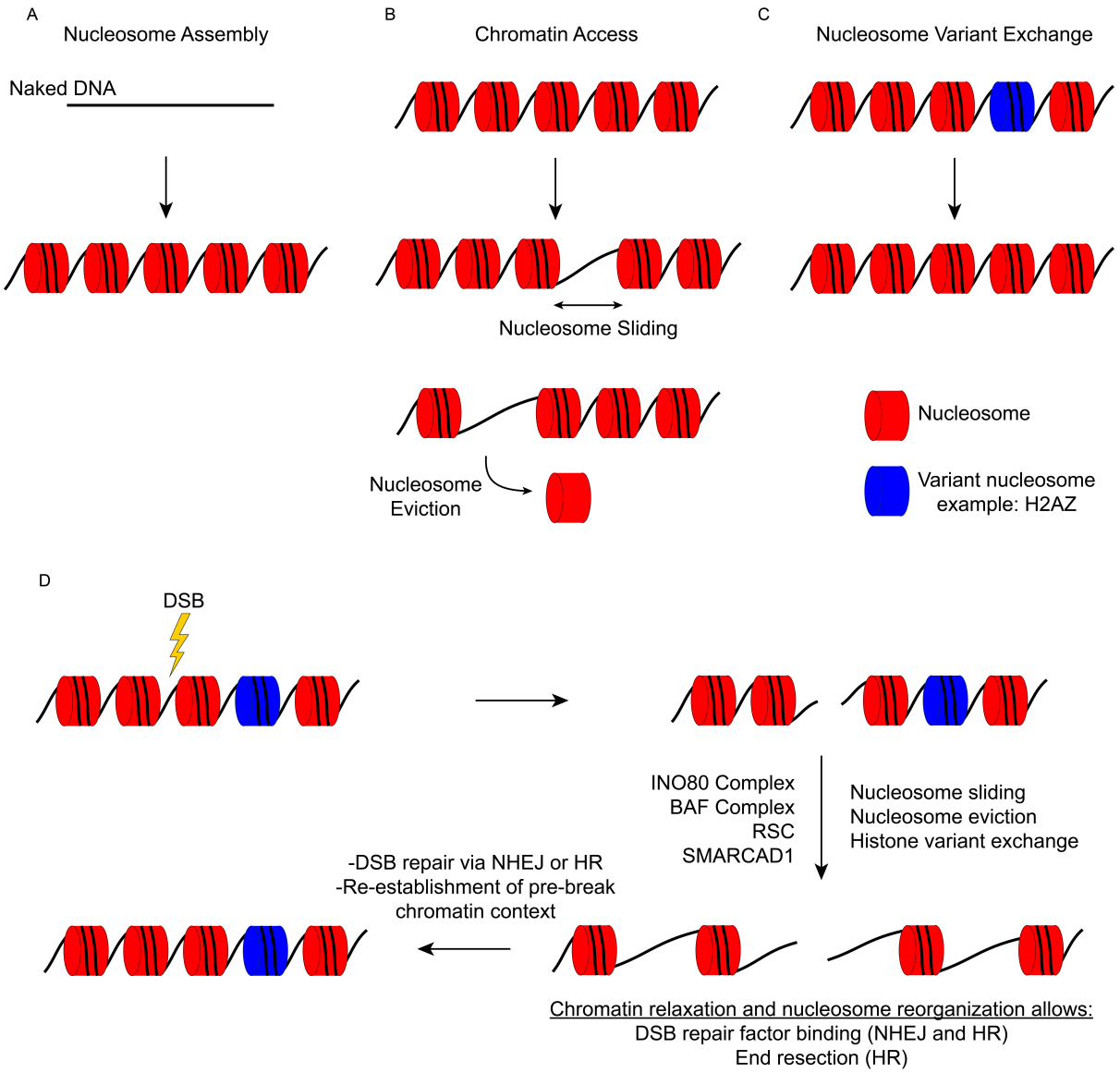

Figure 1.5: Chromatin remodeling mechanisms and function in DSB repair

(A) Chromatin remodelers incorporate nucleosomes to establish chromatin

(B) Access to DNA is modified by chromatin remodelers. Nucleosome sliding and eviction are both used to modify the sequences and genomic features that are available.

(C) Nucleosomes can contain variant histones that alter stability, function, and signaling. Chromatin remodelers catalyze the incorporation and removal of these variant histones.

(D) A model for chromatin-mediated DSB repair showing how chromatin remodelers slide and evict nucleosomes, and alter the histone variants present in the local region of a DSB. Relaxation of chromatin structure and incorporation/removal of specific histone variants allows DSB repair factor binding and processing for NHEJ and HR.
Adapted from (Sokpor et al., 2018).

Chromatin remodelers catalyze critical functions throughout the body and are responsible for numerous human diseases, often with particular effect on neurodevelopment when mutated. It remains to be determined how each remodeling complex is important in brain development. The majority of previous studies have focused on the gene regulatory aspects of chromatin, despite known roles of multiple remodelers in other processes such as DSB repair. My work investigated the role of the INO80-C in corticogenesis, specifically focused on dissecting and separating the dual functions of *Ino80* in gene regulation and DNA damage repair. In a larger sense, the importance of chromatin-mediated DDR and DSB repair has not been well investigated in brain development and remains a field with extensive questions.

Closing Remarks and Overview of Thesis

This dissertation seeks to answer questions fundamental to understanding how the cerebral cortex develops. As previously noted, chromatin remodelers have been increasingly implicated in critical functions in cortical development. However, the majority of these investigations have focused on the role of these remodeling complexes in a gene regulatory capacity. Despite the fact that these complexes remodel chromatin to facilitate DNA damage repair, it remains unknown whether these functions are important in brain development. In particular, the *INO80* chromatin remodeling complex, which has gene regulatory and genome stability functions in other contexts, has not been investigated in the developing brain.

In this work, I used conditional mutant mouse models to determine the role of *Ino80* in cortex development. Work in Chapter 2 showed that *Ino80* was necessary for

proper NPC maintenance, as *Ino80*-deficiency led to massive apoptosis of progenitors in medial neocortex. Developmental analysis showed that this cell death resulted from p53-mediated apoptosis secondary to impaired DSB repair. A novel *in vivo* DSB repair assay enabled me to differentiate between NHEJ- and HDR-mediated repair and demonstrated a specific deficit in HDR in *Ino80* cKO cortex. To ascertain the role of impaired HDR in the developmental phenotype, I co-deleted *Ino80* and *Trp53*, demonstrating a rescue of microcephaly and indicating that p53-mediated apoptosis was the key driver of the phenotype. Further phenotypic and bioinformatic analyses of the *Ino80* cKO and *Ino80;Trp53* dKO were employed to molecularly parse the gene regulatory and genome stability functions. Chapter 3 is focused on work to probe the dynamics of *Ino80* necessity by gene deletion with fine spatiotemporal control during corticogenesis. I also investigated the exciting and surprising finding that NPCs dividing symmetrically in cortex development are exquisitely sensitive to HR impairment via *Ino80* deletion, whereas later asymmetric, neurogenic divisions of NPCs in the cortex were unaffected by gene deletion. Using a *bona fide* HR gene, *Brca2*, I showed that this finding was generalizable to the HR process and was not specific to chromatin-mediated HR via INO80-C. Finally, Chapter 4 offers a perspective on broader implications of the work and directions for future investigations.

Chapter 2: *Ino80* is essential for chromatin-mediated homology-directed repair in developing cortex

Abstract

Chromatin regulates spatiotemporal gene expression during neurodevelopment, but it also mediates DNA damage repair crucial to proliferating NPCs. Here, I uncovered molecularly dissociable roles for the nucleosome remodeling INO80-C in chromatin-mediated transcriptome and genome maintenance in corticogenesis. I found that conditional *Ino80* deletion from cortical NPCs impaired DSB repair, triggering p53 activation, robust apoptosis, and microcephaly. However, co-deletion of the p53 gene, *Trp53*, with *Ino80* led to remarkable reversal of all *Ino80* phenotypes. Using an *in vivo* DSB repair assay, I found that *Ino80* deletion selectively impaired HDR in the embryonic cortex. Transcriptome analysis of *Ino80* cKO and *Ino80;Trp53* dKO brains revealed that INO80 function in genome stability was mechanistically distinct from YY1-associated transcriptional control. Together, this work uncovered molecularly dissociable functions of INO80 during brain development *in vivo*.

Introduction

Emerging human genetic findings implicate dysregulation of chromatin as a key contributor to disorders of brain development (De Rubeis et al., 2014; Gabriele et al., 2018; Iwase and Martin, 2018). Recent studies have shown that altered chromatin function can perturb neural cell fates, circuit function, or neuronal plasticity via defective transcriptional regulation (Gallegos et al., 2018). Chromatin, however, also plays a key

role in DNA damage detection and repair. How disruption of chromatin-mediated genome maintenance affects brain development and whether it contributes to neurodevelopmental disorders remain largely unexplored.

Safeguarding genome integrity in proliferating neural progenitor cells (NPCs) is essential for normal neurodevelopment. In the fetal cerebral cortex, neurons and glia are generated by NPCs via successive rounds of cell division (Kwan et al., 2012). In this process, potentially mutagenic genome damage in the form of DSBs inevitably arise during DNA synthesis and mitosis. DSBs are mainly repaired by one of two major pathways that can yield divergent genomic outcomes: HR and NHEJ. HR uses homologous genomic sequence in S- and G2-phases of the cell cycle to seamlessly repair DSBs, whereas NHEJ ligates free DNA ends throughout the cell cycle in a homology-independent manner that can introduce indels or structural rearrangements (Ceccaldi et al., 2016). DSB repair occurs in the context of chromatin. Repair pathway choice and efficiency are regulated by nucleosome remodelers that control the accessibility, flexibility, and mobility of chromatin. Disruption of chromatin regulators during brain development can therefore contribute to neurodevelopmental disorders by impairing DNA repair in dividing NPCs, which could lead to brain somatic mutations (Wei et al., 2016). Although emerging evidence strongly suggests that somatic mutations can contribute to disorders of the brain (McConnell et al., 2017; Poduri et al., 2012), whether they can arise as a result of chromatin dysregulation remains unknown.

Here, I uncovered mechanistically distinct roles of *Ino80* in chromatin-mediated transcriptional regulation and genome maintenance in cortical development. INO80 is the namesake and catalytic subunit of the INO80 complex that mediates nucleosome

remodeling and histone variant exchange in gene regulation and DNA damage repair. *INO80* was recently identified as a candidate gene for human microcephaly and intellectual disability in a consanguineous pedigree (**Figure 2.1A**) (Alazami et al., 2015)**.** However, the neurodevelopmental roles of INO80 and how deficiency of INO80-C function may contribute to disordered brain development have not been explored.

Within this consanguineous family, affected individuals carry two missense mutations in each homologous *INO80* gene. The mutations occur at positions Chr15:40987186 and Chr15:41071953 (GRCh38) within the NM_017553.3 mRNA. Respectively, the mutations are 3737G>A (p.Arg1246Gln) and 1501T>C (p.Ser501Pro). These mutations are present homozygously in all six affected individuals and are heterozygous in six other unaffected members of the family, therefore segregating as a potential disease-causing recessive haplotype (Alazami et al., 2015). Utilizing the gnomAD database of phenotypically unaffected individuals (Lek et al., 2016), *INO80* loss-of-function mutations are present at much lower frequency (observed/expected ratio = 0.03, pLI (Probability of being Loss-of-function Intolerant) = 1) than would be expected. This suggests that such mutations have detrimental effects on health or development. These genetic observations suggest that the familial *INO80* mutations may function as a hypomorphic allele, whereby significant pathology is only unmasked in the homozygous state. The Arg1246Gln mutation occurs in the C-terminal domain of the protein, which is dispensable for *in vitro* catalytic activity (Chen et al., 2011). This amino acid change from arginine to glutamine represents a charge and size switch, however the conservation of this residue is not strong. Notably, the analogous position in *Saccharomyces cerevisiae* is a glutamine residue, suggesting that glutamine does not

disrupt the function of the protein. The Ser501Pro mutation represents a more strongly conserved residue (Ser, Thr, or Glu back to *S. cerevisiae*). The change to proline represents a polarity switch and is potentially damaging due to the cyclic nature of proline, which dictates a rigidity to the peptide structure not present in other amino acids. And whereas conservation is not phylogenetically perfect, all surveyed species back to *S. cerevisiae* have a phosphorylatable (Ser or Thr) or negatively charged (Glu) residue at this position, which differs dramatically from the mutated proline residue. Additionally, the 501 amino acid residue is near the ATPase catalytic domain, which has very high sequence conservation. Though these points implicate the Ser501Pro mutation to be functionally significant, neither missense mutation has been experimentally investigated, singly or in tandem, and therefore conclusions cannot be made about their impact on INO80 function.

INO80 was originally found in a yeast screen designed to identify necessary components of the inositol biosynthetic pathway. Directed analysis demonstrated that INO80-C was necessary for expression of genes regulated by inositol/choline-responsive elements (Ebbert et al., 1999). And more global approaches to investigate gene regulation showed pleiotropic expression defects including housekeeping genes as well as members of diverse pathways like phosphate metabolism, respiration, and gluconeogenesis. Subsequent work also identified the INO80 complex as necessary for expression of stress-responsive genes (Klopf et al., 2009), suggesting that these remodeling activities coordinate gene expression following a range of stimuli.

It remains controversial as to the exact mechanism by which INO80-C effects changes in gene expression, and owing to the chromatin remodeling and nucleosome eviction activities of the complex, multiple activities may be responsible. H2AZ has been described as a molecular rheostat for gene expression control, with H2AZ-containing nucleosomes often present in the nucleosomes flanking the transcription start sites of genes (Subramanian et al., 2015). The INO80 complex can evict H2AZ-containing nucleosomes, and indeed, depletion of INO80 in yeast leads to globally altered distribution of H2AZ and transcriptional changes (Papamichos-Chronakis et al., 2011). Importantly, H2AZ distribution has been linked to gene transcription control in the mouse brain, and specifically the alteration of H2AZ-containing nucleosomes immediately up- and down-stream of the transcription start site (Zovkic et al., 2014). Removal or maintenance of H2AZ-containing nucleosomes may explain how gene expression is altered, but provides no rationale for the selectivity of gene induction or inhibition. For the cell to coordinate a response to various stimuli, some other factor must provide instructions for the chromatin remodeler. Multiple transcription factors have been reported to interact with the INO80 complex. The most well characterized example is the transcription factor YY1 that binds and recruits INO80 to YY1-activated genes. The INO80 complex is used to locally remodel the chromatin, functioning as a necessary coactivator, to provide access to gene promoters and activate transcription (Cai et al., 2007). This role as a transcriptional coactivator is well established, though multiple studies have also reported large numbers of genes that are upregulated in INO80-deficiency (Yao et al., 2016), suggesting it may also have repressive function. And though it is difficult to discern primary transcriptional targets from downstream

secondary effects in these studies, the function of INO80 in gene transcription can be characterized as complex, likely activating and inhibiting many genes.

In addition to effects on gene regulation, chromatin remodeling by the INO80 complex has also been implicated in maintenance of genome stability. Deletion or knockdown of *INO80* in cultured mammalian cells leads to a number of karyotypic abnormalities including the presence of marker chromosomes, translocations, and alterations in chromosome number (Hur et al., 2010). Although the gene was identified in yeast due to transcription regulation functions, investigations in subsequent years focused on other roles in genome stability and the DDR in organisms as diverse as *S. cerevisiae* (van Attikum et al., 2004) and *A. thaliana* (Fritsch et al., 2004). Initial work demonstrated hypersensitivity to genotoxic agents (Shen et al., 2000) including hydroxyurea, methyl methanesulphonate, and ionizing radiation, all of which can induce DSBs among other types of DNA damage. Seminal work by the Gasser lab demonstrated that the INO80 complex was recruited to Homothallic switching (HO) endonuclease-induced DSBs in a process that was dependent on phosphorylation of histone H2A at the Ser129 position (van Attikum et al., 2004), the phospho-histone analogous to γH2AX in higher eukaryotes. This work also showed diminished production of ssDNA near the induced DSB, suggesting that end resection-dependent mechanisms of DSB repair may be compromised in an *ino80*-deficient state due to inability to produce the necessary single-stranded intermediate.

Despite these insights into INO80 complex recruitment and effects on chromatin structure near DSBs, mechanistic insights remained elusive. The Peterson lab reported novel functionality of INO80, where the complex catalyzed the removal of H2AZ-H2B

variant dimers from nucleosomes, therefore allowing H2A/H2B dimers to be incorporated (Papamichos-Chronakis et al., 2011). Indeed, in the absence of *INO80*, the genomic landscape of H2AZ distribution changes, which leads to gene expression changes and genome instability. Further evidence in yeast (Lademann et al., 2017) and mammalian cells (Alatwi and Downs, 2015) found H2AZ-containing nucleosomes may be an impediment to proper DSB repair by HR. These two studies showed in distinct organisms using diverse methodologies that INO80-deficiency led to impaired HR, and that co-deletion of H2AZ normalized HR. This suggests that H2AZ may not necessarily be important in the process of HR, but that presence within the genome can inhibit proper HR. If cells are deficient in the INO80 complex, which evicts H2AZ-H2B dimers, these H2AZ-containing nucleosomes may inhibit proper processing and preparation of post-break free DNA ends for HR. A recent investigation utilized ChIP-seq to profile how chromatin features, particularly histones and histone post-translational modifications, change in the region of a DSB (Clouaire et al., 2018). H2AZ was depleted in the immediate vicinity of DSBs (500 bp on each side of break), however it was not significantly depleted in larger genomic regions surrounding the break (500 kb pairs on each side of break), suggesting a necessity for H2AZ removal in the local region of damaged DNA. DSBs were also stratified by the type of repair that occurred at each break depending on whether NHEJ or HR was used to repair the break. Interestingly, H2AZ was depleted in the 1 kb surrounding DSBs that were repaired by HR, but was not changed from baseline in the region of DSBs repaired by NHEJ. This provides evidence that H2AZ removal occurs selectively during HR processing, and may indicate that INO80 only affects processing of DNA ends for HR. It is also a critical insight that

H2AZ removal occurs locally to the DSB, across a 2-4 kb span. This contrasts with the spread of γH2AX (Savic et al., 2009), the removal of histone H1, and the addition of ubiquitin conjugates, which all occur over a large stretch that can spread to 2 megabases (Clouaire et al., 2018). This indicates rather specific signaling and a necessary function for H2AZ removal in the proximate DSB region, where chromatin needs to be relaxed for critical functions such as end resection and RAD51 binding.

Other groups have investigated the role of H2AZ post-translational modifications, notably H2AZ acetylation, on the function of *INO80* in genome stability. Yeast strains deficient in endogenous htz1 (the yeast homologue of H2AZ) were made to re-express versions that had all lysines mutated to glutamine to mimic acetylation (HTZ1 4KQ) or all lysines mutated to arginine to prevent acetylation (HTZ1 4KR). Genome instability in *ino80*-mutant strains was reversed with the acetylation-mimic, but was further exacerbated in strains where acetylation was prevented (Papamichos-Chronakis et al., 2011). This demonstrated that H2AZ-acetylation dynamics have an important function in DSB repair and suggested that un-acetylated H2AZ may need to be removed by INO80 for normal DSB processing to occur.

Numerous studies have implicated INO80 in the process of end resection, presumably through modification of chromatin so that CtIP and the MRN complex can process the free ends to ssDNA as needed. Lademann *et al*. recently confirmed this using ChIP-seq in yeast following induction of a specific DSB using HO endonuclease. They proposed that the switch of the single-stranded binding protein RPA to the homology search molecule RAD51 was also impaired in INO80-deficiency. They hypothesize that the RPA-to-RAD51 switch is the portion of the process that is H2AZ-

dependent and furthermore, that it is responsible for the impaired HR (Lademann et al., 2017). It remains unclear how INO80, a chromatin remodeling complex, and H2AZ-containing nucleosomes would affect this process, which occurs on ssDNA. Without invoking novel, untested biology like single-stranded nucleosome wrapping or INO80-C:RAD51 binding, many questions remain.

To delineate the function of INO80-C in the brain, given known roles in gene regulation and genome stability (**Figure 2.1B**), I utilized a mouse with a conditional allele of *Ino80* (Qiu et al., 2016). I created *Ino80* cKO models using multiple Cre-driver lines to determine the effect of deletion with fine spatial and temporal control (**Figure 2.1C**). Conditional deletion of *Ino80* led to apoptosis of early NPCs and postnatal microcephaly, phenocopying the reported individuals who carry recessive mutations. Although *Ino80* functions in multiple genomic processes, the observed cell death and microcephaly in the *Ino80* cKO mouse was downstream of DNA damage and unrepaired DSBs. To investigate the repair of these DSBs *in vivo*, I developed a reporter assay utilizing CRISPR-Cas9 and molecularly distinct repair templates able to distinguish NHEJ and HDR events. This assay obviated the need for a germline-integrated reporter and enabled *in vivo* interrogation of DSB repair in mutant mice. This assay demonstrated a substantial impairment of HDR in *Ino80*-deficient cortex. Strikingly, the dramatic microcephaly of the *Ino80* cKO was completely rescued by concomitant deletion of *Trp53*, demonstrating that p53-mediated mechanisms of apoptosis were downstream of unrepaired DSBs. The *Ino80;Trp53* dKO enabled molecular dissection of the gene regulatory functions of the INO80-C, demonstrating dissociable roles of INO80 in YY1-associated transcription regulation and HR repair.

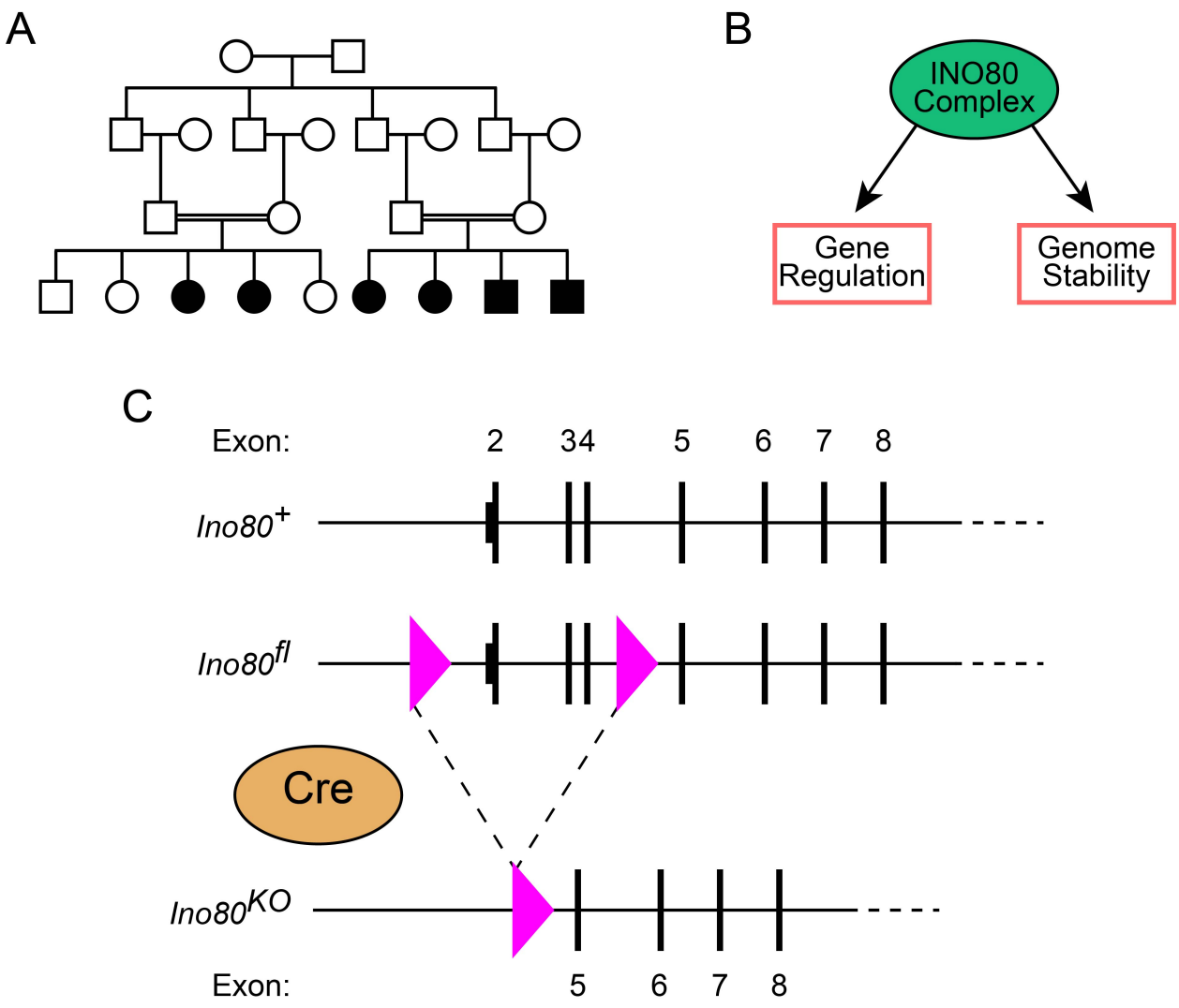

Figure 2.1: *INO80* is a candidate gene for microcephaly

(A) A consanguineous pedigree in which affected individuals share mutations in *INO80*, the catalytic subunit of the INO80 chromatin remodeling complex. Modified from (Alazami et al., 2015).

(B) INO80-C remodels chromatin by sliding and evicting nucleosomes, with effects on gene regulation and genome stability.

(C) A conditional *Ino80* allele allows deletion with spatiotemporal control. LoxP sites flanking exons 2-4 (including the translation start site) prevent the functional production of INO80 protein. Modified from (Qiu et al., 2016).

Results

Microcephaly and hippocampal agenesis following Ino80 deletion from NPCs

Available bulk and single-cell transcriptomic data showed moderate *Ino80* expression in all analyzed tissues and cell types across developmental stages, which is consistent with near ubiquity of the INO80 remodeling complex in cells. In cortical development, *Ino80* is present in both proliferating NPCs and post-mitotic neurons throughout neurogenesis. Constitutive *Ino80* deletion causes embryonic lethality on embryonic day (E)7.5 (MGI:5755273). I therefore leveraged a conditional *Ino80* allele (Qiu et al., 2016) to study *Ino80* in cortical development.

To distinguish potential *Ino80* functions in proliferating NPCs versus post-mitotic neurons, I first used two complementary Cre lines for conditional *Ino80* deletion - $Emx1^{Cre}$ and $Neurod6^{Cre}$ (also known as Nex^{Cre}). $Emx1^{Cre}$ mediates recombination in cortical NPCs starting at E10.5 (Gorski et al., 2002), near the onset of excitatory neurogenesis, whereas $Neurod6^{Cre}$ mediates recombination in newly post-mitotic excitatory neurons and spares NPCs from deletion (Goebbels et al., 2006) (**Figure 2.2**). To confirm proper Cre activity and visualize cells that have undergone recombination, I used Cre-dependent fluorescent reporter alleles (e.g. $ROSA^{nT\text{-}nG}$) to generate conditional mutants. The presence of Cre and appropriate spatial activity was visualized by epifluorescence in whole mounts and brain slices.

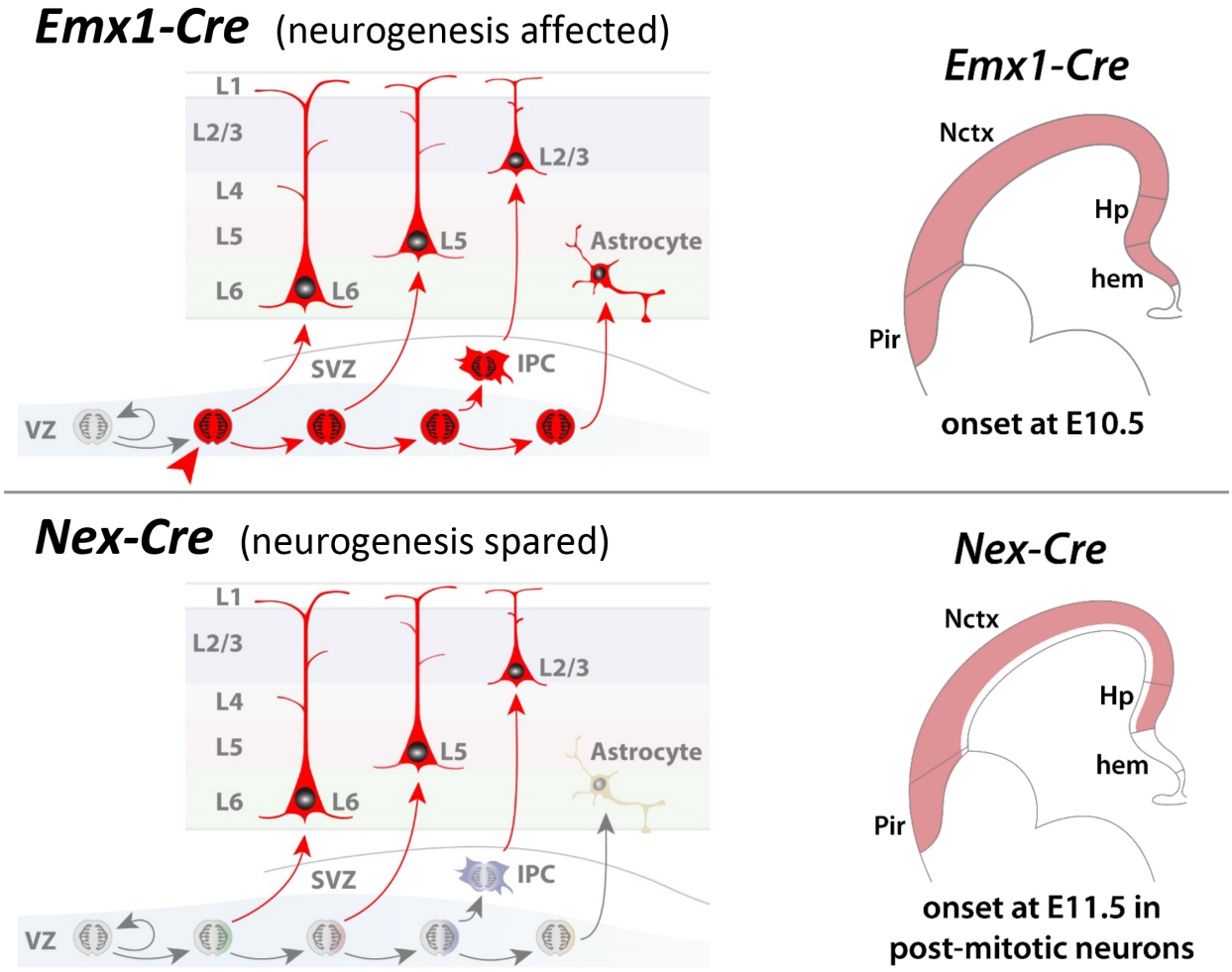

Figure 2.2: Cre expression in *Emx1*^{Cre} and *Neurod6*^{Cre}

Emx1^{Cre} is expressed in the NPCs of the developing cortex, beginning at E10.5. *Neurod6*^{Cre} (*Nex-Cre*) is expressed in cortical neurons when they become post-mitotic, therefore sparing deletion of floxed alleles in dividing NPCs.

L1: layer 1, L2/3: layer 2/3, L4: layer 4, L5: layer 5, L6: layer 6, VZ: ventricular zone, SVZ: subventricular zone, IPC: intermediate progenitor cell, Pir: piriform cortex, Nctx: neocortex, Hp: hippocampus.

Following *Ino80* deletion from NPCs, *Emx1*^{Cre};*Ino80*$^{fl/fl}$ (**cKO-E**), or from post-mitotic excitatory neurons, *Neurod6*^{Cre};*Ino80*$^{fl/fl}$ (**cKO-N**), mice were viable at birth, aged into adulthood without premature lethality, and were fertile as adults. On post-natal day (P)0, cKO-E, but not cKO-N, cortex was characterized by a 40% decrease in cortical area (**Figure 2.3A**) (ctrl, 8.19 mm^2; cKO-E, 4.88 mm^2; cKO-N, 8.66 mm^2; ANOVA with Tukey post-test, ctrl:cKO-E, *p*=1.6e-6; ctrl:cKO-N, *p*=0.22; cKO-E:cKO-N, p=1.1e-6, n≥3 animals per genotype), a 17% reduction in cortical thickness (ctrl, 0.47 mm; cKO-E, 0.39 mm; cKO-N, 0.48 mm; ANOVA with Tukey post-test, ctrl:cKO-E, *p*=0.028; ctrl:cKO-N, *p*=0.93; cKO-E:cKO-N, *p*=0.024; n≥3 animals per genotype), and a 42% decrease in mediolateral extent of the cortex (**Figure 2.3B and C**) (ctrl, 4.32mm; cKO-E, 2.49mm; cKO-N, 4.35mm; ANOVA with Tukey post-test, ctrl:cKO-E, *p*=1.1e-6; ctrl:cKO-N, *p*=0.97; cKO-E:cKO-N, *p*=1.5e-6; n≥3 animals per genotype). These *Ino80* cKO-E phenotypes are consistent with microcephaly in human patients carrying homozygous *INO80* mutations (Alazami et al., 2015). In addition, cKO-E cortex showed agenesis of the corpus callosum and hypoplasia of the hippocampus, two cortical structures near the midline. In contrast to the anatomical defects in cKO-E cortex, *Ino80* deletion from post-mitotic excitatory neurons in cKO-N did not lead to microcephaly, callosal defects, or hippocampal agenesis. Together, data from these conditional mutants implicated an NPC requirement for *Ino80* function in cortical development, including acquisition of normal cortex size and formation of cortical structures near the midline.

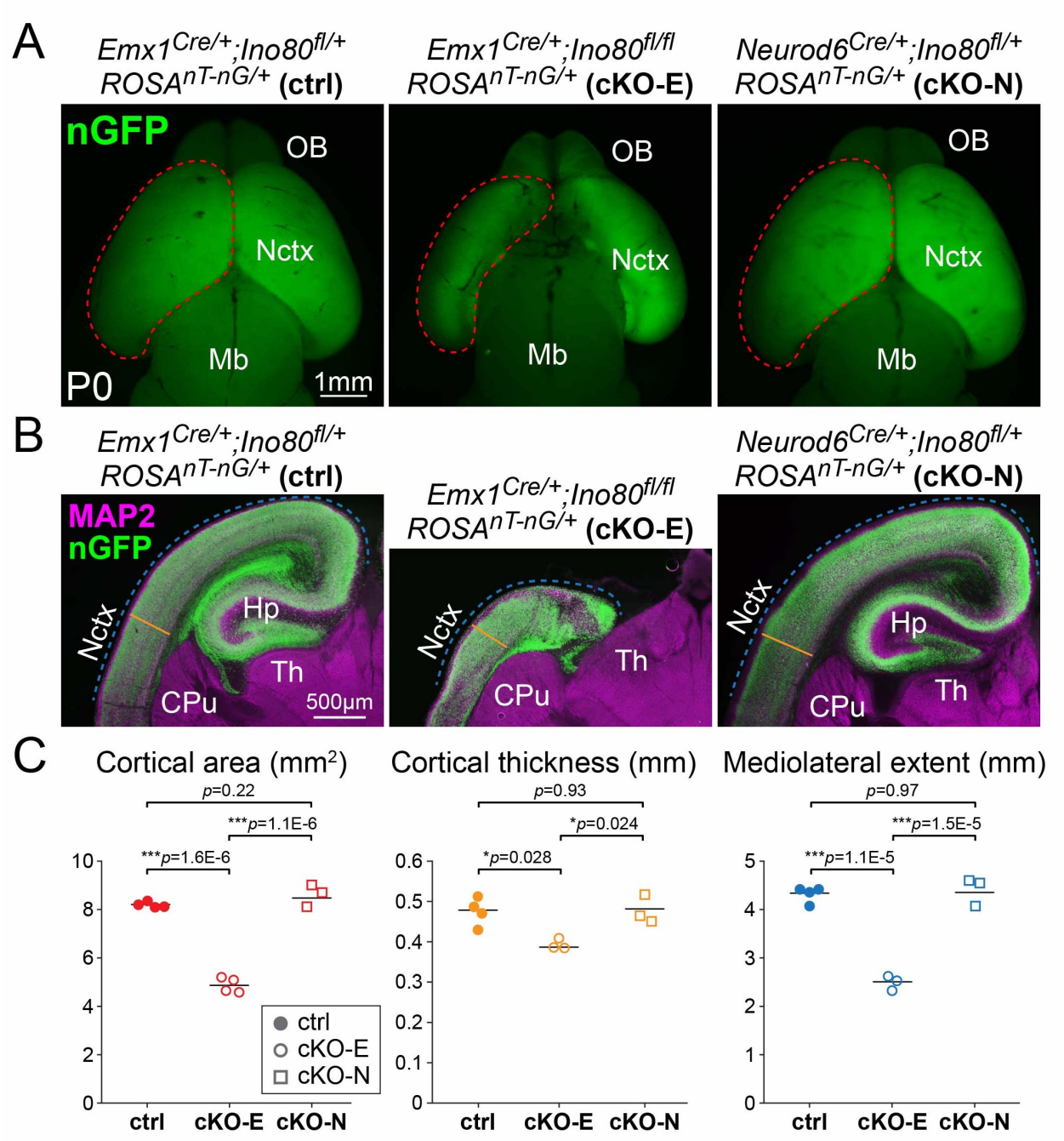

Figure 2.3: *Ino80* deletion in NPCs led to microcephaly

(A) Dorsal whole mount of ctrl, cKO-E, and cKO-N brains. Each brain has Cre-dependent expression of nuclear GFP (nGFP) from the ROSA$^{nT\text{-}nG}$ allele to illustrate proper Cre expression and can be used as a proxy for floxed gene deletion. *Emx1*^{Cre}-mediated deletion of *Ino80* in NPCs led to microcephaly, whereas *Neurod6*^{Cre} cKO did not alter cortical size or appearance. Red dashed lines indicate cortical area.

(B) Coronal sections of ctrl, cKO-E, and cKO-N brains stained for Cre-dependent nGFP expression and the dendritic marker, MAP2. cKO-E brains were microencephalic, with severe disruption to medial structures, including the hippocampus and corpus callosum. Blue lines trace the mediolateral extent of the cortex, from laterally-specified neocortex to the midline. Orange lines indicate the thickness of the cortex, using MAP2, measured laterally to the dorsal aspect of the CPu.

(C) Cortical area (mm^2), cortical thickness (mm), and mediolateral extent (mm) of ctrl, cKO-E, and cKO-N brains. Images in (A) and (B) are representative of measurements. Cortical area (red), cortical thickness (orange), and mediolateral extent (blue) were all reduced in cKO-E, but cKO-N were not significantly different from ctrl (mean, $n \geq 3$ animals, one-way ANOVA with Tukey post-test).

OB: Olfactory bulb, Nctx: Neocortex, Mb: Midbrain, CPu: Caudate putamen, Hp: Hippocampus, Th: Thalamus.

Ino80 deletion from NPCs preferentially disrupted medial corticogenesis

To assess potential alterations in neocortical lamination following NPC deletion of *Ino80*, I analyzed layer markers by immunostaining P0 brains. This revealed a striking mediolateral regional difference in layer formation in *Ino80* cKO-E. In lateral neocortex, TLE4+ layer (L)6, BCL11B+ (CTIP2+) L5, and LHX2+ L2-5 neurons were present in the correct location and properly ordered in cKO-E. The medial cortex, however, was hypoplastic and layer organization was severely disrupted; neurons were aberrantly clustered without forming distinct horizontal layers. The effects of *Ino80* deletion from NPCs were therefore regionalized and graded on the mediolateral axis in cKO-E: lateral neocortex was grossly normal in lamination, medial neocortex was hypoplastic and severely disorganized, and hippocampus, a 3-layered cortical structure normally medial to neocortex, was absent (**Figure 2.4**). In contrast to cKO-E, post-mitotic deletion of *Ino80* in cKO-N did not alter medial or lateral neocortical lamination or hippocampal development (**Figure 2.4**). Together, these data suggested that *Ino80* deletion from NPCs, but not neurons, preferentially disrupted medial cortex development but largely spared lateral corticogenesis.

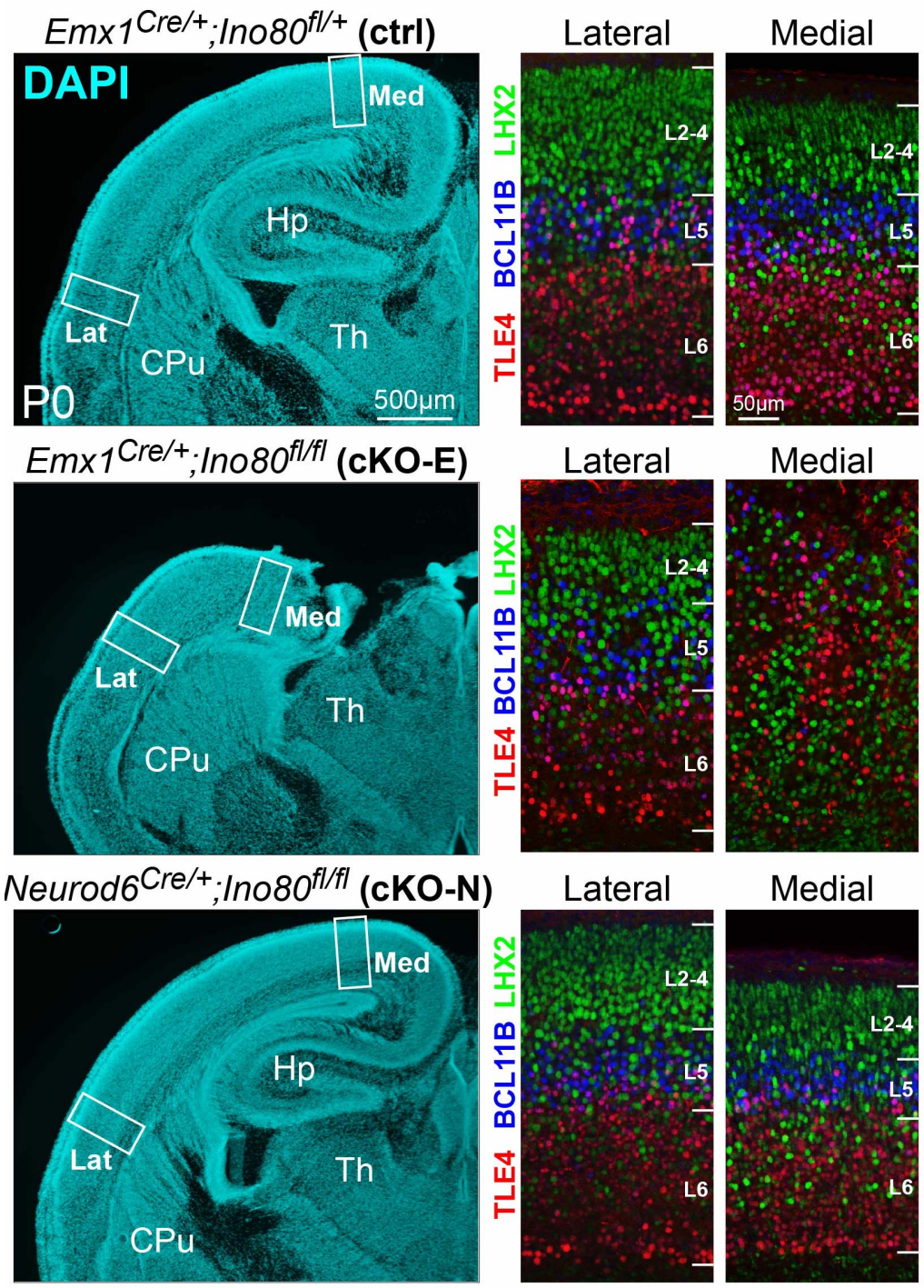

Figure 2.4: cKO-E brains had medial defects

Coronal sections of P0 ctrl, cKO-E, and cKO-N brains were stained for markers of L2-5 (LHX2, green), L5 (BCL11B, blue), and L6 (TLE4, red). ctrl and cKO-N brains had no differences in cellular organization. cKO-E lateral neocortex was appropriately specified, but the medial neocortical structures were severely dysplastic.

Lat: Lateral, Med: Medial, Hp: Hippocampus, Th: Thalamus, CPu: Caudate putamen.

To determine whether altered lamination was associated with altered axonal projections, I used the Cre-dependent *ROSA*^{EYFP} reporter for anterograde tracing of cortical axon tracts at P2 (**Figure 2.5A**). In the cKO-E brain, corticofugal tracts were reduced, but they were correctly targeted, innervating thalamus, pons, and medullary pyramids along the typical trajectory (**Figure 2.5B and C**). The anterior commissure was properly targeted. And whereas the corpus callosum was absent, it was unclear if callosal axons were not properly specified and directed or if medial structural defects prevented the structural formation of the midline appropriate for crossing (**Figure 2.5D**). These observations suggested that despite cortical hypoplasia and laminar disruption, some remaining neurons were correctly specified and projected to their normal targets.

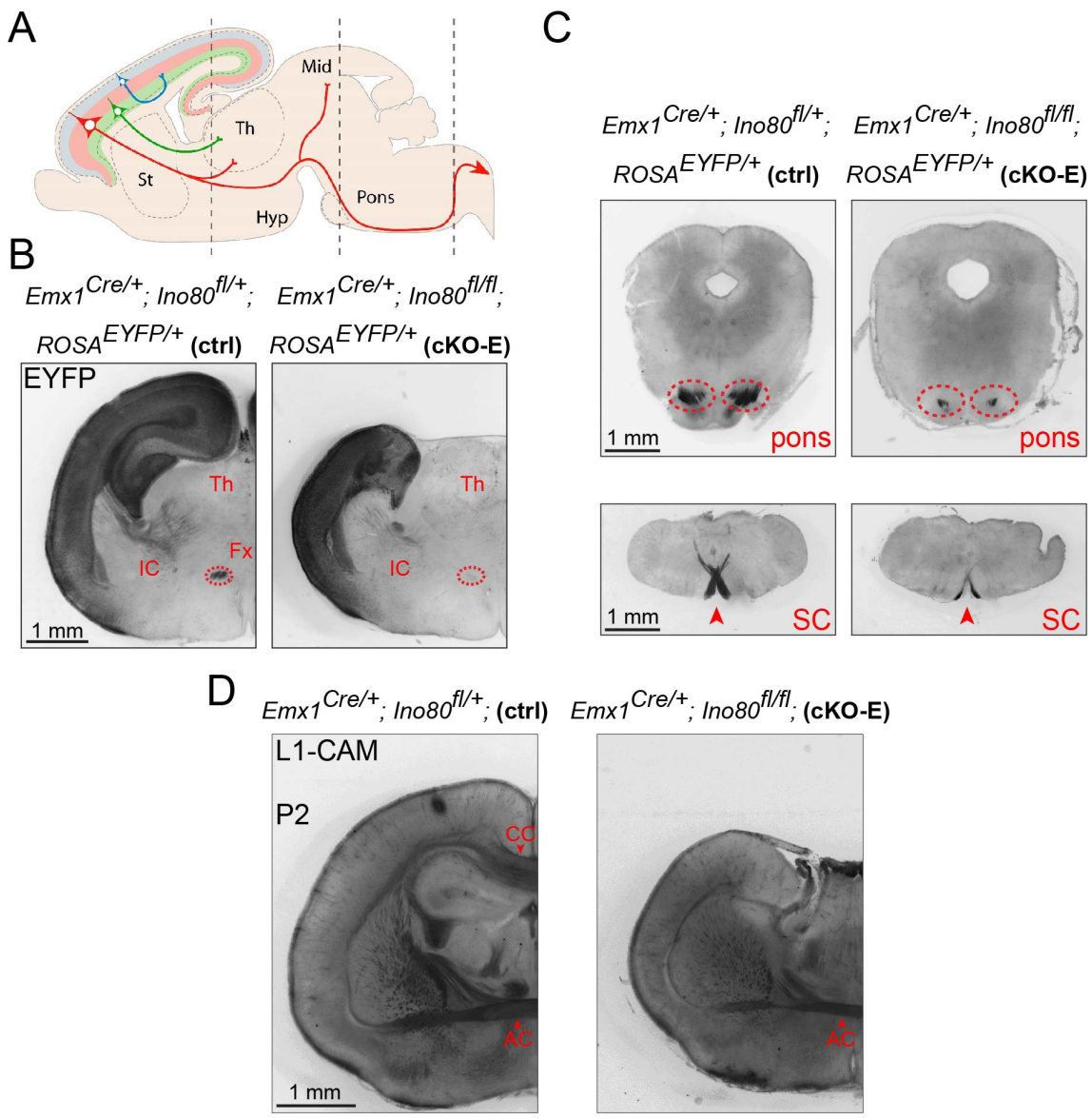

Figure 2.5: cKO-E cortical projections were appropriately targeted

(A) Schematic diagram illustrating the three abundant types of cortical projection neurons. Callosal axons (blue) from L2-4 neurons project through the corpus callosum to a similar location in the contralateral hemisphere. Corticospinal axons (red) from L5 neurons make connections in the thalamus and the spinal cord. L6 neurons are mainly corticothalamic (green), with targets in the thalamus. Vertical dashed lines represent the approximate levels of coronal sections in (B) and (C)

(B) Coronal sections of P2 ctrl and cKO-E brains immunostained for Cre-dependent expression of *ROSA*^{EYFP}. Corticothalamic projections were present in cKO-E brains, but diminished in number. Fornix was absent in cKO-E brains, as hippocampus, from which forniceal fibers are derived, was absent.

(C) Corticospinal tracts were visualized by immunostaining of EYFP and were present, but diminished in fiber number in cKO-E brain, at the level of the pons and the pyramidal decussation in the spinal cord.

(D) L1-CAM immunostaining showed the commissural axons of the corpus callosum and anterior commissure. Anterior commissure was present in ctrl and cKO-E brains. Corpus callosum was not present in cKO-E, possibly due to lack of appropriate midline anatomy for the callosum to form.

St: striatum, Hyp: hypothalamus, Th: thalamus, Mid: midbrain. Fx: fornix, IC: internal capsule, SC: spinal cord, AC: anterior commissure, CC: corpus callosum.

Specific loss of medial cortical NPCs to apoptosis following Ino80 deletion

The mediolateral differences in *Ino80* cKO-E phenotypes were congenital, and therefore likely embryonic in origin. I analyzed whether the medial cortex defects in cKO-E were associated with regional alterations in NPCs. In E15.5 cKO-E cortex, SOX2+ apical progenitors and EOMES+ (TBR2+) basal intermediate progenitors were each significantly reduced in number in medial (SOX2-positive progenitors per 100 um column, ctrl mean - 142, cKO-E mean - 55.8, a 61% decrease, p=5.5e-4, two-tailed t-test; n=4 animals; TBR2-positive progenitors per 100 um column, ctrl mean - 82.8, cKO-E mean - 10.5, an 87% decrease, p=1.4e-4, two-tailed t-test; n=4 animals; **Figure 2.6A and B**) but not lateral cortex (SOX2-positive progenitors per 100 um column, ctrl mean - 138.5, cKO-E mean - 148, p=0.35, two-tailed t-test; n=4 animals; EOMES-positive progenitors per 100 um column, ctrl mean - 89.8, cKO-E mean - 90, p=0.98, two-tailed t-test; n=4 animals; **Figure 2.6A and B**). This regional NPC loss selectively affected the neocortical and hippocampal anlagen, and did not affect the hem (**Figure 2.6A**).

To determine whether the marked NPC loss from cKO-E medial cortex was associated with cell death, I analyzed apoptosis earlier in cortical neurogenesis. At E13.5, cleaved-caspase 3 (CC3), an executioner caspase and marker of apoptosis, was widespread in medial (Med, **Figure 2.6C**) but not lateral cortex (Lat, **Figure 2.6C**). Similarly, pyknosis, the irreversible condensation of chromatin during apoptosis, was significantly increased in medial (pyknotic nuclei per 100 um column, ctrl mean - 1, cKO-E mean - 56.3, p=1.2e-6, two-tailed t-test; n=4 animals), but not lateral cortex (pyknotic nuclei per 100 um column, ctrl mean - 1.25, cKO-E mean - 2.25, p=0.70, two-tailed t-test; n=4 animals; **Figure 2.6D**). Together, these results showed that the post-

natal anatomical defects in medial cortex were associated with embryonic apoptosis and NPC loss in medial cKO-E cortex.

To ascertain that this spatial sensitivity to *Ino80* deletion was independent of potential regional non-uniformity in $Emx1^{Cre}$ activity, I analyzed the extent of cell ablation by $Emx1^{Cre}$ and the Cre-dependent suicide gene $ROSA^{DTA}$. At E13.5, widespread cell ablation was present throughout the entire mediolateral extent of the $Emx1^{Cre};ROSA^{DTA}$ cortex (**Figure 2.6E**). Consistent with the absence of regional difference in cell ablation in this model, analyses of $Emx1^{Cre}$ activity using multiple Cre-dependent fluorescent reporters have consistently shown cortex-wide expression of reporter genes without regional preference (Gorski et al., 2002; Liang et al., 2012). Together, these data indicated that cKO-E phenotypes were not the result of non-uniform Cre activity and supported that medial cortex was preferentially sensitive to NPC deletion of *Ino80* in cKO-E.

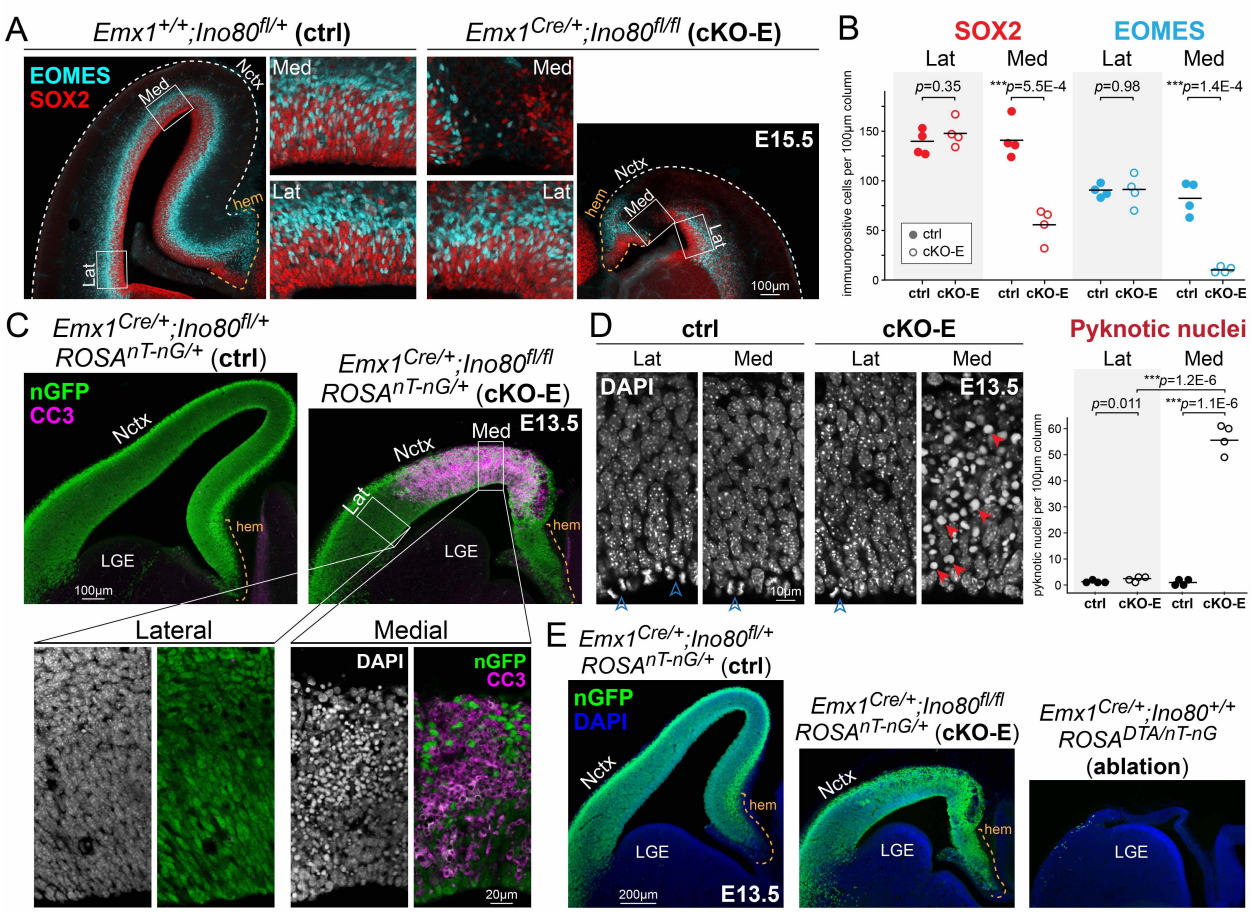

Figure 2.6: *Ino80*-deficiency led to medial NPC loss via massive apoptosis

(A) Immunostaining of NPC markers EOMES (TBR2) and SOX2 from E15.5 ctrl and cKO-E brains. cKO-E brains had severe loss of NPCs medially, but were unaffected in the lateral compartment of the neocortex. The cortical hem was also unaffected by *Ino80* deletion.

(B) Quantification of SOX2+ and EOMES+ cells in medial and lateral compartments of ctrl and cKO-E brains. Positively-staining cells were counted within 100 um columns. SOX2+ and EOMES+ cells were substantially decreased in the medial compartment of cKO-E, compared to ctrl. Cell counts in lateral neocortex were not statistically different in cKO-E compared to ctrl (mean, n=4, two-tailed unpaired *t* test).

(C) Immunostaining of nGFP and CC3 in ctrl and cKO-E brains at E13.5. Massive apoptosis was observed in the medial portion of the cKO-E cortex, but lateral neocortex was unaffected by gene deletion. nGFP immunostaining indicates Cre recombination has occurred, and is therefore a proxy for gene deletion. Higher magnification images demonstrate robust apoptosis and pyknotic nuclei, not present in the lateral cortex. The cortical hem was also unaffected by *Ino80* deficiency.

(D) Pyknotic nuclei (red arrowheads) were present in medial cKO-E cortex and were counted within 100 um columns (mean, n=4, two-tailed unpaired *t* test). Mitotic figures (blue arrowheads) were present at the ventricular surface of ctrl brain as well as in the lateral cortex indicating cell divisions.

(E) ctrl, cKO-E, and *Emx1*^{Cre}*; ROSA*$^{DTA/nT\text{-}nG}$ brains showed that ablation of the *Emx1* lineage led to total loss of cortex, including the lateral neocortex and cortical hem. cKO-E brains demonstrated selective loss of the medial neocortex.

Lat: lateral, Med: medial, Nctx: neocortex, LGE: lateral ganglionic eminence

Next, I investigated the possibility that altered cortical hem development can contribute to the *Ino80* cKO-E phenotypes. The cortical hem is a medial developmental center that gives rise to the Cajal-Retzius cells of the marginal zone and secretes signaling molecules to set up gradients across the cortex. Genetic ablation of the hem leads to microcephaly, disordered cortical development and inappropriate specification of neocortical cells via disordered neocortical *Lhx2* expression (Chou et al., 2009; Monuki et al., 2001; Shetty et al., 2013). In cKO-E, $Emx1^{Cre}$ induced deletion of *Ino80* in the cortical hem; however, no apoptosis was observed in the hem. Although the structure of the hem was intact, deletion of *Ino80* within these cells could lead to transcriptional dysregulation, effecting signaling center function of the hem, which could subsequently lead to disordered cortical development. To test this hypothesis, I obtained *Tg(Lmx1a-Cre)* that drives Cre expression selectively in the cortical hem and developing choroid plexus (**Figure 2.7A)** (Chizhikov et al., 2006). Conditional knockout of *Ino80* with *Tg(Lmx1a-Cre)* (cKO-L) demonstrated normal brain development at P0. Embryonic analysis showed appropriate and widespread Cre activity in the hem (nGFP) at E12.5. Importantly, no apoptosis was found in the *Ino80*-deficient cortical hem, indicating a lack of cell autonomous lethality in these cells. There was also no appreciable cell death or mis-specification in *Ino80*-proficient neocortical progenitors as a result of *Ino80* deletion in the hem. This demonstrated that any transcriptional dysregulation that occurred in *Ino80*-deficient hem was not affecting neocortical development (**Figure 2.7A**). Hem ablation can alter *Lhx2* expression. I therefore immunostained for LHX2 in the cortex at E12.5 in ctrl and cKO-E brains. LHX2 staining

was similar in intensity and pattern, indicating that cortical hem was likely not playing a role in the apoptosis or microcephaly phenotype (**Figure 2.7B**).

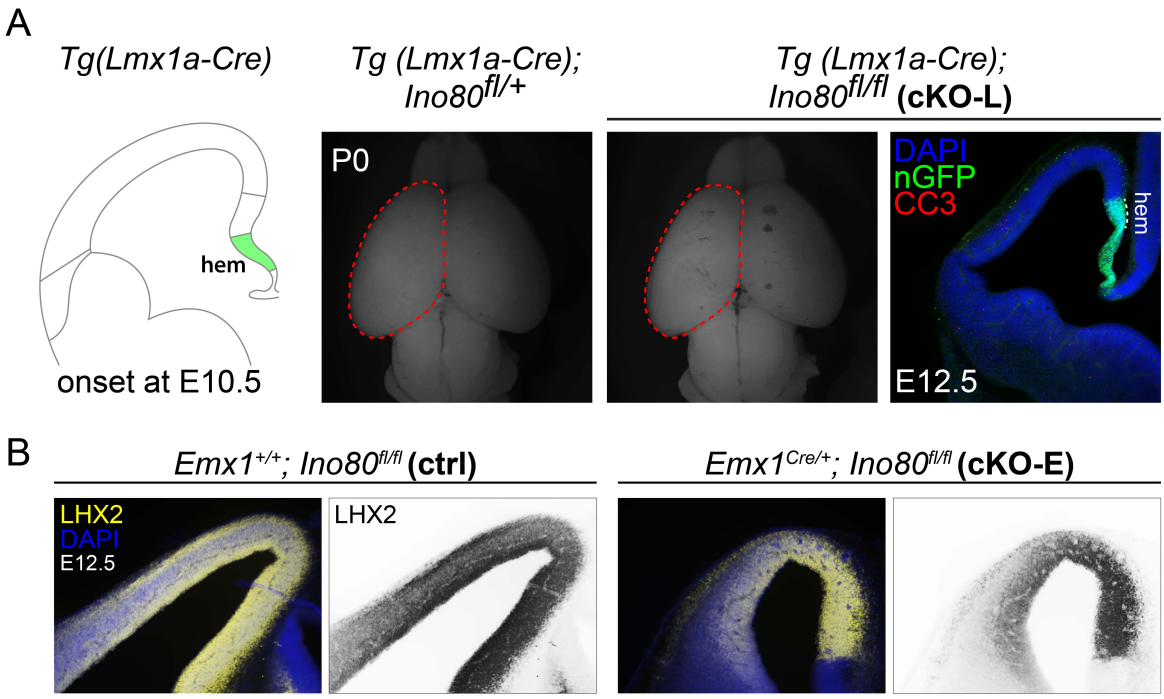

Figure 2.7: Deletion of *Ino80* in cortical hem did not disrupt corticogenesis

(A) *Tg(Lmx1a-Cre)* drives Cre expression in the cortical hem starting at E10.5. cKO of *Ino80* with *Tg(Lmx1a-Cre)* did not lead to microcephaly in P0 brains or apoptosis (CC3) at E12.5. nGFP immunostaining demonstrated *Tg(Lmx1a-Cre)* activity in the cortical hem and very few CC3-positive cells were present in neocortex. This presented a contrast to $Emx1^{Cre}$ deletion of *Ino80*, which led to widespread apoptosis.

(B) Cortical hem controls expression of *Lhx2* in neocortical progenitors. In cKO-E, which deletes *Ino80* from cortical hem and neocortical progenitors, LHX2 is expressed in the cortical VZ at similar levels and in a similar pattern as control cortex.

Transcriptomic signature of p53 activation in Ino80 cKO-E

Multiple mechanisms, including transcriptional dysregulation, could contribute to marked apoptosis in *Ino80* cKO-E. To gain insights into potential changes in gene expression contributing to apoptosis, I performed transcriptome analysis of E13.5 cKO-E by unique molecular identifier (UMI) RNA-seq using Click-seq (Routh et al., 2015) (ctrl: *n*=7, cKO-E: *n*=5 animals). In UMI RNA-seq, Click addition of a UMI tag to each individual cDNA molecule enabled post-sequencing de-duplication of PCR-amplified reads. Analysis of spike-in ERCC standards revealed excellent quantification over a wide dynamic range, indicating that transcriptomic changes could be determined with high confidence. Analysis of differential gene expression using edgeR (Robinson et al., 2010) revealed a total of 205 significantly upregulated and 418 significantly downregulated genes in cKO-E with a stringent false discovery rate (FDR) of < 0.001 (**Figure 2.8A**). Strikingly, of the 205 significantly upregulated genes, 30 are known to be either transcriptionally activated by the tumor suppressor protein p53 (TRP53), bound at their genomic locus by p53, or both (**Figure 2.8A**).

In an unactivated state, p53 is constantly monoubiquitinated by MDM2 and degraded. Abrogation of MDM2-p53 interaction blocks p53 degradation and activates p53 (Zilfou and Lowe, 2009). p53 can be activated via numerous stimuli and regulates differing sets of genes depending on the cellular context (Kastenhuber and Lowe, 2017; McKinley and Cheeseman, 2017). To understand what stimuli are causing p53 signaling in cKO-E cortex, I performed intersectional analysis with p53 gene target lists. These analyses demonstrated that target genes were significantly enriched from genome-wide studies of p53-mediated upregulation (P_{hyper}=0.011) and candidate gene studies

(P_{hyper}=0.025). However, genes targeted by p53 following a DSB-causing stimulus (X-irradiation), were highly and significantly enriched (P_{hyper}=3.6E-20) and the number of genes observed was greater than 10-fold higher than would be expected in a normal distribution (**Figure 2.8B**).

Consistent with p53 target activation in cKO-E, stabilized p53 protein was present at E13.5 in medial (p53-positive nuclei per 100 um column, ctrl-2.3, cKO-E-39.5, 17-fold, p=9.1e-6, two-tailed t-test; n=4 animals) but not lateral cortex (p53-positive nuclei per 100 um column, ctrl-1.3, cKO-E-2.3, 1.77-fold, p=0.11, two-tailed t-test; n=4 animals; **Figure 2.9A**), a gradient comparable to apoptosis and NPC loss in cKO-E. Together, the clear p53 transcriptome signature and the spatial specificity of p53 protein localization strongly suggested that p53 activation underpinned the apoptosis, NPC loss, and anatomical defects in medial cKO-E cortex.

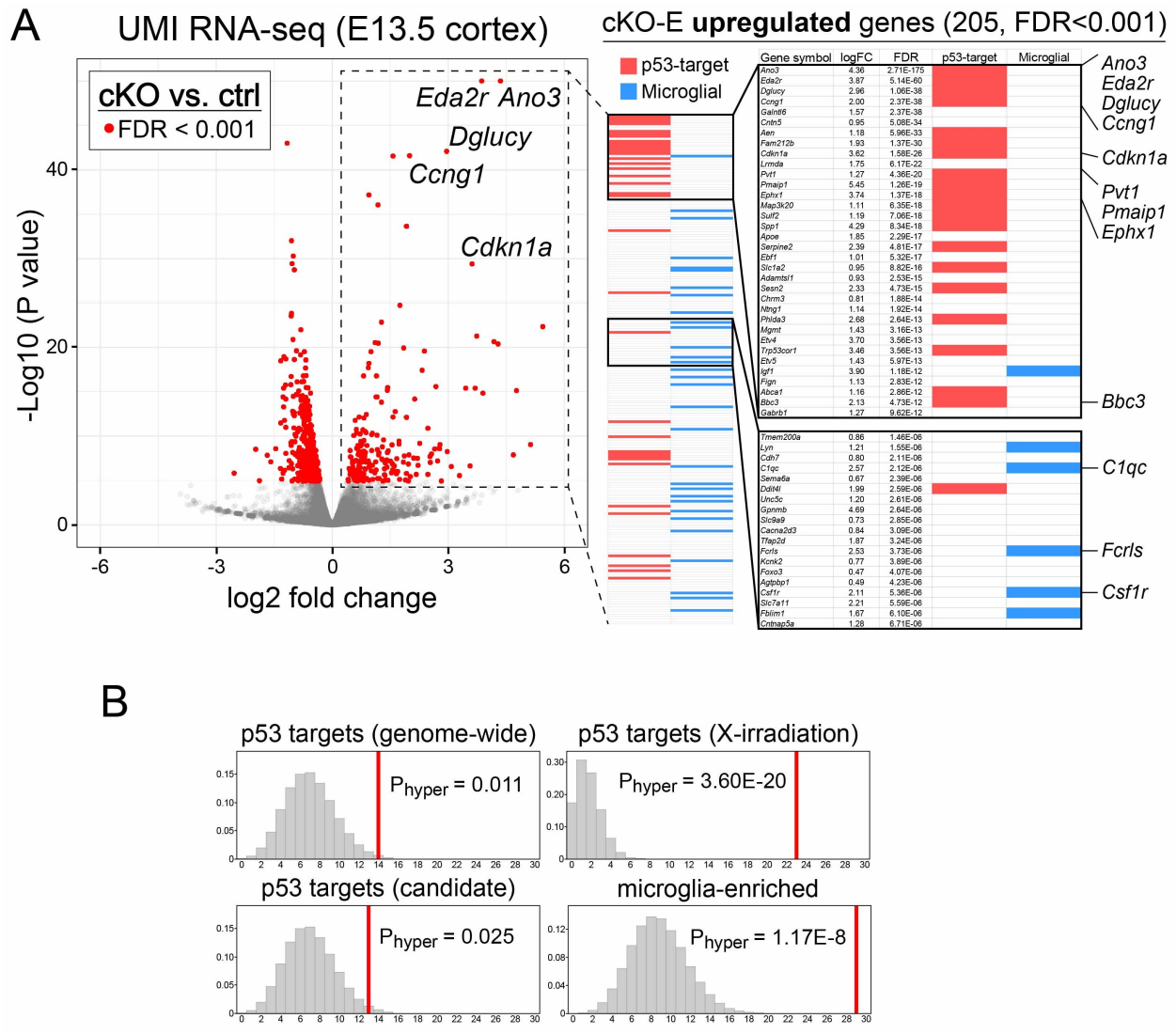

Figure 2.8: *Ino80* deficiency leads to p53 activation

(A) Volcano plot of log2 fold change plotted against -Log10 (P value) from transcriptome analysis of E13.5 ctrl and cKO-E cortex. 205 genes were significantly upregulated with a stringent FDR<0.001 (n = 7 ctrl, n = 5 cKO-E). Of those 205 genes, 30 were known targets of p53 (red) and 29 were genes expressed specifically in microglia (blue).

(B) Intersectional, hypergeometric analyses of upregulated p53 target genes compared to the expected number of p53 target genes from a hypothetical transcriptome analysis. Using genome-wide or candidate p53 gene lists resulted in p-values of 0.011 and 0.025, respectively. However, using p53 targets that are specifically upregulated after X-irradiation, a DSB-causing stimulus, led to a p-value of 3.6E-20 and a 10-fold increase in the number of targets detected compared to a hypothetical dataset. Hypergeometric analysis of microglia enriched genes showed a highly significant p-value of 1.17E-8.

In addition to the p53 activation signature, I also found a transcriptomic signature consistent with microglia in cKO-E. Based on available single-cell and cell type-specific transcriptome data, 29 of the 205 upregulated genes were specifically expressed in microglia in wild-type brain (e.g. *Csf1r*, *C1qc*, *Cd33*, and *Igf1*) (**Figure 2.8A**). Intersectional analysis of this gene list with confirmed microglia-specific genes showed a significantly enriched group of microglial genes were upregulated (P_{hyper}=1.17E-8) (**Figure 2.8B**). Microglia are the resident phagocytes of the brain and can increase in number and undergo activation in response to apoptosis. Our lab has previously shown that microglia are activated following widespread apoptosis in embryonic cortex (Shi L, Qalieh A, Lam MM, Keil JM and Kwan KY, In press, Nature Communications). Immunostaining for the macrophage/microglia marker ADGRE1 (F4/80) showed an increase in microglia number and phagocytic morphology in medial but not lateral E13.5 cortex in cKO-E, consistent with the regional gradient of p53 activation and apoptosis (**Figure 2.9B**). Consistent with one known function of microglia in the developing brain, pyknotic nuclei from apoptotic cells were present within the phagocytic microglia (**Figure 2.9B**).

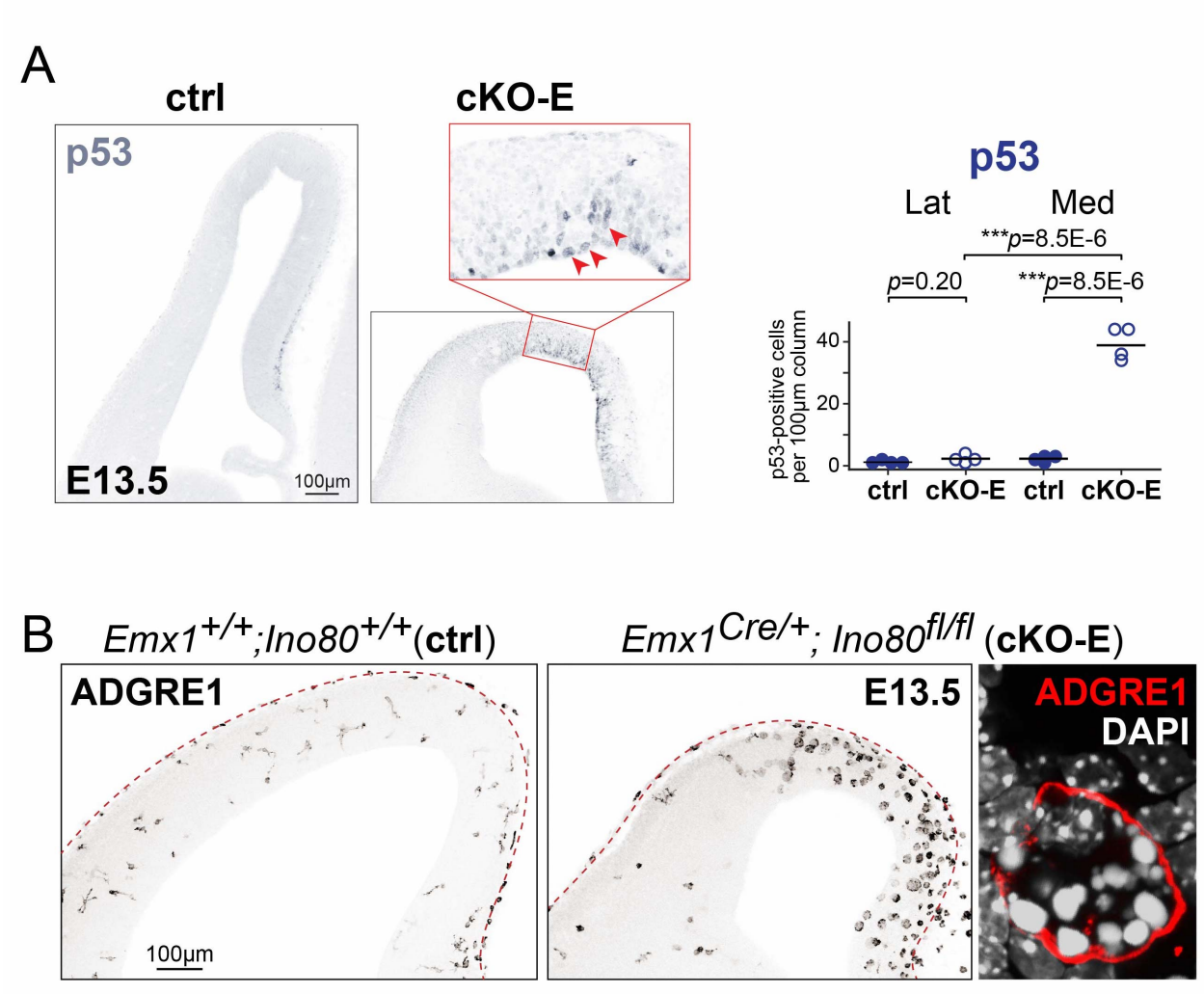

Figure 2.9: cKO-E showed p53 stabilization and microglial activation

(A) Coronal sections of E13.5 ctrl and cKO-E brains demonstrated a dramatic upregulation of p53-positive cells in medial neocortex of *Ino80*-deficient brains. p53-positive cell counts in a 100 um column. (mean, n=4, two-tailed unpaired *t* test).

(B) ADGRE1 immunostaining demonstrated increased microglial number and morphological change in the medial neocortex of cKO-E. Higher magnification image showed microglia (ADGRE1-positive, red) phagocytosing dead, pyknotic nuclei (DAPI hyperintense).

DNA damage in the form of double-strand breaks in Ino80 cKO-E

Activation of p53 is triggered by DNA damage, often via ataxia telangiectasia-mutated kinase (ATM), and drives downstream processes in DNA repair, cell cycle arrest, and cell death to safeguard genome stability (Banin et al., 1998; Cheng and Chen, 2010; Maréchal and Zou, 2013). I therefore immunostained for ATM substrate histone variant γH2AX to assess potential DNA damage in cKO-E (**Figure 2.10A**).

In cKO-E cortex, increased γH2AX staining in medial compared to lateral cortex at E12.5, indicated accumulation of DNA damage in cKO-E cortex with a mediolateral gradient similar to p53 and apoptosis (**Figure 2.10A**). The observed accumulation of DSBs in cKO-E could result from increased DNA damage or impaired DNA repair. Studies from multiple systems have shown that DNA synthesis is prone to DSBs, and DSBs are thought to be prevalent in rapidly dividing NPCs. Analysis of wild-type E12.5 cortex showed that γH2AX puncta were normally present in S-phase NPCs labeled by a 1-hour pulse of EdU (**Figure 2.10A**) and were also present in G2-phase and mitotic cells near the ventricular surface, suggesting that DNA repair occurs through G2 to properly repair damage before mitosis. In *Ino80* cKO-E, γH2AX puncta were present, but notably not increased in S-phase NPCs. However, hyperintense γH2AX immunostaining was present in *Ino80*-deficient mitotic NPCs, suggesting that the repair of synthesis-associated DNA damage was impaired following *Ino80* deletion in cKO-E. This possibility is supported by the absence of increased DNA damage or apoptosis following *Ino80* deletion from post-mitotic neurons in cKO-N.

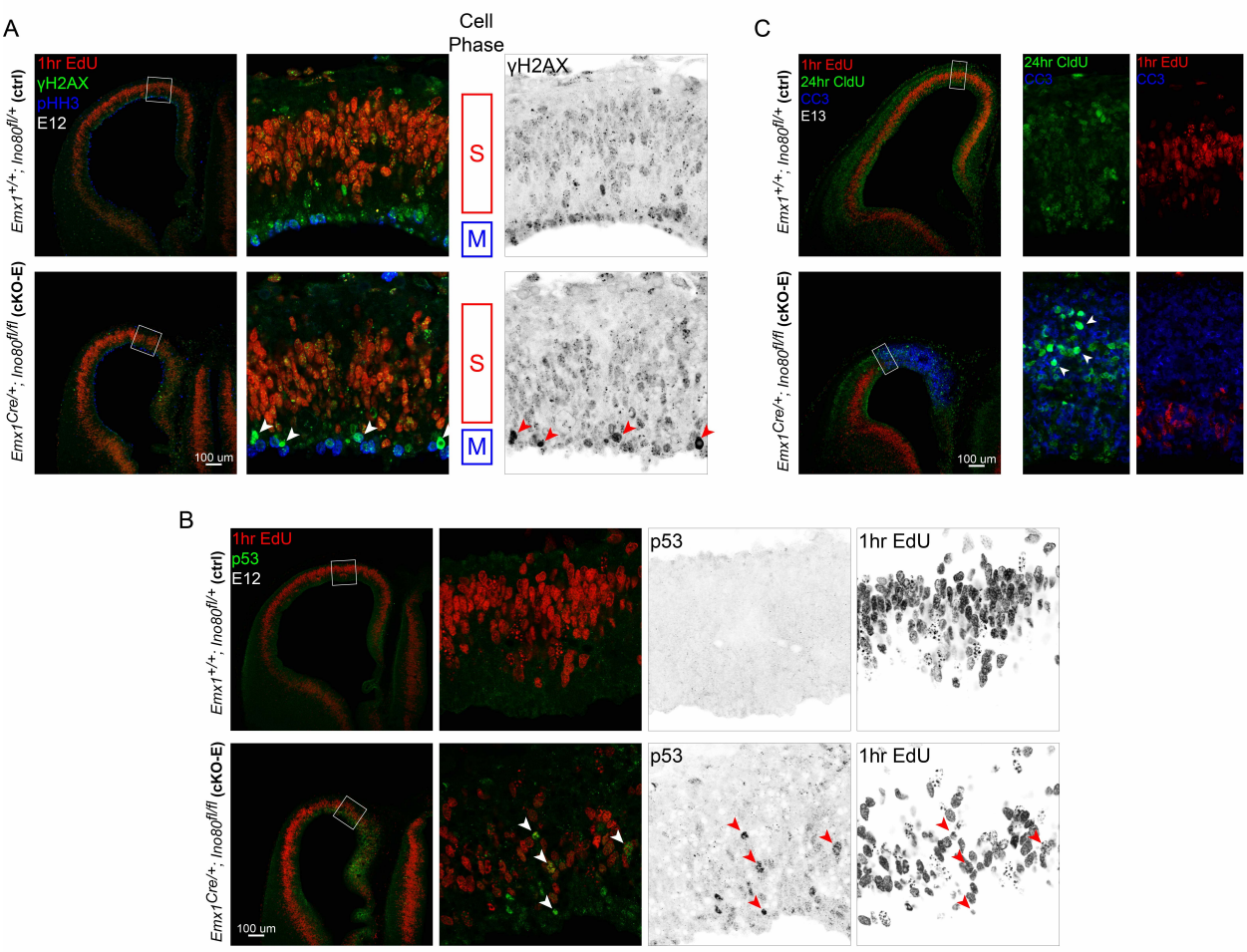

Figure 2.10: S-phase-associated DNA damage led to apoptosis

(A) One hour pulse with thymidine analog EdU labeled S- and G2-phase cells in ctrl and cKO-E cortex at E12.5. The EdU-positive (red) cells indicates the pool of cells in S-phase undergoing genome replication, whereas the pHH3-positive (blue) cells at the ventricular surface are the population of cells in M-phase. ctrl and cKO-E brain demonstrated γH2AX (green) staining in actively dividing cells as well as cells preparing to divide near the ventricular surface, indicating physiological DNA damage in replicating cells. However, cKO-E brains demonstrated hyper-intense γH2AX staining in likely G2- and M-phase cells lining the ventricular surface (arrowheads).

(B) One hour pulse with EdU labeled dividing cells (red) and immunostaining revealed p53-positive cells in S-phase (arrowheads) and likely G2-phase cells near the ventricular surface in cKO-E brains. Ctrl brains demonstrated few p53-positive cells.

(C) Before sacrificing animals at E13.5, mice were given a 24 hour exposure to CldU and a 1 hour exposure to EdU. cKO-E cortex had multiple apoptotic cells with CldU, but no cells with EdU (arrowheads), indicating that cells had died within the last day but not within the last hour.

To better assess DSBs, I immunostained for phospho-(p)KAP1 (TRIM28), an ATM substrate and marker of heterochromatic DSBs (Goodarzi et al., 2008; White et al., 2012; Ziv et al., 2006). At E12.5, the cKO-E brain was characterized by a marked increase in pKAP1+ VZ cells in medial but not lateral cortex, consistent with region-dependent accumulation of DSBs (**Figure 2.11A**). pKAP1 immunostaining was concentrated near the ventricular surface. This localization within the VZ suggested that cells nearing mitosis carried unrepaired heterochromatic DSBs, as the interkinetic nuclear migration (IKNM) demonstrates that cells finishing S-phase move towards the ventricular surface in preparation for M-phase (**Figure 2.11B**). Additionally, multiple cells were pKAP1-positive with EdU staining from a 1 hour pulse, indicating DNA damage associated with genome replication (**Figure 2.11A**).

If S-phase-associated DSBs were not being properly repaired, I reasoned that p53 accumulation and function may occur in S- and G2-phase cells. Indeed, I found multiple p53-positive nuclei that were also EdU-positive following a 1 hour pulse. This indicated that p53 accumulation occurred in S- or G2-phase cells and was likely related to S-phase-associated DNA damage (**Figure 2.10B**). My transcriptomic analysis provided additional support that the form of accumulated DNA damage in cKO-E was DSBs. Diverse target gene expression can be activated by p53 in a context-dependent manner. My analyses showed that *Ino80* deletion did not lead to global increase of all p53 targets. However, intersectional analysis with genes activated by radiation-induced DSBs showed a significant overrepresentation (P_{hyper}=3.6e-20) (**Figure 2.8B**). Thus, the transcriptomic signature of p53 activation suggested that DSBs were a trigger of p53 and an important, if not predominant, form of DNA damage in cKO-E.

To determine the timing of apoptosis relative to phases of the cell cycle, I used incorporation of thymidine analogs CldU (24 hours pre-sacrifice) and EdU (1 hour pre-sacrifice). This analysis showed the presence of multiple pyknotic, apoptotic nuclei positive for CldU, but none positive for EdU (**Figure 2.10C**). This indicated that cKO-E cells underwent apoptosis within one day of S-phase, but not within the last hour. This timing is consistent with my other findings that S-phase-associated DSBs led to upregulation of p53 signaling and to eventual apoptosis.

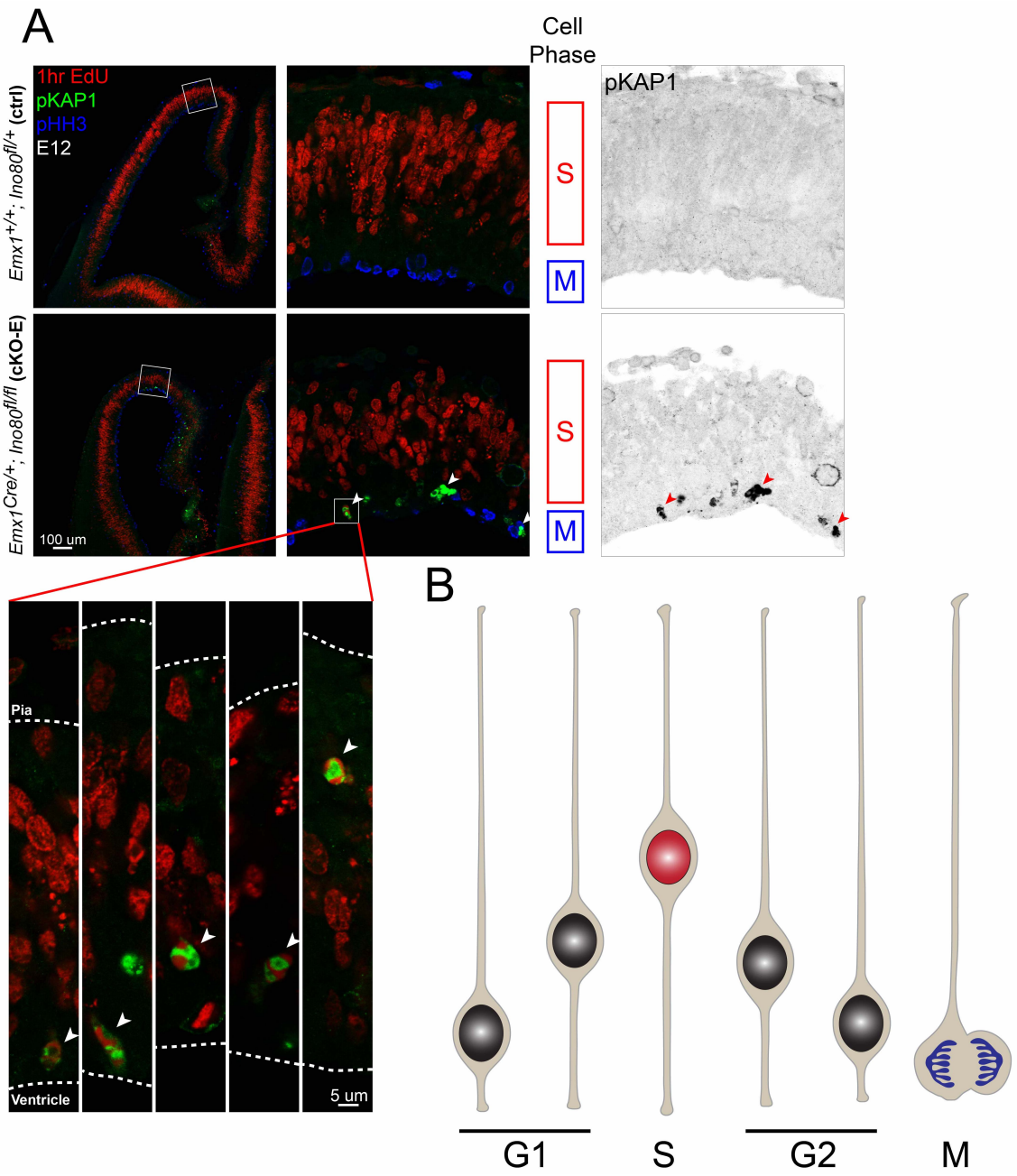

Figure 2.11: Persistent unrepaired DSBs were present in cKO-E NPCs

(A) One hour EdU and immunostaining of pKAP1 in E12.5 ctrl and cKO-E cortex. pKAP1-positive cells were present in S-phase cells and in cells near the ventricular surface, likely in G2- or M-phase cells. Colocalization of EdU and pKAP1 suggested that S-phase-associated DSBs may be unrepaired. Higher magnification of representative examples of pKAP1+, EdU+ cells indicating S-phase unrepaired damage.

(B) Schematic of interkinetic nuclear migration showing location within VZ of S-, G2-, and M-phase cells.

Selective disruption of homology-dependent DNA repair in Ino80 cKO

INO80 has previously been shown to be important for DSB repair by mediating removal of histone subunit H2AZ (Alatwi and Downs, 2015; Papamichos-Chronakis et al., 2011) or exchange of RPA for RAD51 in crucial steps for DNA repair by HR (Lademann et al., 2017). To test the possibility that *Ino80* deletion impaired HR in cKO-E, I designed an assay to interrogate DNA repair pathway choice *in vivo*. In this assay, I used CRISPR-Cas9 to generate a targeted DSB within the mouse genome at the C-terminus of the *Actb* coding region (Yao et al., 2017). To assess the mode of DNA repair, I generated an HDR reporter template with 800bp arms of complete homology to either side of the genomic DSB. With this template, successful HDR repair would lead to an in-frame knock-in of a *3xMyc* epitope tag at the C-terminus of *Actb*, resulting in a clear readout of ACTB-3xMYC translation. Complementary to the HDR template, I also generated an NHEJ template that is flanked by sgRNA target sites on either side of a *3xHA* epitope tag. CRISPR/Cas9 cleavage would generate a short NHEJ repair template with no homology to the *Actb* locus and successful NHEJ repair would lead to in-frame expression of ACTB-3xHA. By providing both repair templates simultaneously, relative pathway choice can be assessed using an HDR/NHEJ ratio (**Figure 2.12**) (Weinstock et al., 2006).

To perform the assay *in vivo*, I used *in utero* electroporation (IUE) to transfect the CRISPR-Cas9 and repair constructs into cKO-E and control embryonic cortex at E12.5. In IUE, plasmid DNA is injected through the uterus, into the lateral ventricles of the embryos, and transfected into cortical NPCs by electroporation. Analyzed at E17.5, electroporated control brains showed an HDR/NHEJ ratio of 0.87. In striking contrast,

HDR was severely impaired relative to NHEJ in electroporated cKO, which showed an HDR/NHEJ ratio of 0.31, a 64% decrease (ctrl mean - 0.87, cKO-E mean - 0.31, p = 8.1E-6, two tailed t-test, n≥4 animals, >100 immunostained cells counted per animal) (**Figure 2.12**). Therefore, DNA repair by HDR was selectively impaired compared to NHEJ in *Ino80* cKO. Although HDR uses exogenous DNA whereas HR uses sister chromatid as template, the molecular mechanisms underpinning homology-dependent repair in HDR and HR are shared. Thus, these data are consistent with a selective impairment of DNA repair by HR in *Ino80* cKO-E and with previous studies on the role of the INO80-C in HR, potentially via nucleosome remodeling or RPA/RAD51 exchange in HR.

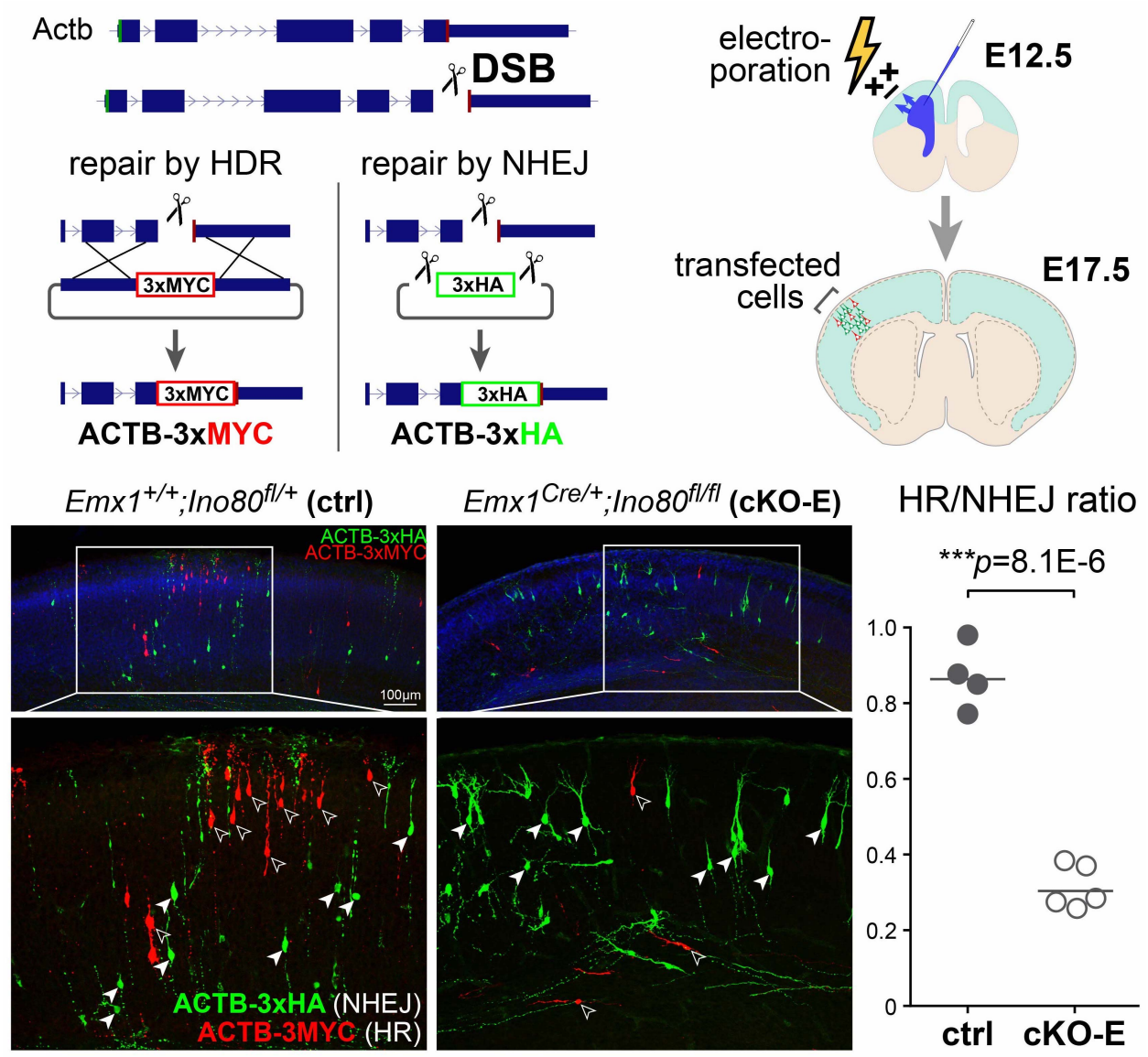

Figure 2.12: A novel DSB repair assay showed impaired HDR in *Ino80* cKO cortex

Schematic illustrating the principle of the DSB repair assay. CRISPR-Cas9 targets the C-terminal coding region of the genomic *Actb* gene and induces a DSB. Two repair templates are supplied, which use different repair mechanisms (NHEJ or HDR), resulting in molecularly distinct tagged-ACTB products. IUE of cortex at E12.5 and resultant analysis at E17.5 enabled analysis of the neurogenic period. Ctrl and cKO-E were immunostained for the NHEJ-repaired ACTB-3xHA product (filled arrowheads) and the HDR-repaired ACTB-3xMYC product (open arrowheads). Quantification of the HDR:NHEJ ratio demonstrated a dramatic decrease in the amount of HDR relative to NHEJ in the cKO-E cortex (mean, two-tailed unpaired *t* test, n≥4 animals, >100 cells counted per electroporated animal).

Impaired HR often leads to genomic instability (Moynahan and Jasin, 2010) from aberrant repair by suboptimal methods like NHEJ or Alt-EJ. One potential manifestation of this genome instability is the presence of micronuclei, DNA that is excluded from the nuclear membrane. Micronuclei can be formed in multiple ways, including impaired HR. DSBs that are aberrantly repaired via NHEJ or other methods often lead to structural variation including large CNVs or translocations. These events can create acentric chromosomal fragments lacking centromeres, which mis-segregate during mitosis and will subsequently not be incorporated into the nuclear envelope (Fenech et al., 2011). Micronuclei are difficult to visualize *in vivo*, so I cultured NPCs from control and cKO-E cortex to ascertain the presence of aberrant micronuclei. I observed micronuclei in cKO-E cells, but never visualized such abnormal events in control cells (**Figure 2.13**). As micronuclei are chromosomal fragments, distinct from the functionally intact nucleus, they do not immunostain for nuclear markers (including transcription factors) as nucleoplasm does. Here, staining for the stem cell marker SOX2 demonstrated that micronuclei were distinct from the rest of the nucleus (**Figure 2.13**).

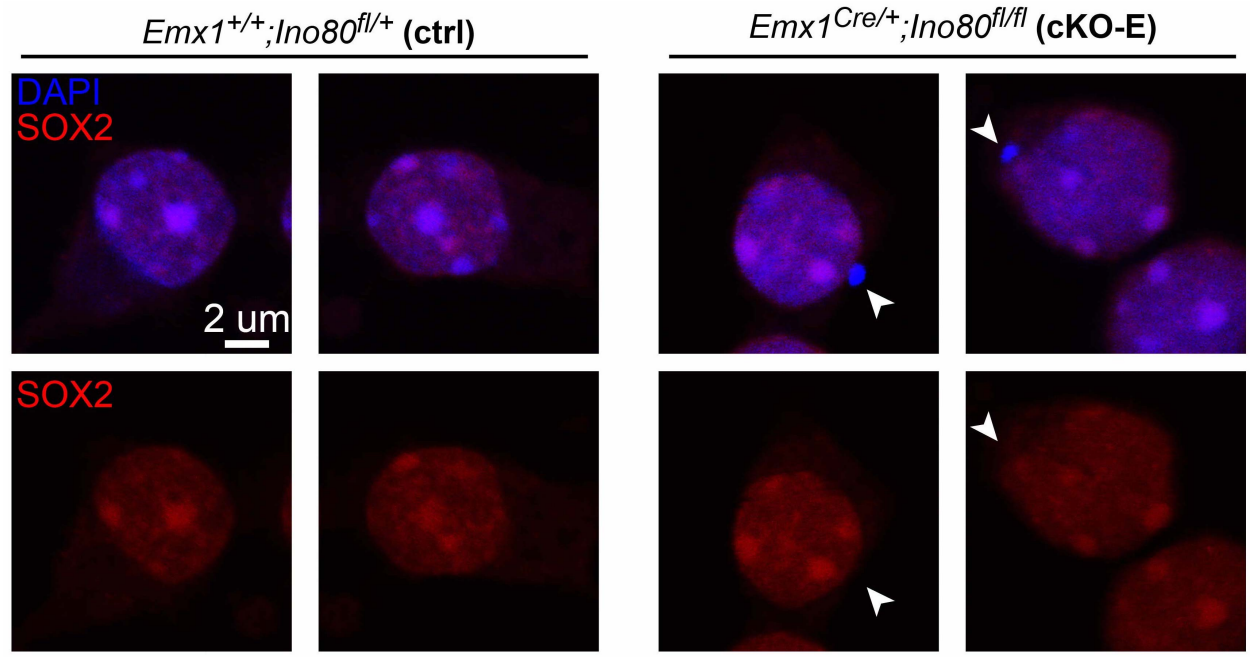

Figure 2.13: *Ino80*-deficient cells showed signs of genome instability

NPCs from cKO-E brains grown in culture demonstrated the presence of micronuclei, which were not observed in ctrl NPCs. Micronuclei were SOX2-negative (arrowheads), indicating that they were excluded from the nuclear envelope, and were likely chromosomal fragments formed during aberrant DSB repair.

HR can occur in actively cycling cells in which the sister chromatid can serve as a homologous template for repair. During development, the proportion of cycling progenitor cells within the cortex decreases with embryonic age, whereas the proportion of post-mitotic neurons increases. ENCODE RNA-seq data from E11.5, E14.5, and E18.5 CNS tissue demonstrated robust decreases in *Brca2* and *Rad51* expression during development. In contrast, NHEJ genes are expressed in a relatively constant fashion because NHEJ can function throughout the cell cycle. This importance in progenitor cells as well as post-mitotic neurons is demonstrated by stable expression of *Lig4* and *Xrcc4*. The INO80 remodeling complex is known to affect transcription in multiple cell types as well as playing an important role in HR within cycling cells. In concordance with these dual roles, the expression of *Ino80* is highest in early CNS (E11) and decreases across the course of development. This higher expression at early age and gradual slight decrease, suggests continued functionality in post-mitotic neurons, in processes other than HR (**Figure 2.14**).

As INO80 could mediate both transcription and DNA repair, I leveraged the RNA-seq data to assess the possibility that disrupted DNA repair in cKO-E resulted from abnormal expression of DNA repair genes. Analysis of E13.5 cKO-E transcriptome revealed that *Ino80* deletion did not significantly affect expression of known HR genes (e.g. *Rad51*, *Brca2*, etc) or DNA repair genes overall. Thus, the role of INO80 in HR was likely not mediated via transcriptional regulation. Together, my data suggest that following *Ino80* deletion, disruption of HR DNA repair led to an accumulation of DSBs in NPCs, thereby triggering p53, robust apoptosis, NPC loss, and medial cortex hypoplasia and disruption.

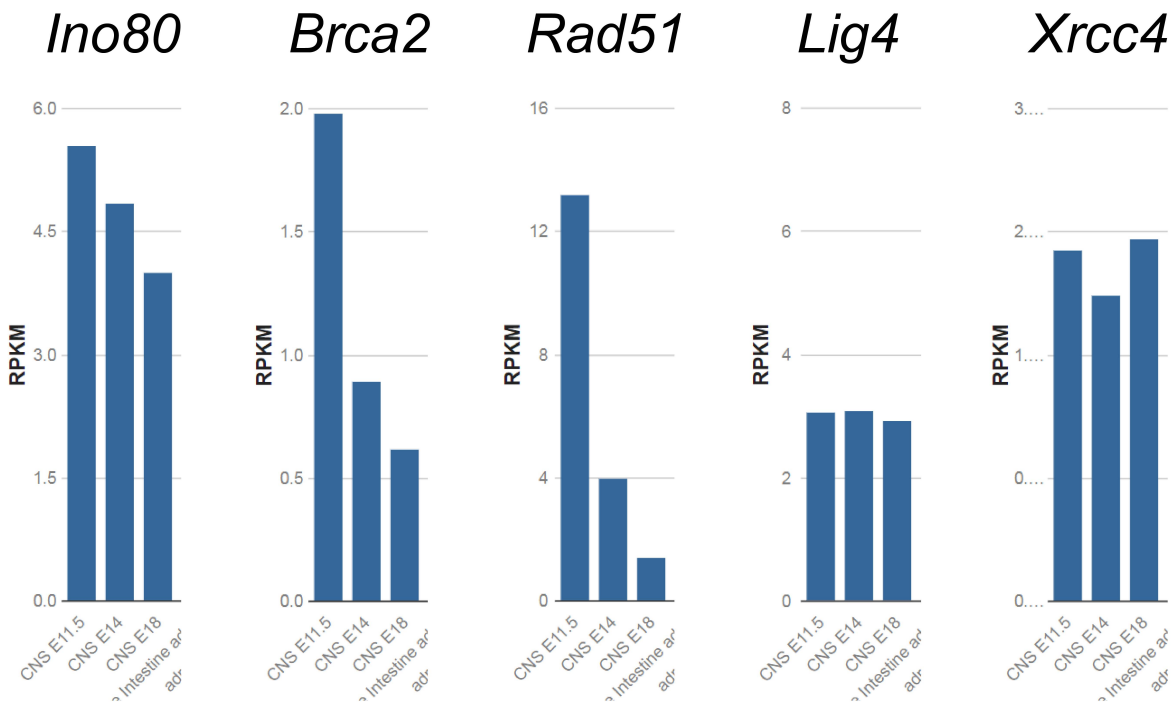

Figure 2.14: *Ino80* expression profile alluded to multiple functions in developing brain

ENCODE RNA-seq data demonstrated differing patterns of gene expression depending on molecular function. Transcriptome analysis from E11, E14, and E18 developing brain. HR genes (*Brca2*, *Rad51*) showed high expression early that decreased dramatically as the brain developed. NHEJ genes (*Lig4*, *Xrcc4*) demonstrated consistent levels of expression. *Ino80* showed a modest decrease over time, indicating that expression may be necessary for multiple processes, including DSB repair via HR as well as transcriptional regulation of gene expression.

CNS: central nervous system, RPKM: reads per kilobase million

Trp53 codeletion completely reversed Ino80 cKO-E phenotypes

Our results revealed a key role for *Ino80* in HR DNA repair in cortical NPCs. As a nucleosome remodeler, however, INO80 is positioned to regulate both gene expression and genome stability. To distinguish these aspects of INO80 function in contributing to *Ino80* cKO-E phenotypes, I simultaneously deleted *Trp53,* the mouse p53 gene, together with *Ino80* (*Emx1*^{Cre}*;Ino80*$^{fl/fl}$*;Trp53*$^{fl/fl}$, **dKO-E**). Codeletion of *Trp53* led to a strikingly complete reversal of all major *Ino80* cKO-E phenotypes. At P0, microcephaly, medial cortex hypoplasia and lamination defects, hippocampal agenesis, and callosal dysgenesis were all markedly reversed by *Trp53* codeletion in dKO-E (**Figure 2.15A and B**). At E13.5, dKO-E cortex showed no increase in apoptosis compared to control and at E15.5, no loss of SOX2+ or EOMES+ NPCs (**Figure 2.16**). This extensive rescue following *Trp53* codeletion indicated that essentially all *Ino80* cKO-E phenotypes were underpinned by the functionality of *Ino80* in DNA repair and p53-dependent responses to resulting DNA damage.

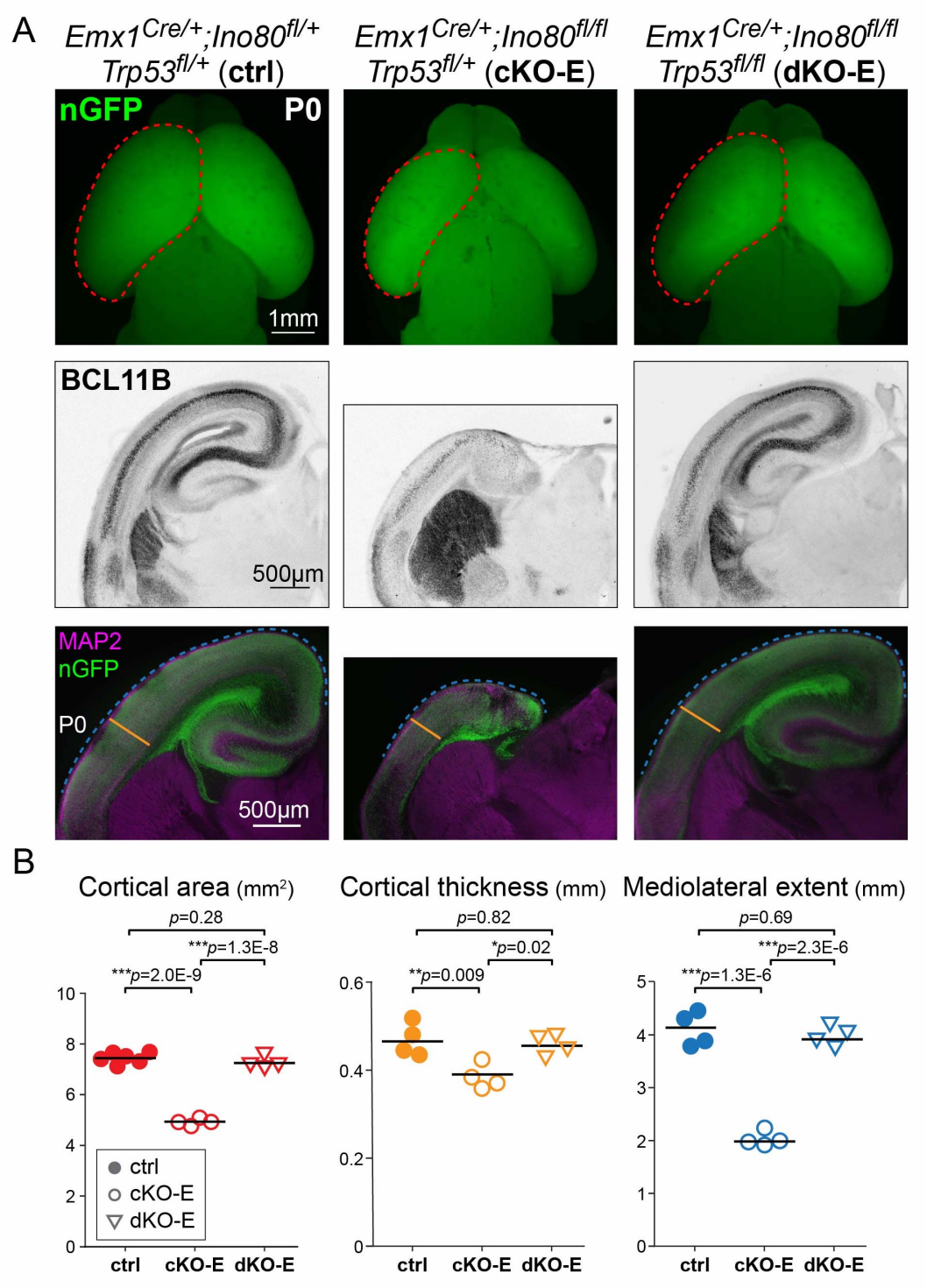

Figure 2.15: p53 co-deletion rescued the *Ino80* cKO-E microcephaly phenotype

(A) Dorsal whole mount images from ctrl, cKO-E, and dKO-E brains demonstrated a rescue of the microcephaly phenotype. Red dashed lines indicate the cortical area. Coronal sections were immunostained for BCL11B, demonstrating proper specification and development of cortex in dKO-E brains compared to ctrl. nGFP immunostaining

illustrated the extent of Cre-mediated recombination and MAP2 stains dendrites. Blue lines trace the mediolateral extent of the cortex, from laterally-specified neocortex to the midline. Orange lines indicate the thickness of the cortex, using MAP2, measured laterally to the dorsal aspect of the CPu.

(B) Cortical area (mm^2), cortical thickness (mm), and mediolateral extent (mm) of ctrl, cKO-E, and dKO-E brains. Images in (A) are representative of measurements. Cortical area (red), cortical thickness (orange), and mediolateral extent (blue) were all reduced in cKO-E, and rescued in dKO-E to ctrl levels (mean, $n \geq 4$, One-way ANOVA with Tukey post-test).

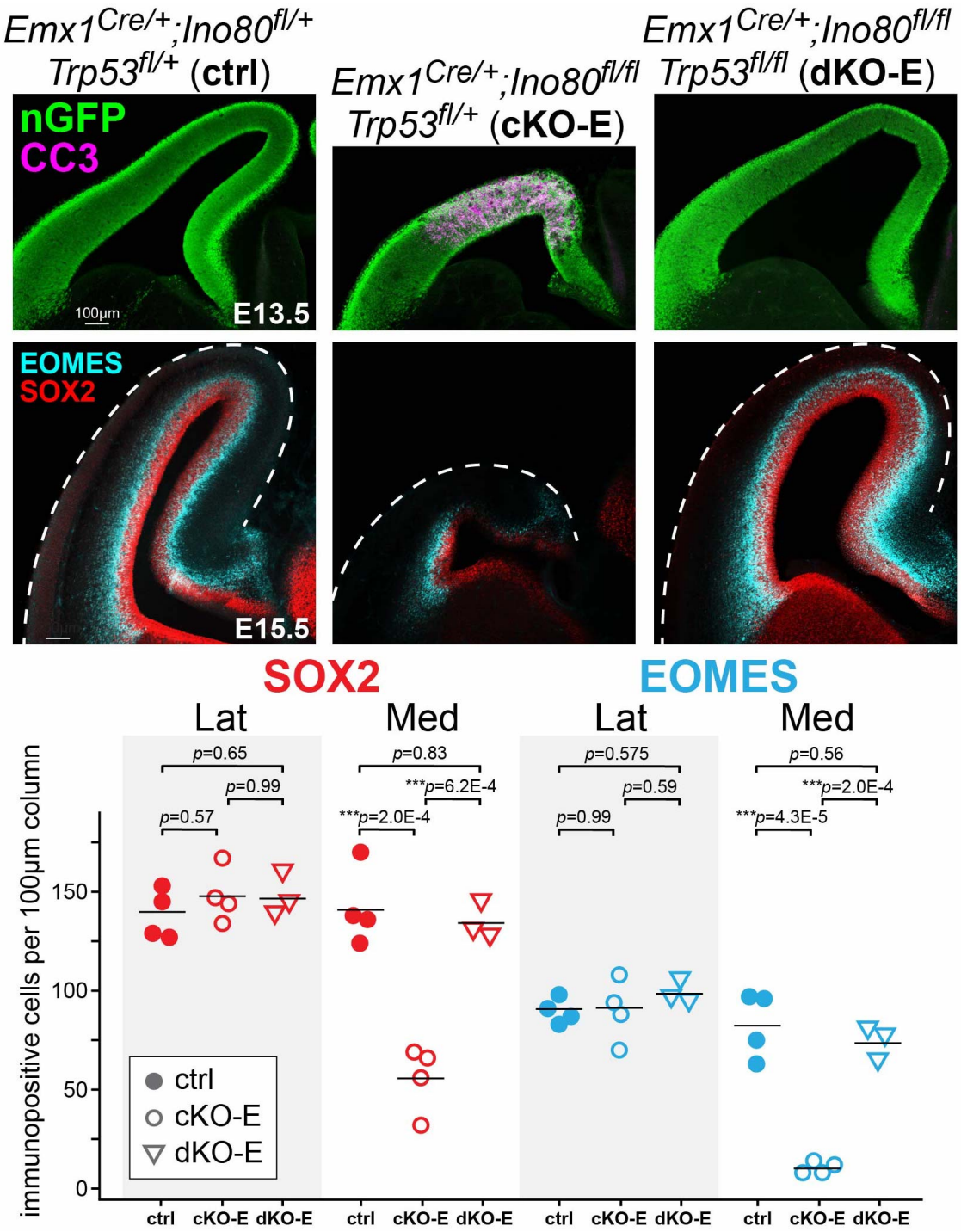

Figure 2.16: *Ino80;Trp53* dKO-E rescued embryonic cortical development

Coronal sections from E13.5 (nGFP, CC3 immunostained) and E15.5 (SOX2, EOMES immunostained) ctrl, cKO-E, and dKO-E brains. E13.5 cortex demonstrated complete rescue of the medial apoptosis phenotype. E15.5 cortex showed reversal of the NPC-loss phenotype in dKO-E compared to cKO-E via cell counts for NPC markers in 100 um cortical columns (mean, n≥3, one-way ANOVA with Tukey post-test).

Molecularly dissociable roles of INO80 in transcriptome fidelity and genome maintenance

Our transcriptome analysis of *Ino80* cKO-E revealed a clear signature of p53 target gene activation and microglia. Using the single *Ino80* cKO-E, however, potential direct transcriptional effects of INO80 could not be isolated from those related to p53 target activation. In contrast, the *Ino80*/*Trp53* dKO-E could be leveraged to identify potential primary effects of INO80 on gene expression unrelated to p53. I therefore performed UMI RNA-seq of E13.5 *Ino80*/*Trp53* dKO-E cortex (n = 7 animals) for direct comparison with cKO-E transcriptome data (**Figure 2.17A**). In single *Ino80* cKO-E cortex, the majority of upregulated genes were attributable to p53-dependent transcription and microglia. Following *Trp53* codeletion, these transcriptomic signatures were nearly completely reversed (FDR>0.001), suggesting that their increase in cKO-E was p53-dependent. In remarkable contrast, a substantial subset of the downregulated genes from cKO-E were not reversed in dKO-E, suggesting that some genes were downregulated in cKO-E independently of p53. Previous studies have shown that the transcription factor YY1 recruits INO80 to gene promoters, facilitating chromatin remodeling near gene bodies. This coactivator function enables transcriptional activation and provides gene specificity to the INO80 complex (Cai et al., 2007). I therefore performed intersection analysis with available YY1 ChIP-seq data from mouse NPCs (Mendenhall et al., 2010). This showed that, as a group, the 135 downregulated genes whose downregulation was not reversed by *Trp53* codeletion (i.e. down in *Ino80* cKO, p53-independent) were characterized by a significant YY1 peak near the TSS, a typical feature of YY1-regulated genes. In striking contrast, neither a set of 135

randomly selected genes nor the 42 *Ino80* downregulated genes whose downregulation was reversed by *Trp53* codeletion (i.e. down in *Ino80* cKO, p53-dependent), showed collective YY1-binding near the TSS or in the gene body (**Figure 2.17B**). These data showed that INO80 regulated the transcription of YY1-associated genes independently of p53, resulting in distinct molecular signatures. Thus, INO80 played mechanistically dissociable roles in gene expression and genome maintenance. Importantly, despite the persistence of YY1-associated transcriptomic dysregulation in *Ino80*;*Trp53* dKO-E, there were no overt cellular or anatomical phenotypes. These data thus provided further support that the *Ino80* cKO-E phenotypes were largely based on the role of INO80 in genome maintenance. Although INO80 functioned in YY1-regulated transcription, disruption of this gene regulatory capacity of INO80 did not significantly contribute to *Ino80* cKO-E phenotypes.

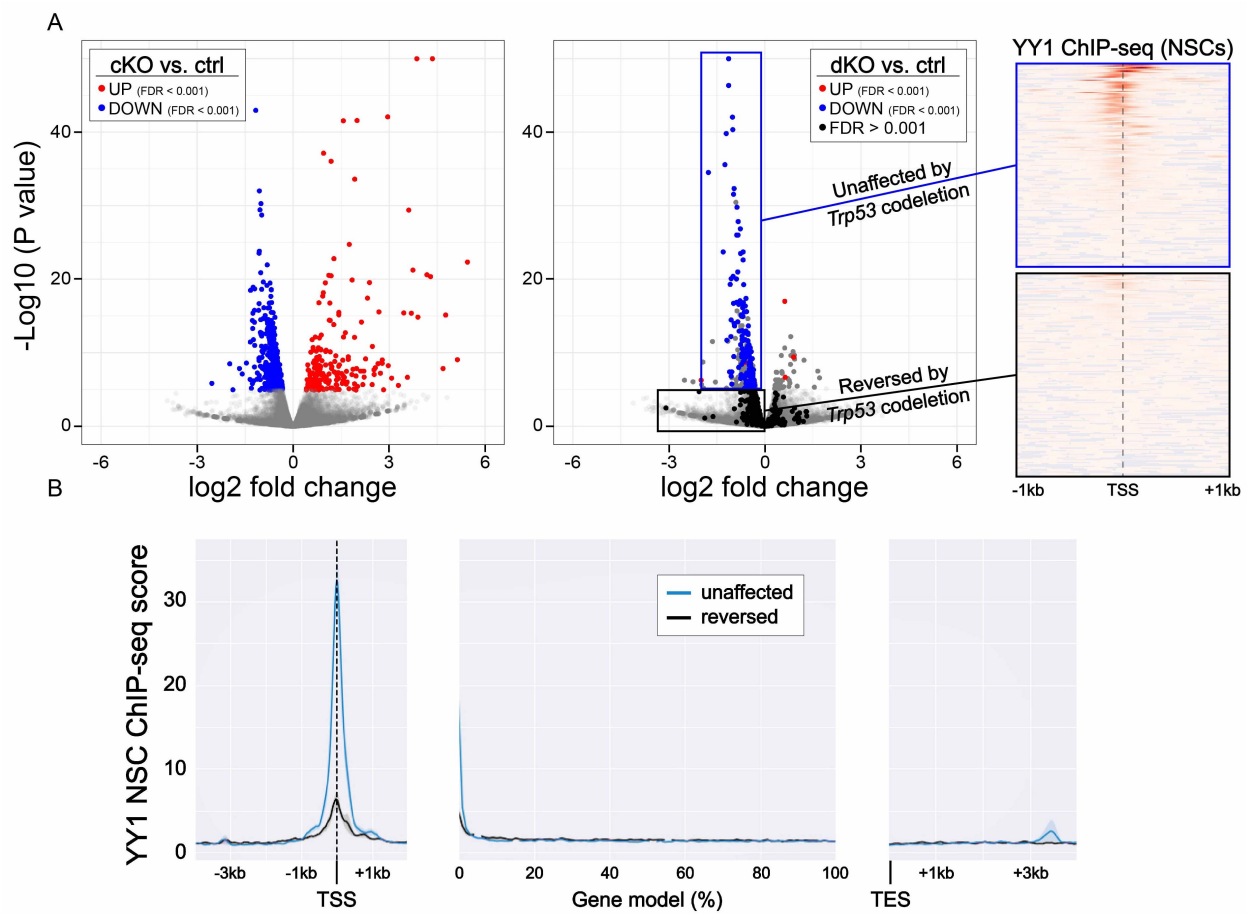

Figure 2.17: Molecularly dissociable roles of *Ino80* in cortex development

(A) Transcriptome analysis of E13.5 neocortex viewed by volcano plots of cKO vs. ctrl and dKO vs. ctrl. In the cKO vs. ctrl plot, red dots indicate genes upregulated in cKO compared to ctrl (FDR<0.001), blue dots indicate genes downregulated in cKO compared to ctrl (FDR<0.001), and gray dots indicate genes that are unchanged in cKO compared to ctrl. In the dKO vs. ctrl plot, the gene identities of the red, blue, and gray dot colors are maintained from the cKO vs. ctrl plot. If the gene maintained upregulated or downregulated status, the color was not changed. If, however, the gene was no longer significantly changed compared to ctrl, the dot representing that gene is now black. The vast majority of upregulated genes were reversed by *Trp53* deletion whereas many of the downregulated genes continued to be downregulated in dKO cortex. Genes that were persistently downregulated were enriched for genes regulated by the transcription factor YY1, a known binding partner of INO80. Published YY1 ChIP-seq data from cultured NSCs (Mendenhall et al., 2010) showed a strong peak of YY1 binding near the TSS of persistently downregulated genes, but not in the genes that were reversed by *Trp53* deletion.

(B) YY1 binding across the gene body from persistently down (unaffected) and reversed genes demonstrated a sharp peak near the TSS in unaffected genes.

Discussion

Chromatin remodelers and chromatin-modifying enzymes participate in many processes and can mediate widespread effects throughout the genome. Gene expression changes have been identified as a main functionality of many chromatin-associated complexes. However, other functions affected by these enzymes remain understudied. The chromatin remodeler INO80, the focus of my work, is implicated in repair of DSBs, but details of the importance of this process in development are limited. Aberrant DSB repair is demonstrably important in numerous neurodevelopmental syndromes, but detailed understanding of the role chromatin-mediated DSB repair plays in brain development and pathology are lacking.

I found that *INO80*, a candidate gene for microcephaly in humans, produces microcephaly in *Ino80* cKO mice from impaired HR repair of DSBs in the developing cortex. The INO80-C catalyzes nucleosome sliding and histone variant exchange to maintain genome stability and regulate gene expression. This leads to a complex developmental role in which gene expression changes and chromatin-mediated DSB repair are both dysregulated in *Ino80* mutant tissue. I molecularly dissected the genome stability and gene expression changes in *Ino80*-deficient cortex and found that altered chromatin-mediated DSB repair was responsible for the developmental phenotypes (**Figure 2.18**).

I used a conditional allele to delete *Ino80* with spatiotemporal control during cortex development. Initial analysis demonstrated that deletion in stem cells resulted in a robust microcephaly phenotype, whereas deletion in post-mitotic neurons had no observable defects. Furthermore, NPC deletion in cKO-E preferentially disrupted medial

cortical development and lateral neocortex was relatively unaffected, with appropriate laminar structure and axonal projections. These changes in postnatal cKO-E brains were interrogated using embryonic developmental analysis. I found massive apoptosis during early cortical development that led to a loss of NPCs, pathologies that were concentrated in the medial compartment and corroborated the medial defects observed in postnatal brains. To interrogate the molecular mechanisms, I utilized UMI RNA-seq from E13.5 cortex and found robust upregulation of microglial activation and p53 response to DSBs.

These analyses, however, also demonstrated a large array of genes that were altered in expression but did not correspond to signatures of microglia or p53-mediated response, indicating that transcriptional changes unrelated to DNA damage may also play a role in the aberrant development. To investigate this possibility, I made a conditional *Ino80;Trp53* dKO to ablate the cellular response to unrepaired DSBs. Strikingly, p53 co-deletion rescued the microcephaly and associated apoptotic phenotypes seen in the *Ino80* cKO. This observation led me to conclude that impaired DSB repair via HR was solely responsible for the developmental phenotypes, even though additional transcriptomic changes were present. Importantly, RNA-seq analyses of ctrl, cKO-E, and dKO-E brains enabled use of a subtractive analysis to define a set of genes that was persistently downregulated in *Ino80*-deficient cortex, and were therefore not altered as a secondary effect of p53 or cell death. These genes were highly enriched for regulation via transcription factor YY1, a known binding partner of the INO80-C. This molecular dissociation of *Ino80* roles in HR and transcriptional control demonstrated dissection of complex functionality in brain development (**Figure 2.18**).

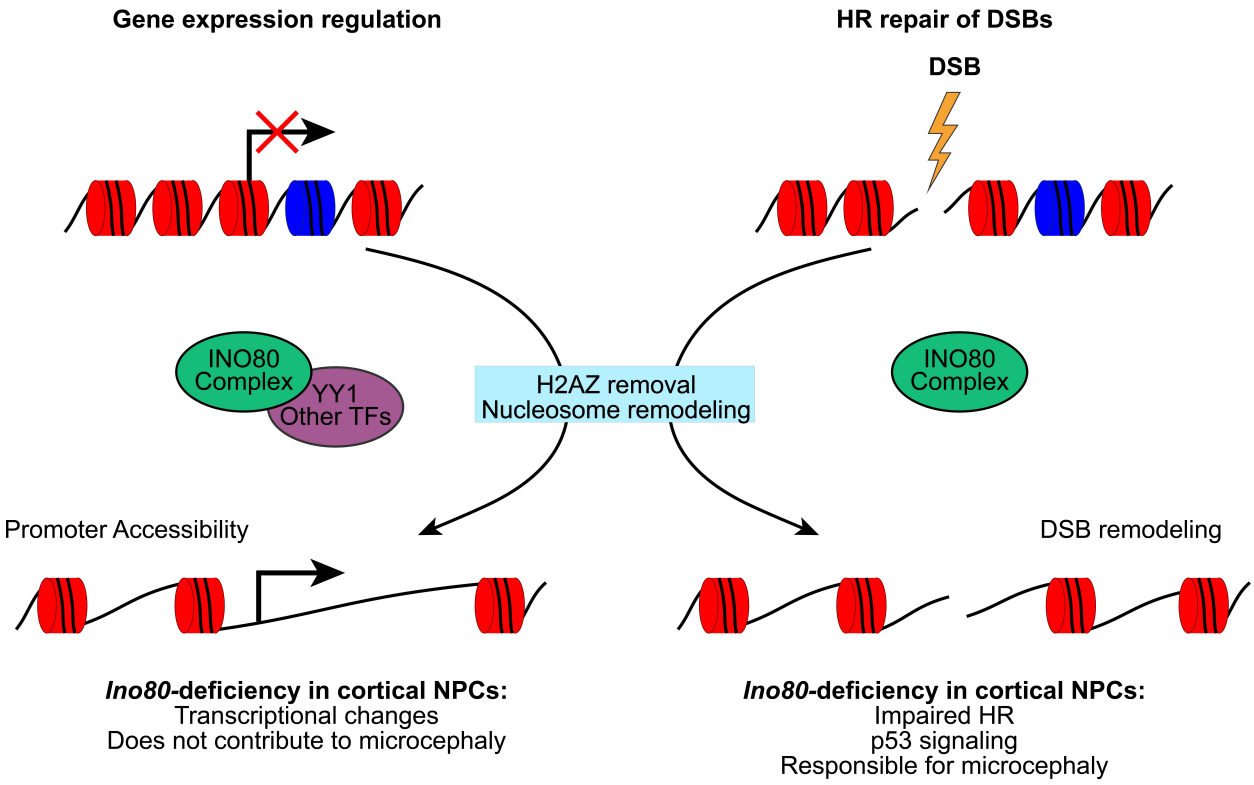

Figure 2.18: *Ino80* deletion led to impaired HR and microcephaly, independent of transcriptional changes

Ino80 cKO-E led to transcriptional changes and impaired HR, from lack of crucial chromatin remodeling necessary for each of these processes. Impaired HR led to unrepaired DSBs and apoptosis downstream of p53 signaling, causing microcephaly. However, other identified transcriptional changes (e.g., INO80/YY1-dependent transcription) did not contribute to the microcephaly phenotype.

To my knowledge, this is the first transcriptome analysis in an *Ino80*-deficient cell or organism that circumvents the confounding effect of transcriptional and cellular responses to p53 signaling. This represents a persistent problem as large numbers of genes may be highly up- or down-regulated, and can cloud interpretation of primary expression changes because of robust responses by p53 to genome damage. The cKO-E and dKO-E models, therefore, provide a powerful tool to isolate potential gene targets or binding partners. YY1 had been previously demonstrated to bind INO80-C

and some mechanistic insight into the binding and functional relationship has been elucidated (Cai et al., 2007). However, it remains unknown whether YY1 is the sole transcription factor binding partner of INO80, and therefore, deeper analysis may yield additional insights into transcriptional regulation by INO80-C.

I have not excluded the possibility that direct gene expression changes in *Ino80*-deficiency affect neural function. My current analyses focused on neurodevelopment within the scope of neuron generation, migration, specification, and axonal tract development. Further analyses are warranted to investigate synapse connectivity, circuitry development, and potential behavioral effects. It is conceivable that *Ino80* deficiency during NPC division or in post-mitotic neurons may disrupt proper neuronal function or circuit development. Correlating circuit or behavioral phenotypic results with expression changes in cKO-E mice would likely be unreliable from microcephaly present in the knockout animals. However, cKO-N mice, with *Ino80* deleted from post-mitotic neurons, and dKO-E mice, with *Ino80* deleted from NPCs (but protected from microcephalic development by p53 deletion), would provide excellent models to interrogate postnatal transcriptional changes, circuitry development, and behavioral effects in morphologically intact brains.

Investigations of suspected DNA damage allowed me to pinpoint unrepaired DSBs as pathogenic in this model. To investigate INO80-C in chromatin-mediated DSB repair, I developed a novel assay using CRISPR-Cas9 and molecularly distinct repair templates used *in utero* in developing cortex. This repair assay demonstrated a dramatic relative reduction in HR, implicating *Ino80* in the complex chromatin-mediated processing of DSBs for proper repair via HR. Since some NPCs survive *Ino80* deletion

and continue to proliferate, this raises interesting questions about how DSBs may be repaired in the context of impaired HR. Other routes for repair, namely c-NHEJ and Alt-EJ, may be used, but are suboptimal due to their inherently mutagenic repair mechanisms.

Despite the robust cell death in the medial neocortex in cKO-E brains, I observed very few p53-positive or dying cells in the lateral neocortex. This striking spatial boundary in sensitivity to *Ino80* deletion does not align with any known neuroanatomical borders. Available transcriptomic resources demonstrate widespread expression in all tissues examined and *in situ* hybridization data from other groups suggests low, but consistent, expression in E14.5 cortical VZ. These points argue against the possibility that *Ino80* expression differs across the mediolateral gradient. If *Ino80* expression is constant among these dividing cell populations, it raises an intriguing possibility that differences in usage of HR underlies the observed differences in cellular sensitivity.

Conclusion

Regulation of chromatin drives many cellular processes and has been implicated in disease, particularly neurodevelopmental disorders. How genetic mutations in chromatin regulators lead to such disease must be investigated individually, because of the varied functions of each particular complex. Here, I investigated the role of the INO80 chromatin remodeling complex in cortex development. Despite robust changes in gene expression in *Ino80*-deficient cortex, I found that the observed microcephaly and developmental defects were a result of impaired DSB repair. To further investigate, I developed a novel assay to test for NHEJ- or HDR-based repair in the developing brain. *Ino80*-deficient cortex displayed dramatically decreased ability to repair breaks using

HR, and massive cellular apoptosis occurred following p53 stabilization and signaling. Using an *Ino80;Trp53* dKO mouse, I demonstrated complete rescue of the phenotype, showing that the microcephaly was dependent on p53 signaling as a result of impaired HR following *Ino80* deletion. These mouse models also enabled the identification of potential primary transcriptional targets of the INO80-C, without confounding transcriptional changes associated with p53 and apoptosis. Many genes that were persistently downregulated shared a gene signature for the transcription factor YY1. These analyses demonstrated that the transcriptional and genome stability mechanisms of INO80-C were molecularly dissociable, and that INO80-mediated HR was critical for cortical development.

Materials and Methods

Mice and mouse husbandry

All mice were maintained on a C57BL/6 background with standard 12 hour day:night cycle with *ad libitum* access to food and water. Copulation plugs were used to determine mating, with noon of the day with visualized plug designated as E0.5 for timed pregnancy identification. Transgenic mice are listed in **Table 2.1**. Genomic DNA was isolated from toe or tail clips and genotyping was performed using DreamTaq Green 2x Master Mix (Thermo Fisher) with oligos listed in **Table 2.2**. All procedures were approved by the University of Michigan IACUC.

Immunostaining

Brains were dissected and fixed in 4% PFA in PBS at 4°C with agitation overnight. Brains were embedded in 4% low-melting agarose and sectioned using a

Leica Vibratome (VT1000S or VT1200S). Some antigens benefit from antigen retrieval in pH 6.1 citrate buffer (Dako, Agilent) at 70°C for 30 minutes (as noted in **Table 2.3**). Sections were then incubated for 1 hour at room temperature in blocking solution consisting of 5% Donkey Serum, 1% BSA, 0.1% glycine, 0.1% lysine and 0.3% Triton X-100. Primary antibodies (**Table 2.3**) were added to blocking solution and incubated with free-floating sections overnight at 4°C with agitation. Sections were washed 3 X 5 minutes in PBS and incubated with fluorescently-linked secondary antibodies (**Table 2.4**) and DAPI, diluted in blocking solution, for 1 hour at RT. Fluorescently-linked primary antibodies were used for immunostaining with multiple primary antibodies raised in the same species. In these cases, fluorescently-linked primaries were diluted in blocking solution and incubated at RT for 1 hour after the secondary antibody incubation. Sections were affixed to slides and allowed to dry, before mounting with VECTASHIELD mounting media (Vector Laboratories). For sections with endogenous fluorescent reporters (nT-nG or EYFP), 100 mM HCl was added to VECTASHIELD to decrease the pH to roughly 6, which reduced the epifluorescence and allowed immunostaining in multiple fluorescent channels.

EdU/CldU incorporation and visualization

EdU or CldU was given by intraperitoneal injection at the indicated time before sacrifice at a final concentration of 5 ug per gram or 50 ug per gram, respectively. Following dissection, brains were fixed in 4% PFA in PBS overnight, embedded in agarose and sectioned using a vibratome (VT1000S or VT1200S) at 70 micron thickness. For EdU staining, sections were permeabilized by incubation for 30 minutes in 0.5% Triton X-100 in PBS followed by 3 X 5 minute washes in PBS. EdU staining

solution was made fresh each time, containing 100 mM Tris, 4 mM CuSO4, and 100 mM ascorbic acid diluted in 1X PBS. The fluorescently-labeled azide molecule was added last and the staining cocktail was immediately added to sections for a 30 minute incubation at room temperature (final concentrations of each fluorescent molecule: 4 mM AlexaFluor488-Azide, 10 mM Cy3-Azide, 16 mM AlexaFluor647-Azide). After incubation, sections were washed 3 X 5 minutes in PBS. After EdU labeling, standard protocols were followed for immunostaining.

For staining of incorporated CldU, sections were treated with 1 M HCl for 15 minutes at 37°C followed by re-hydration and neutralization with 3 X 15 minute washes in PBS. Sections were permeabilized and blocked in 0.3% Triton X-100 in normal donkey serum for 1 hour at RT followed by addition of anti-CldU antibody (Accurate Chemical YSRTMCA2060GA, 1:500). For staining of EdU- and CldU-containing brains, EdU labeling was completed first followed by HCl treatment and subsequent overnight antibody incubation.

DSB Repair Assay

A gRNA sequence targeting the c-terminus of the Actb coding sequence (5'-AGTCCGCCTAGAAGCACTTG) was cloned into eSpCas9Opt1.1, a vector expressing enhanced-specificity Cas9 molecule and an optimized gRNA scaffold. To construct Actb_NHEJ_3xHA, tandem HA tag sequences were cloned between two Actb gRNA recognition sequences in the same orientation. This orientation is reversed from that in the genome, which prevented re-cutting of properly NHEJ-repaired genomes. Actb_HDR_3xMyc was constructed by cloning tandem Myc tags between 800 bp homology arms of the c-terminal Actb gene (Yao et al., 2017). The previously targeted

Actb_gRNA sequence was altered at 7 base pairs in the HDR-repairable template, to prevent cleavage of the repair template or subsequent re-cutting after HDR-mediated repair. Timed-pregnant dams were anesthetized using Ketamine at 100 mg/kg and Xylazine at 10 mg/kg given by intraperitoneal injection. Mice were also given carprofen at 5 mg/kg via subcutaneous injection for analgesia. A midline incision was made through skin and abdominal muscle to expose the uterine horns. Ring forceps were used to gently maneuver both uterine horns from the body cavity of the dam. A pulled micropipette was loaded with plasmid DNA solution and injection was controlled using a World Precision Instruments Micro4 MicroSyringe Pump Controller. The micropipette was inserted into the fluid-filled lateral ventricle through the uterus, amniotic sac, skull and cortex of the embryo. Injection solutions were composed of eSpCas9opt1.1-Actb_gRNA, Actb_NHEJ_3xHA, Actb_HDR_3xMyc, and CAG-Lifeact3xBFP, to visualize successful electroporation of the brains. Each plasmid was present at 1 ug/ul in the final solution, along with 0.1% Fast Green FCF to visualize the solution during intraventricular injection. Following injection of plasmid solutions, electroporation paddles were positioned on opposing sides of the ventricle and 4 - 5 pulses of 27 volts (45 milliseconds each) were delivered, with 950 milliseconds between pulses in a unipolar fashion. Pulses were delivered using a BTX Harvard Apparatus ECM 830 power supply. In utero electroporations were performed on E12.5 embryos and brains were isolated 5 days later. Following serial sectioning, BFP-positive sections were isolated and immunostained using anti-HA (Sigma-Aldrich 11867423001, 1:250) and anti-Myc (Absolute Antibody Ab00100-22.0, 1:1000) antibodies. Sections were imaged using an Olympus SZX16 dissecting scope and counts of HA-positive and Myc-positive

neurons were completed in multiple sections from each embryo. For each electroporated animal, at least 100 positively-labeled cells were counted to determine a ratio of NHEJ:HDR repair.

RNA isolation

E13.5 embryos were isolated and immediately submerged in ice-cold PBS. Neocortical tissue was dissected and flash-frozen in a dry ice-ethanol bath and stored at -80°C until further processing. Tissue was resuspended in 0.5 mL Trizol and homogenized using metal beads in a bullet blender. Chloroform was added to sample and the aqueous phase was isolated following centrifugation for 15 minutes at >20000g at 4°C. The sample was transferred to a Zymo Research Zymo-Spin IC column and was processed following the manufacturer's protocols, including on-column DNA digestion. Pure RNA was eluted in DNase/RNase-free water and quantified using a Qubit fluorometer.

Click-seq

Libraries for RNA-seq were generated from 600 ng of RNA following a previously published Click-Seq protocol (Routh et al., 2015). In brief, ribosomal RNA was removed from total RNA using NEBNext rRNA Depletion Kit (NEB). ERCC RNA spike-in was included for library quality assessment (Thermo Fisher). Superscript II (Thermo Fisher) was used for reverse transcription with 1:30 5 mM AzdNTP:dNTP and 3' Genomic Adapter-6N RT primer (GTGACTGGAGTTCAGACGTGTGCTCTTCCGATCT NNNNNN). RNaseH treatment was used to remove RNA template and DNA was purified with DNA Clean and Concentrator Kit (Zymo Research). Azido-terminated cDNA was combined with the click adaptor oligo

(/5Hexynyl/NNNNNNNNAGATCGGAAGAGCGTCGTGTAGGGAAAGAGTGTAGATCTC GGTGGTCGCCGTATCATT) and click reaction was catalyzed by addition of ascorbic acid and Cu2+, with subsequent purification with DNA Clean and Concentrator Kit. Amplification of the library was accomplished using the Illumina universal primer (AATGATACGGCGACCACCGAG) and Illumina indexing primer (CAAGCAGAAGACGGCATACGAGATNNNNNNGTGACTGGAGTTCAGACGTGT) and manufacturer's protocols from the 2x One Taq Hot Start Mastermix (NEB). To preference amplification products larger than 200 bp, PCR products were purified using Ampure XP (Beckman) magnetic beads at 1.25x ratio. Libraries were analyzed on TapeStation (Agilent) for appropriate quality and distribution and were sequenced at the University of Michigan sequencing core on the Illumina NextSeq 550 platform (75 cycle, high output).

RNA-seq analysis

RNA-seq data were subject to quality control check using FastQC v0.11.5 (https://www.bioinformatics.babraham.ac.uk/projects/download.html#fastqc). Adapters were trimmed using cutadapt version 1.13 (http://cutadapt.readthedocs.io/en/stable/guide.html). Processed reads were aligned to the GENCODE GRCm38/mm10 reference genome (https://www.gencodegenes.org/mouse_releases/current.html) with STAR (v2.5.2a) (Dobin et al., 2013) and deduplicated according to UMI using UMI-tools (v0.5.3) (Smith et al., 2017). Read counts were obtained with htseq-count (v0.6.1p1) with intersection-nonempty mode (Anders et al., 2015). Differential expression was determined with edgeR (Robinson et al., 2010). The *p*-value was calculated with likelihood ratio tests

and the adjusted *p*-value for multiple testing was calculated using the Benjamini-Hochberg procedure, which controls false discovery rate (FDR).

Droplet digital PCR (ddPCR)

500 ng of RNA was reverse transcribed to cDNA using Superscript II (Thermo Fisher). Diluted cDNA was used as template for ddPCR analysis of individual gene products. Reactions were composed of 2X ddPCR Supermix (no dUTP), cDNA template, and primer/probe sets (IDT) targeting individual genes identified in the unbiased RNA-seq analysis. Gene target probes were labeled with FAM, whereas *Srp72* was used as a housekeeping gene, with a HEX-labeled probe. Primer and probe sequences are listed in **Table 2.5**. Reaction mixtures were partitioned into thousands of small reactions using the QX200 droplet generator (Bio-Rad) and subjected to thermocycling. Droplets were analyzed in the QX200 droplet reader (Bio-Rad), where the number of FAM- and HEX-positive droplets in each reaction allowed for calculation of relative gene expression.

NPC single cell isolation and culture

Cortical hemispheres were dissected from E13.5 embryos and incubated in PPD solution (Papain, Dispase, DNaseI) at 37°C for 30 minutes, with trituration every 10 minutes to disrupt cell clumps into single cells. Single cells were resuspended in Neurobasal media supplemented with B27 lacking Vitamin A, GlutaMAX, sodium pyruvate, pen-strep, and 10 ng/mL bFGF. Cells were seeded on ornithine- and laminin-coated coverslips at 5000 cells per well in a 24-well plate. Cells were fixed for 15 minutes in 4% PFA in PBS at 4°C following 24 hours of culture.

Imaging

Whole mount and early postnatal brain images were taken on an Olympus SZX16 dissecting scope with Olympus U-HGLGPS fluorescent source. Q-Capture Pro 7 software was used to operate a Q-Imaging Retiga 6000 camera. Confocal images were obtained using an Olympus Fluoview FV1000 confocal microscope utilizing Olympus FV10-ASW software.

Statistical analysis

Statistical calculations were performed in GraphPad Prism (7 or 8). Values were compared using a two-tailed, unpaired Student's *t*-test or one-way ANOVA with Tukey post-test. A p-value <0.05 was considered statistically significant.

Image processing and analysis

Images were exported as TIFF files and processed in Adobe Photoshop. Counts and measurements were performed in Photoshop or using ImageJ software.

Acknowledgements

I owe many thanks to the following people. Nitesh Mohan, Stephen Harvey, and Nikita Khan completed critical work like genotyping, sectioning, and immunostaining. Mandy Lam performed Click-seq library preparation on cortical RNA samples. Adel Qalieh built the pipeline for RNA-seq quantification, produced figures related to the RNA-seq studies, and performed the YY1 ChIP-seq analysis. Dr. Lei Shi contributed a great deal of knowledge regarding analysis of microcephaly and genome instability. Dan Doyle and Owen Funk assisted in running bioinformatics analyses. The Tg(Lmx1a-Cre) mouse line was generated and provided by Kathleen Millen and Parthiv Haldipur facilitated this

transfer. Finally, all members of the Kwan lab have provided thoughtful analysis and input about scientific questions, figure organization, and technical support.

Table 2.1: Mice used in this study.

Mouse	Description	ID	Citation
B6.129(C3)-*Ino80*$^{tm1.1Jland}$/J *Ino80*^{fl}	Floxed exons 2-4 of *Ino80*	JAX# 027920	(Qiu et al., 2016)
B6.129P2-*Gt(ROSA)26Sor*$^{tm1(DTA)Lky}$/J *ROSA*^{DTA}	Cre-dependent expression of *DTA* at ROSA26 locus	JAX# 009669	(Voehringer et al., 2008)
B6N.129S6-*Gt(ROSA)26Sor*$^{tm1(CAG-tdTomato*,-EGFP*)Ees}$/J *ROSA*$^{nT-nG}$	Cre-dependent switch from *nTdTomato* to *nEGFP*	JAX# 023537	(Prigge et al., 2013)
B6.129X1-*Gt(ROSA)26Sor*$^{tm1(EYFP)Cos}$/J *ROSA*^{EYFP}	Cre-dependent expression of *EYFP* at ROSA26 locus	JAX# 006148	(Srinivas et al., 2001)
B6.129P2-*Trp53*^{tm1Brn}/J *p53*^{fl}	Floxed exons 2-10 of *Trp53*	JAX# 008462	(Marino et al., 2000)
B6.129S2-*Emx1*$^{tm1(cre)Krj}$/J *Emx1*$^{IRES-Cre}$	Knock-in of *Cre* to *Emx1* locus driven by IRES	JAX# 005628	(Gorski et al., 2002)
Neurod6$^{tm1(cre)Kan}$ *Neurod6*^{Cre}	Knock-in of *Cre* to *Neurod6* locus	MGI# 2668659	(Goebbels et al., 2006)
Tg(Lmx1a-cre)1Kjmi *Tg(Lmx1a-Cre)*	Transgenic line with *Lmx1a* promoter driving *Cre*	MGI# 4359769	(Chizhikov et al., 2006)

Table 2.2: Oligos used for genotyping mice in this study.

Gene Target	Oligo Name	Sequence (5' - 3')	Notes
Cre	Cre-F	TCGATGCAACGAGTGATGAG	Detects all Cre lines tested 500 bp
	Cre-R	TTCGGCTATACGTAACAGGG	
Ino80^{fl}	Ino80-F	GCACTTCCTGGTTTTGCTGT	WT = 290 bp Floxed = 350 bp
	Ino80-R	CACTGACTGGCGTGTTCAGA	
Ino80^{fl}	Ino80-P1	CTGGATGTGAAGGGAGAAGG	WT = 416 bp Floxed = 482 bp (-) allele = 352 bp
	Ino80-P2	CATCTCTCCAGCCAGCACACT	
	Ino80-P3	TGCCACTCTACCTGCATCTG	
DTA	DTA-F	CGACCTGCAGGTCCTCG	650 bp
	DTA-R	CTCGAGTTTGTCCAATTATGTCAC	
EYFP	EYFP-F	AGGGCGAGGAGCTGTTCA	384 bp
	EYFP-R	TGAAGTCGATGCCCTTCAG	
p53^{fl}	p53-F	GGTTAAACCCAGCTTGACCA	WT = 270 bp Floxed = 390 bp
	p53-R	GGAGGCAGAGACAGTTGGAG	

Table 2.3: Primary antibodies used in this study

Primary Antibody	Company and product number	Dilution	Notes
Chicken anti-MAP2	Novus Biologicals NB300-213	1:2000	
Rabbit anti-GFP	Thermo Fisher A-11122	1:250	
Chicken anti-GFP	Abcam ab13970	1:2000	
Rabbit anti-LHX2	EMD Millipore ABE1402	1:2000	
Rat anti-BCL11B	Abcam ab18465	1:500	
Mouse anti-TLE4	Santa Cruz Biotechnology sc-365406	1:250	
Rat anti-L1-CAM	EMD Millipore MAB5272	1:500	
Rat anti-EOMES	Thermo Fisher 14-4875-80	1:500	
Rabbit anti-SOX2	Millipore/Chemicon AB5603	1:2000	
Goat anti-SOX2	Santa Cruz Biotechnology sc-17320	1:250	
Rabbit anti-CC3	Cell Signaling 9661S	1:500	
Rabbit anti-CC3-Alexa555	Cell Signaling 9604S	1:100	Alexa555-labeled
Rabbit anti-pHH3-Alexa647	Cell Signaling 3458S	1:400	Alexa647-labeled
Rabbit anti-TRP53	Leica P53-CM5P-L	1:500	
Rat anti-F4/80	Abcam ab6640	1:500	
Rabbit anti-pKAP1	Bethyl Laboratories A300-767A	1:200	
Rat anti-HA	Sigma-Aldrich 11867423001	1:250	
Hamster anti-Myc	Absolute Antibody Ab00100-22.0	1:1000	
Rabbit anti-γH2AX	Cell Signaling 9718S	1:250	
Anti-BrdU (CldU)	Accurate Chemical YSRTMCA2060GA	1:500	HCl pre-treatment

Table 2.4: Fluorescently-linked secondary antibodies used in this study.

Secondary Antibody	Company	Dilution
AlexaFluor 488 AffiniPure Donkey anti-Rabbit IgG (H+L)	Jackson ImmunoResearch Labs	1:250
AlexaFluor 488 AffiniPure Donkey anti-Rat IgG (H+L)	Jackson ImmunoResearch Labs	1:250
AlexaFluor 488 AffiniPure Donkey anti-Goat IgG (H+L)	Jackson ImmunoResearch Labs	1:250
AlexaFluor 594 AffiniPure Donkey anti-Mouse IgG (H+L)	Jackson ImmunoResearch Labs	1:250
Cy3 AffiniPure Donkey anti-Rabbit IgG (H+L)	Jackson ImmunoResearch Labs	1:250
Cy3 AffiniPure Donkey anti-Rat IgG (H+L)	Jackson ImmunoResearch Labs	1:250
AlexaFluor 647 AffiniPure Donkey anti-Goat IgG (H+L)	Jackson ImmunoResearch Labs	1:250
AlexaFluor 647 Affinipure Donkey anti-Rabbit IgG (H+L)	Jackson ImmunoResearch Labs	1:250
AlexaFluor 647 Affinipure Donkey anti-Rat IgG (H+L)	Jackson ImmunoResearch Labs	1:250
AlexaFluor 647 Affinipure Donkey anti-Chicken IgG (H+L)	Jackson ImmunoResearch Labs	1:250

Table 2.5: Primers and probe sequences used in ddPCR analyses.

Gene	Primer_1 (5' - 3')	Primer_2 (5' - 3')	Probe (5' - 3')
Eda2r	GCATCTACCTTCA CTAAGCTCA	GTTCTACCGAAAG ACACGCAT	/56-FAM/TGCATCCCA /Zen/TGTACAAAGCAGACTCC/3IABkFQ/
Pvt1	GCCACTGCCAATG TCTGT	CACTGAAAACAAG GACCGAAAC	/56-FAM/TCCAGGTAG /Zen/CCCGAGAGATGACA/3IABkFQ/
Ano3	CGAAGAAAACTGT CCCTCCAT	GTCTTCATGTGTCC TCTATGTGA	/56-FAM/AGCTGTCGT /Zen/TGAGTCTCTGCAGTG/3IABkFQ/
Ino80	CTCTCATACTCTG CACTTCTGTC	GCTACCTCCTCACT TCGTTG	/56-FAM/CTGCGGTGA /ZEN/CTCGTGGACTGG/3IABkFQ/
Srp72	CTCTCCTCATCATA GTCGTCCT	CTGAAGGAGCTTT ATGGACAAGT	/5HEX/CCAAGCACT /Zen/CATCGTAGCGTTCCA/3IABkFQ/

Chapter 3: Symmetric and asymmetric NPC divisions differ in requirement for homologous recombination

Abstract

Cortical neurons are generated by two distinct modes of divisions. Early NPCs begin by dividing symmetrically, thereby exponentially expanding the number of NPCs with each division. To produce neurons, NPCs transition to an asymmetric type of division, producing one post-mitotic neuron and regenerating one NPC. Here, I found that symmetric divisions and asymmetric divisions have differing requirements for DSB repair. Conditional deletion of *Ino80*, a chromatin remodeler necessary for HR, using multiple Cre-driver lines demonstrated that symmetric divisions strictly require HR whereas asymmetric, neurogenic divisions can continue neuron production even with impaired HR. Confirmation of these developmental phenotypes using conditional deletion of a *bona fide* HR gene, *Brca2*, demonstrated that this observation was generalizable to multiple components of the HR machinery and not confined to chromatin remodeling at the DSB.

Introduction

The neocortex is a highly ordered structure made via a complex series of developmental processes to generate a six-layered neocortex with multiple subtypes of neurons and complicated circuitry. During early corticogenesis, NPCs called apical radial glia (aRG) divide in a symmetric fashion, with each division giving rise to two daughter aRG cells. The multipotent pool of NPCs that results from this symmetric

expansion then transitions to asymmetric division, where a cell divides giving rise to one post-mitotic cortical neuron and re-generates one daughter cell into an aRG. This daughter aRG then continues to divide in an asymmetric fashion, iteratively giving rise to additional cortical neurons that will migrate to the cortical plate and develop connections appropriate for their location and identity.

This description of cortex development forms the basis for the radial unit hypothesis, which describes the brain as a collection of ontogenetic columns containing post-mitotic neurons that originated from single progenitor cells. Understanding the transitions and differences between the symmetric and asymmetric modes of NPC division is crucial for a complete picture of cortical development. Generally, the number of symmetric divisions dictates the surface area of the cortex, since each additional progenitor gives rise to an additional ontogenetic column of post-mitotic cells. In contrast, the number of asymmetric divisions of each NPC determines the thickness of the cortex, as each post-mitotic neuron born from a progenitor will populate the column from that progenitor and increase the cortex in a radial direction. Changes in the timing and ratio of these modes of division have dramatic effects on the resulting brain. For instance, the human neocortex has a surface area of roughly 1900 cm^2 (Schnack et al., 2015), about 1000X greater than that of a mouse (Rakic, 1995). Cortical thickness, however, varies by less than 2-fold. Human cortical thickness ranges between 1 and 4.5 mm, with an average around 2.5 mm (Fischl and Dale, 2000). Mouse cortex varies slightly, but is between 1.5 and 2 mm (Fenlon et al., 2015). The hugely disparate ratios of thickness and surface area between the species indicate that humans have greatly expanded the number of progenitors, through symmetric divisions, whereas the number

of asymmetric divisions of each individual progenitor has increased by a much more modest margin.

Each symmetric division of the neural progenitor pool doubles the potential number of neurons that can be produced. The exponential nature of these symmetric divisions can dramatically increase the number of cortical minicolumns that can be produced (Rakic, 1988), thereby altering the surface area of the resultant cortex. Each additional asymmetric division only generates one additional neuron per column and would produce a thicker cortex, but only increases the cortical neuron total in a linear fashion. Each of these types of cell division has important consequences for cortex development. Therefore, understanding these two modes of NPC division has dramatic importance for a complete picture of the development of the human brain, both in physiologic and disordered states.

Regulation of the transition from symmetric to asymmetric NPC divisions is driven by a number of known factors. Chief among these is the Notch pathway, which relies on cell-cell signaling via Delta-like ligand 1 (Dll1) to activate transmembrane Notch receptors. Receptor activation triggers a cleavage event that liberates the Notch intracellular domain (NICD) that then translocates to the nucleus to alter transcription of a wide array of genes. In NPCs, Notch primarily activates pro-stem cell genes to maintain the expression profile of a symmetrically dividing cell. Inhibition or loss of Notch signaling disrupts the process and leads to acquisition of pro-neural gene expression and subsequent asymmetric, neurogenic division. Notch1 has been described as mediating this process in the cortex (Chenn and McConnell, 1995; Rash et al., 2011; Yang et al., 2004), however, the Notch family has multiple members that are

expressed in the brain. Notch1 and Notch3 have similar functionality, and show redundant signaling in cortex (Dang et al., 2006) and striatum (Mason et al., 2005). Another mechanism relies on the symmetric or asymmetric inheritance of cellular and apical membrane contents based on the orientation of the cleavage plane between dividing cells. Cells dividing with perpendicular cleavage plane to the ventricle will both retain apical contact to the ventricle and inherit receptors that allow for continuation of stem cell behavior. In divisions with orientations other than 90-degrees, asymmetric segregation of membrane and receptors will predispose one daughter to shed the stem cell identity and become a post-mitotic neuron. Multiple players including mPar3 (Bultje et al., 2009), Numb (Zhong et al., 1996), and Notch1 (Chenn and McConnell, 1995) participate in this process.

In mouse, the transition from symmetric to asymmetric division begins around E11 and gradually shifts to all cells dividing asymmetrically towards the end of the neurogenic period (Haydar et al., 2003). Importantly for this discussion, neurogenesis through asymmetric divisions is not induced throughout the cortex simultaneously. Rather, neurogenesis begins in the rostrolateral region of the cortex and sweeps in a caudomedial direction towards the midline. This is called the transverse neurogenetic gradient (TNG) and is a common feature of corticogenesis in mammals including rodents, ferrets, and humans (Hicks and D'Amato, 1968; McSherry and Smart, 1986; Takahashi et al., 1999).

As the neurogenic gradient progresses and cells switch from symmetric to asymmetric divisions, there are also pronounced changes in molecular and cellular behavior. Notch signaling decreases, which leads to downregulation of pro-stem genes

(*Hes1, Hes3, Hes5*) (Kageyama et al., 2007) and increases expression of pro-neural genes (*Ngn1, Ngn2, Mash1, Math1, Tis21*) (Bertrand et al., 2002; Iacopetti et al., 1999). These gene expression programs along with changes in chromatin marks (Albert et al., 2017) alter the behavior of the cell and enable the production of neurons. A notable change following this cellular transition is an alteration in cell cycle parameters. In mice, symmetrically dividing aRG progress through the cell cycle in 22.4 hours. In asymmetrically dividing aRG, this time decreases substantially to 15.8 hours. Importantly, this reduction in cycle time is driven completely by a reduction in the length of S-phase. The length of the total cell cycle with the exception of S-phase (Tc-Ts) is roughly 14 hours in each population, demonstrating a dramatic decrease in S-phase length from 8.3 hours in symmetrically dividing NPCs to 1.8 hours in asymmetrically dividing NPCs (Arai et al., 2011). This decrease in S-phase as cells progress to neurogenic fates has also been observed in ferrets (Reillo and Borrell, 2012; Turrero García et al., 2016). And though primate cortical development is more difficult to study due to experimental constraints and more complex hierarchies of neuron generation, variability in cell cycle and particularly in S-phase is a consistent observation (Betizeau et al., 2013; Kornack and Rakic, 1998).

In addition to proliferative differences, NPCs in different modes of division also show differential sensitivity to stress. It has been observed in multiple systems that early NPC divisions are more susceptible to DNA damage than later NPC divisions. This has been observed in genetic deletion of *Brca1* (Pulvers and Huttner, 2009), important in the early steps of HR, and *TopBP1* (Lee et al., 2012), a topoisomerase that functions in DNA replication. Additionally, this is not only observed in genetic models of impaired

DNA repair, but is also seen in wild-type brain exposed to DSB-causing radiation at different developmental timepoints (Lee et al., 2012). This indicates a fundamental difference in the tolerance of different NPCs for DNA damage. Despite these consistent findings, a molecular understanding of the timing involved with these events as well as the cellular processes driving this differential susceptibility remain to be fully understood (McKinnon, 2013).

Here, I report that the requirement for HR repair of DSBs differs dramatically between these two modes of NPC divisions: symmetrically dividing NPCs are exquisitely sensitive to impairment of HR, whereas later neurogenic cell divisions are relatively unaffected by loss of HR. In Chapter 2, I investigated the function of *Ino80* in the developing cortex and determined that it was a critical component of chromatin-mediated HR repair in NPCs. Using multiple Cre driver lines with spatiotemporal expression differences, I deleted *Ino80* at differing developmental timepoints to investigate the necessity for HR in symmetric and asymmetric NPCs. I found that impaired HR led to massive cellular apoptosis in symmetrically dividing NPCs, but did not cause apoptosis in asymmetrically dividing, neurogenic NPCs. I further validated this observation using a conditional allele of *Brca2*, a known HR gene, demonstrating that these observations are generalizable to the process of HR, and not restricted to chromatin-mediated processing of DSBs.

Results

Ino80 cKO-E phenotypic severity spatiotemporally correlates with symmetric NPC-NPC divisions

Our analyses of embryonic apoptosis and NPC loss, and postnatal cortical lamination in cKO-E consistently showed a markedly higher sensitivity of medial cortex to *Ino80* deletion compared to lateral cortex. Normally, from approximately E10.5 to E13.5, NPCs in wild-type cortex gradually transition from symmetric self-renewing NPC-NPC divisions to asymmetric neurogenic NPC-neuron divisions. Importantly, this transition does not occur simultaneously in NPCs throughout the cortex, and the spatial gradient in the timing of this transition could contribute to the mediolateral difference in sensitivity to *Ino80* deletion in cKO-E.

Previous studies have suggested that lateral cortex transitions to asymmetric divisions earlier than medial cortex following a transverse neurogenetic gradient (rostrolateral first, caudomedial last). To ascertain this, I analyzed NPCs and neurons in medial versus lateral wild-type cortex at E12.5, when the first cohort of cortical excitatory neurons have been generated and some have migrated into the cortical plate (CP). At this stage, the thickness of the SOX2+ NPC-containing ventricular zone (VZ) was not significantly different between medial and lateral cortex (**Figure 3.1A**). However, the lateral cortex was characterized by a more developed CP that contained several layers of RBFOX3+ (NeuN+) neurons in thickness. In contrast, the medial CP was significantly thinner and contained only a single layer of RBFOX3+ neurons. The TNG was also directly visualized by immunostaining for NEUROG2 (also called NGN2), a pro-neural gene expressed by NPCs during neurogenic divisions. In wild-type E11.5

cortex, a large majority of NPCs were NEUROG2- (data not shown), consistent with symmetric NPC-NPC divisions at this age. From E12.5 to E15.5, the wild-type cortex was characterized by an increase in number of NEUROG2+ NPCs following a lateral first, medial last gradient (**Figure 3.1C**). Notably, at E12.5 and E13.5, a transition zone delineated NEUROG2-positive and NEUROG2-negative neocortex along the mediolateral axis (red arrowheads). By E15.5, the entire mediolateral extent of the wild-type cortex showed high NEUROG2 expression, consistent with largely asymmetric, neurogenic divisions at this age. My data thus confirmed that neurogenesis occurred with a lateral to medial gradient, with lateral NPCs entering asymmetric NPC-neuron divisions earlier than medial NPCs.

At E12.5 and E13.5, *Ino80* cKO-E showed a marked increase in apoptotic markers in medial but not lateral cortex (**Figure 3.1C**). Strikingly, the border of medial apoptotic and lateral non-apoptotic cells in cKO-E aligned with the NEUROG2+/NEUROG2- transition zone present in wild-type cortex at these ages, suggesting that the mode of NPC division may be associated with NPC sensitivity to *Ino80* deletion. To determine whether apoptosis persisted throughout neurogenesis and through transition into asymmetric NPC-neuron divisions, I analyzed the cKO-E cortex at E15.5, an age when NPCs have largely transitioned to asymmetric neurogenic divisions. Remarkably, cKO-E showed no persistent apoptosis at E15.5. An essential absence of apoptosis suggested that the remaining NPCs were no longer sensitive to *Ino80* deletion. Together, these data support that NPC sensitivity to *Ino80* deletion is spatiotemporally associated with the mode of NPC division. Near the onset of *Ino80* deletion in cKO-E, the severely-affected medial NPCs were largely undergoing

symmetric NPC-NPC divisions, whereas the mildly-affected lateral NPCs had begun to transition to asymmetric NPC-neuron divisions (**Figure 3.1B**). By mid-neurogenesis, NPCs had largely transitioned to asymmetric neurogenic division and were no longer undergoing apoptosis in cKO-E.

To investigate the rostrocaudal extent of the disordered development, I analyzed the dorsal view of whole mount brains from P0 mice. The TNG moves in a rostrolateral-to-caudomedial direction (**Figure 3.2A**). Ctrl and cKO-E brains demonstrate drastically different phenotypes, with the cKO-E brain deficient in medial cortex and hippocampal formation. Superimposition of the cortical area of ctrl brain on the cKO-E brain shows the area that is most affected by *Ino80* deletion lies along the midline and extends throughout the rostrocaudal axis (**Figure 3.2B**). This pattern of medial defect supports the hypothesis that symmetric divisions are selectively susceptible to impaired HR.

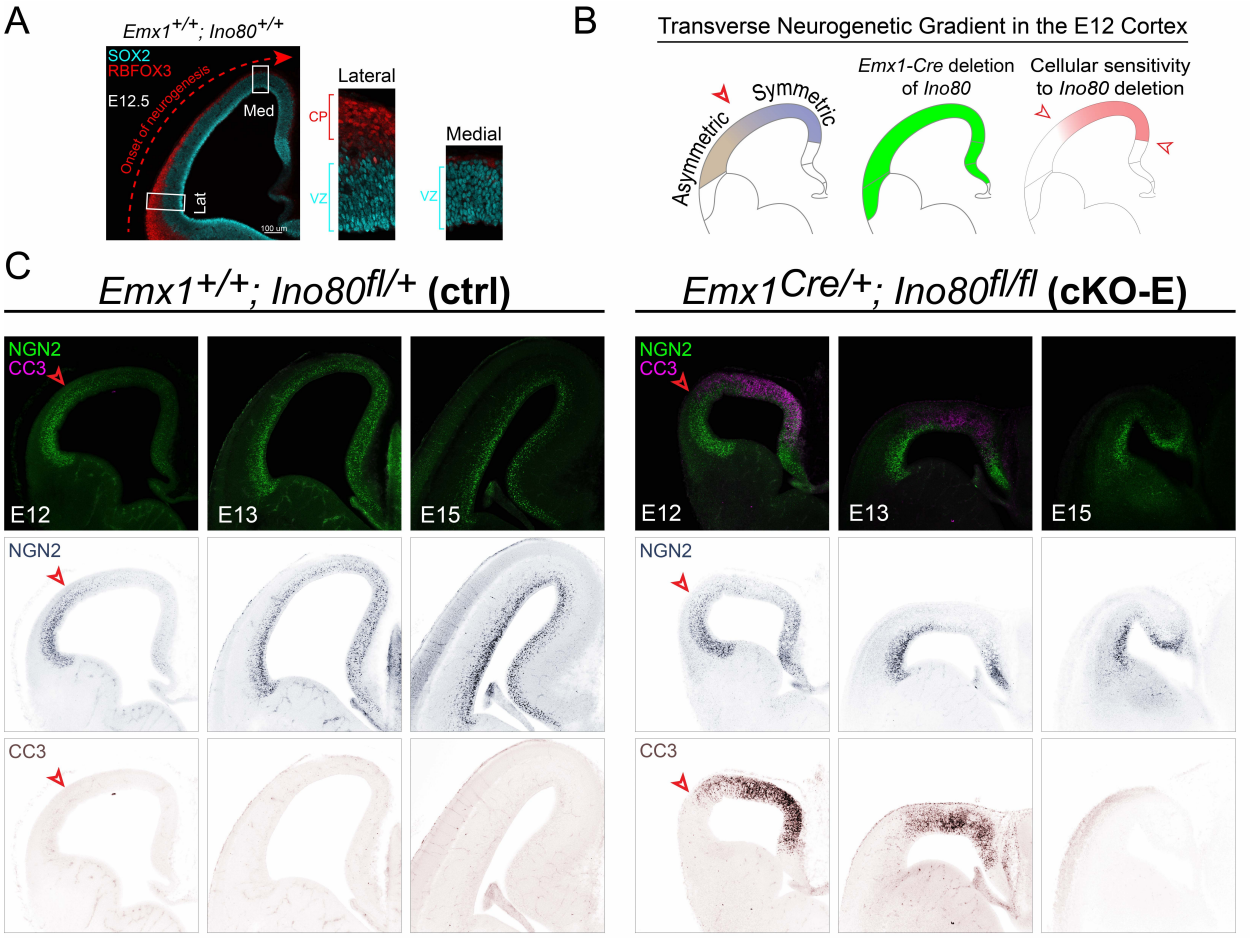

Figure 3.1: Regions of symmetrically dividing NPCs had high cell death in cKO-E

(A) Immunostaining in E12.5 cortex for stem cell marker (SOX2) and post-mitotic neuron marker (RBFOX3) showed the cortical plate developed laterally before medially. Red arrow indicates the direction that neurogenesis proceeds, along the transverse neurogenetic gradient.

(B) Schematic showing the population of symmetric and asymmetric divisions at E12.5 in the transverse neurogenetic gradient. *Emx1*^{Cre} mediates deletion throughout the entire neocortex, though *Ino80* deletion only leads to cellular apoptosis in the medial compartment of the cortex, corresponding to symmetrically dividing cells.

(C) Ctrl and cKO-E brains immunostained for NGN2, a marker of neurogenic stem cells, and CC3, a marker of apoptosis. At E12.5, the advancing frontier of neurogenic stem cells is visible progressing along the TNG (red arrowheads). In cKO-E brains, robust apoptosis occurs in medial, symmetrically dividing NPCs at E12.5 and E13.5, but not in lateral cortex where cells are neurogenic. E15.5 ctrl and cKO-E brains have NGN2+ cells throughout the mediolateral extent of the cortex. No apoptosis was observed in cKO-E brains, as most cells have transitioned to asymmetric division by E15.5.

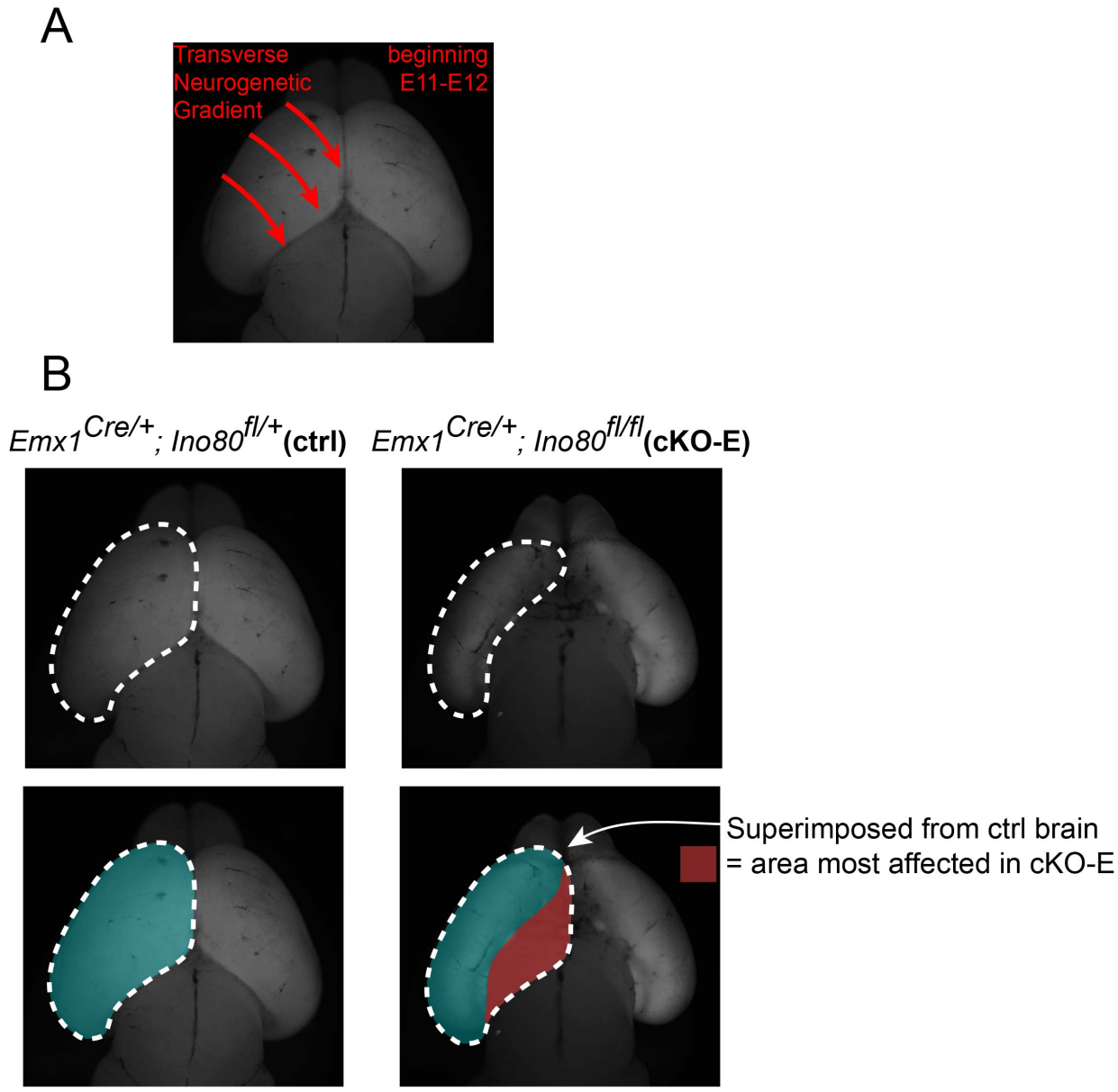

Figure 3.2: The most affected regions of the cKO-E brain correlated with the TNG

(A) Schematic showing the rostrolateral-to-caudomedial direction of the transverse neurogenetic gradient projected on a P0 brain. Neurogenic divisions to produce post-mitotic neurons occur first in the lateral aspect of the brain and follow the general direction of the arrows.

(B) (Top panel) Ctrl and cKO-E P0 brains with tracing of cortical area. (Bottom panel) The same brain images are each overlaid with a cortical tracing of the ctrl brain (cyan). The red portion is the most susceptible region to Ino80-deficiency in cKO-E brain. This portion of cortex along the rostrocaudal gradient transitions latest to asymmetric divisions.

In addition, I investigated the proliferation of cells in the medial and lateral cortex by a 1 hour pulse of EdU pre-sacrifice at each of these ages (**Figure 3.3**). At E12.5, many cells in control and cKO-E brains were dividing in both medial and lateral neocortex. In E13.5 and E15.5 cKO-E brains, medial cortex had few dividing cells due to apoptotic loss of NPCs. However, E13.5 and E15.5 cKO-E brains continued to have robust NPC proliferation in lateral neocortex, where NPCs have largely transitioned to asymmetric, neurogenic division. Additionally, E15.5 cKO-E cortex did not show apoptotic cells, even in medial cortex, indicating that the cells dividing medially in E15.5 brains were no longer sensitive to *Ino80*-deficiency at an age when most NPCs have transitioned to asymmetric division. These data further support the finding that NPC sensitivity to *Ino80* deletion is spatiotemporally associated with the mode of NPC division; symmetric NPC-NPC divisions are much more sensitive to *Ino80* deletion compared to asymmetric NPC-neuron divisions.

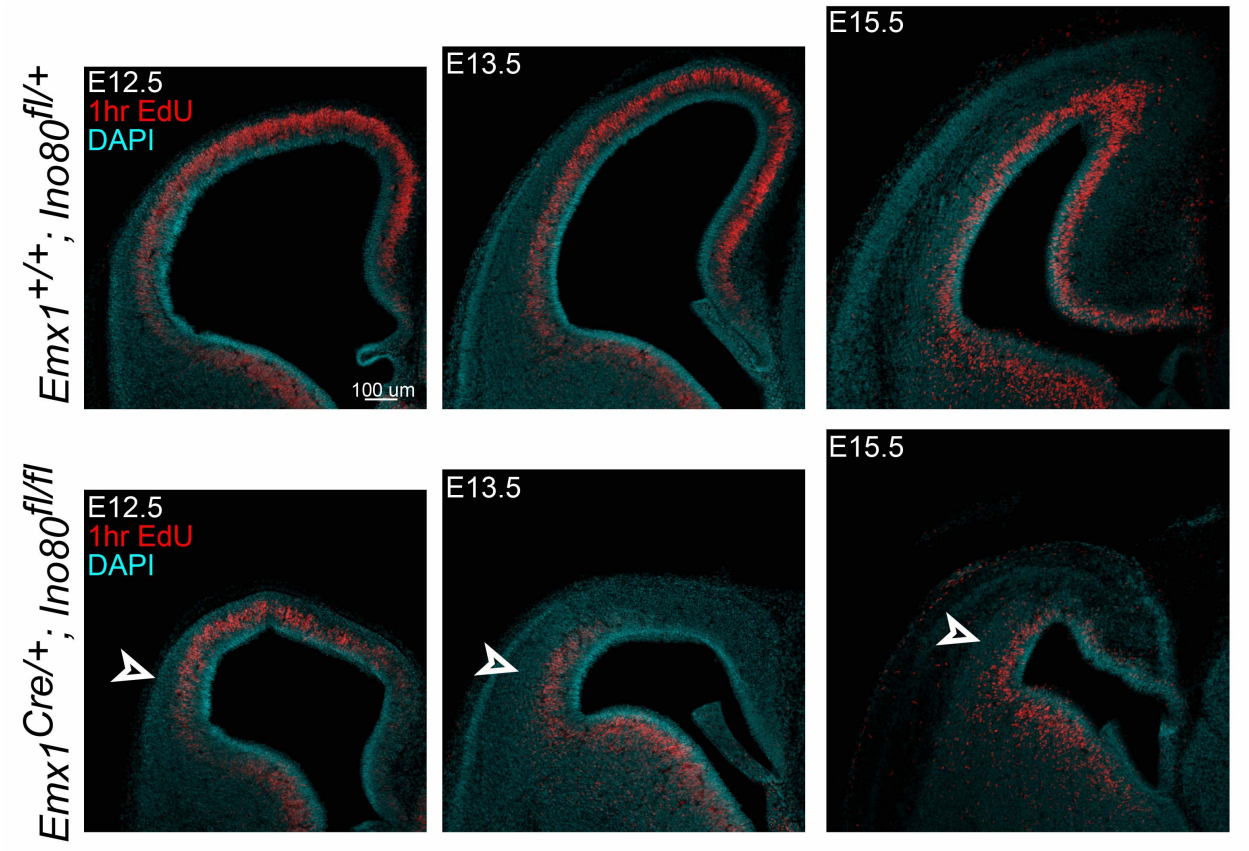

Figure 3.3: NPC division continued following *Ino80* deletion

EdU was administered to pregnant dams 1 hour before sacrifice to label S-phase cells in E12.5, E13.5, and E15.5 ctrl and cKO-E brains. cKO-E brains showed diminished EdU-labeling in medial neocortex from loss of stem cells. Despite deletion of *Ino80* throughout the extent of the cortex, lateral cortex maintains a robust stem cell population and continues to proliferate throughout corticogenesis (open arrowheads).

Early Ino80 deletion during exclusive symmetric NPC-NPC divisions led to cortical agenesis

To directly assess the possibility that symmetric NPC-NPC divisions are much more sensitive to *Ino80* deletion, I generated an *Ino80* cKO using *Foxg1*^{Cre} (*Foxg1*^{Cre};*Ino80*$^{fl/fl}$, **cKO-F**). *Foxg1*^{Cre} mediates floxed gene deletion from embryonic forebrain starting at E8.5 (Hébert and McConnell, 2000), at an early developmental stage when NPCs divisions are exclusively symmetric NPC-NPC, and several days prior to transition into asymmetric NPC-neuron divisions (**Figure 3.4A**). Remarkably, *Foxg1*^{Cre} deletion of *Ino80* led to widespread apoptosis throughout the entire mediolateral extent of the cKO-F cortex at E11.5 (**Figure 3.4B**). Therefore, at a stage when both medial and lateral NPCs were undergoing symmetric NPC-NPC divisions, they were equally sensitive to *Ino80* deletion. This extensive apoptosis manifested postnatally as complete forebrain agenesis (**Figure 3.4C**). To ascertain that cKO-F phenotypes were associated with loss of INO80-mediated DNA repair, I analyzed by immunostaining γH2AX and p53. Both markers of DNA damage were markedly increased in cKO-F at E11.5, throughout the mediolateral extent of the developing cortex (**Figure 3.5A**). To determine whether the remarkable forebrain agenesis phenotype in cKO-F was p53-dependent, I generated *Foxg1*^{Cre};*Ino80*$^{fl/fl}$;*Trp53* $^{fl/fl}$ (**dKO-F**). The dKO-F brain was characterized by a near complete reversal of cKO-F phenotypes (**Figure 3.5B**). Thus, the cortical agenesis of cKO-F was underpinned by p53 activation, and at this earlier stage also, INO80 function in DNA repair was a key driver of cKO phenotypes. Together, these data indicated that the spatiotemporal difference in phenotypic severity in the *Emx1*^{Cre} cKO-E was underlain by a difference in

mode of NPC division and that symmetric NPC-NPC divisions were highly sensitive to *Ino80* deletion.

To assess the effects of *Ino80* deletion following transition into asymmetric neurogenic division mode, I generated and analyzed an *Ino80* cKO using Tg(*hGFAP-Cre*) (Tg(*hGFAP-Cre*);*Ino80*$^{fl/fl}$, **cKO-hG**). Tg(*hGFAP-Cre*)-mediated gene deletion starts at E12.5 and is extended throughout the embryonic cortex at E13.5, a stage when the majority of NPCs have transitioned to asymmetric NPC-neuron divisions. At E15.5, the cKO-hG showed no increase in apoptosis or DNA damage (**Figure 3.4B**). Furthermore, at P0, the cortex was similar in size to control and had normal lamination and hippocampal development (**Figure 3.4C**). Therefore, after NPCs have largely transitioned into asymmetric divisions, they were no longer sensitive to *Ino80* deletion. Together, these data converge on a selective requirement for INO80-dependent HR DNA repair in symmetric NPC-NPC divisions.

To ensure that *Tg(hGFAP-Cre)* was effectively catalyzing recombination in the intended cells, I used the *ROSA*^{DTA} suicide gene to ablate the lineage of cells. This model caused a dramatic cortical developmental phenotype, and was starkly different than the *Ino80* cKO-hG (**Figure 3.6**).

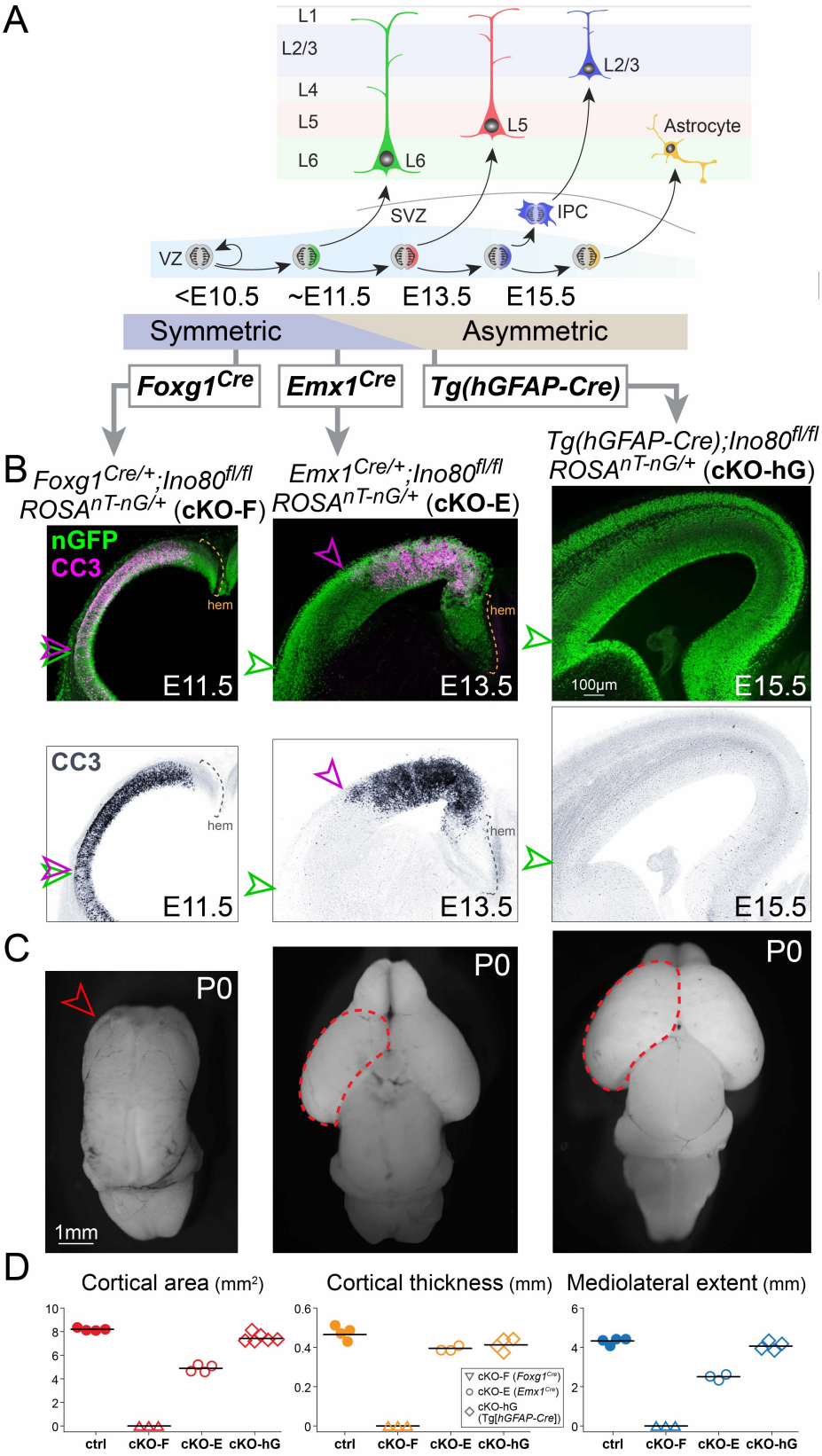

Figure 3.4: *Ino80* deletion phenotype varied by mode of NPC division

(A) Cortical development diagram illustrating the developmental timepoints when each Cre line is expressed in NPCs. *Foxg1^{Cre}* turns on around E8.5 when cell divisions are exclusively symmetric. *Emx1^{Cre}* is expressed around E10.5 near the transition between symmetric and asymmetric divisions, therefore deleting *Ino80* from NPCs undergoing both different modes of division, with a mediolateral differentiation. Tg*(hGFAP-Cre)* is expressed starting on E12.5, with full cortical deletion by E13.5, when most cells have transitioned to asymmetric division.

(B) Immunostaining of nGFP from Cre-dependent *ROSA^{nT-nG}* allele and CC3 in cKO-F, cKO-E, and cKO-hG. Each cKO model was evaluated three days after Cre becomes active in the cortex: E11.5, E13.5, and E15.5, respectively. The lateral aspect of the neocortex is indicated in each section (green arrowhead), and the mediolateral extent of apoptotic cells is indicated by the purple arrowhead. Deletion in symmetric NPCs (*Foxg1^{Cre})* caused apoptosis throughout the forebrain. Deletion via *Emx1^{Cre}* produced a sharp border of apoptotic cells in the mid-neocortex. Deletion in asymmetric NPCs (*Tg(hGFAP-Cre*)) demonstrated few apoptotic cells.

(C) Dorsal view of P0 cKO-F, cKO-E, and cKO-hG brains. cKO-F deletion, during expansive, symmetric divisions caused agenesis of the forebrain. cKO-E brains exhibit microcephaly with severe medial defects. cKO-hG brains are similar in size and shape to control brains.

(D) Quantification of cortical area, cortical thickness, and mediolateral extent showed dramatic reductions in cKO-F and cKO-E, but little difference in cKO-hG compared to control.

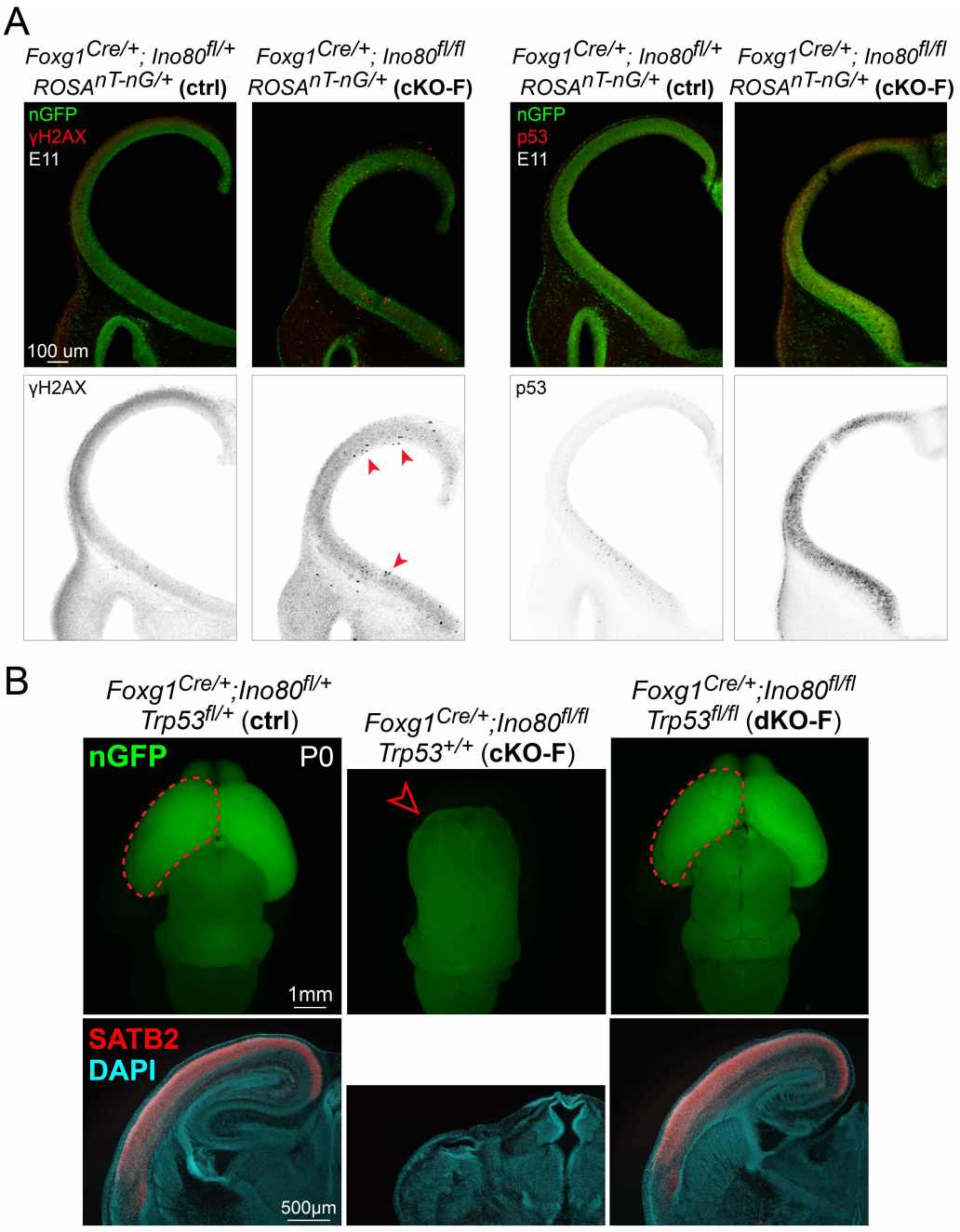

Figure 3.5: *Ino80* deletion during symmetric division caused p53-dependent forebrain agenesis

(A) cKO-F at E11.5 had elevated γH2AX and p53 staining, indicating that *Ino80* deletion impacted genome stability in early, symmetrically dividing cells.

(B) Co-deletion of *Ino80* and *Trp53* with *Foxg1*^{Cre} led to a substantial rescue of the forebrain development phenotype. SATB2 staining demonstrated that upper layer neurons were generated and properly specified.

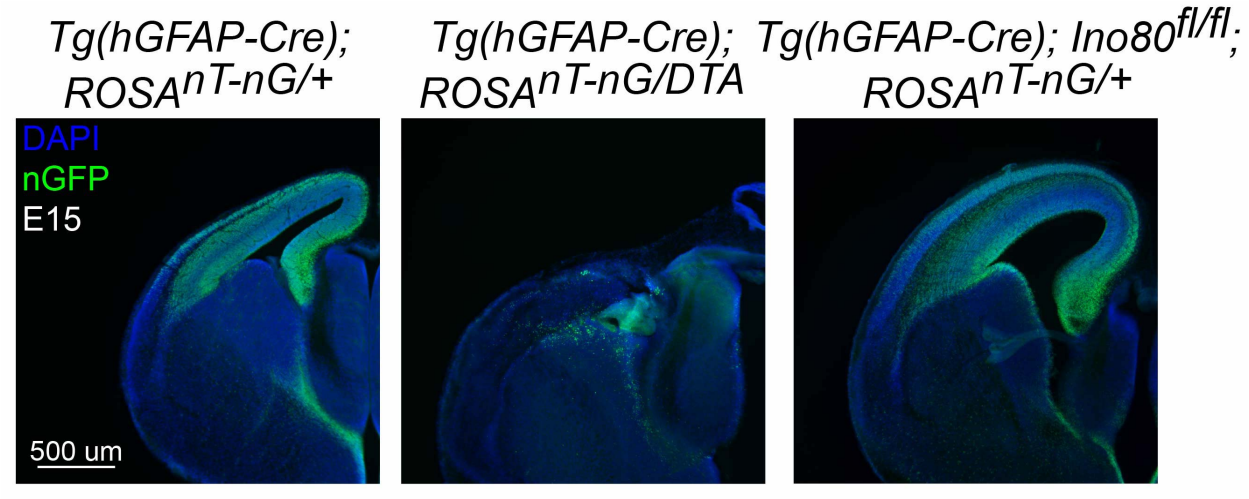

Figure 3.6: Ablation of the *Tg(hGFAP-Cre)* lineage led to cortical agenesis

Tg(hGFAP-Cre) is expressed in cortical NPCs beginning around E12.5. Ablation of the *Tg(hGFAP-Cre)* lineage using $ROSA^{DTA}$ showed that Cre recombined widely and effectively, causing severe microcephaly at E15.5. cKO-hG at E15.5 had no obvious defects.

Defective HR following Brca2 conditional deletion phenocopied Ino80 cKO-E

Chromatin-mediated DSB repair has not been well studied in developmental processes, and therefore it is unclear whether the observations made in the context of *Ino80*-deficiency are true for other components of the HR machinery. To investigate this question, I utilized a conditional allele of *Brca2*, the breast cancer-associated tumor suppressor gene. BRCA2 has a critical role in HR, as a necessary component of the machinery aiding the switch from ssDNA-binding protein RPA to the homology-searching molecule RAD51. This process is necessary to form the presynaptic filament, which invades dsDNA in search of an appropriate template for homology-directed repair of the DSB. BRCA2 facilitates this reaction through a series of BRC repeat domains, which bind RAD51 and serve as a scaffold for the RPA-to-RAD51 switch (Chen et al., 1998; Wong et al., 1997) in cooperation with other genes like *Brca1* and *Palb2* (Sy et

al., 2009). This central role in the HR process makes the protein essential for effective HR repair and functions as a useful *bona fide* HR molecule to compare with the observations made in *Ino80*-deficient cortex.

Indeed, conditional deletion of *Brca2* using $Emx1^{Cre}$ (*Brca2* cKO-E) led to microcephaly at P0, as visualized by the dorsal view of whole mount brains (**Figure 3.7**). Similarly to the *Ino80* cKO-E, the medial portion of the neocortex was most severely affected, exposing the underlying diencephalon.

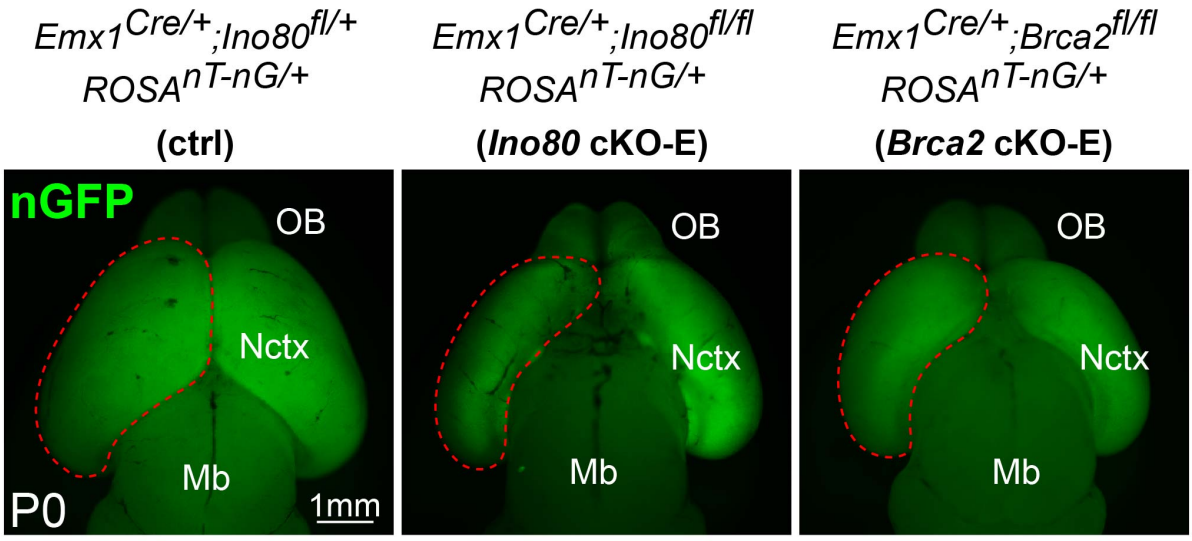

Figure 3.7: *Brca2* cKO-E was microcephalic with medial neocortical disruption

Dorsal view of P0 brains from ctrl, *Ino80* cKO-E, and *Brca2* cKO-E. The *Ino80* and *Brca2* cKOs both demonstrated microcephaly with preferential disruption of the medial compartment of the neocortex.

To better understand the dynamics of HR during critical periods of cortical development, I isolated embryonic brains of E13.5 ctrl and *Brca2* cKO-E embryos. As observed in *Ino80* cKO-E cortex, there was robust upregulation of pKAP1, marking unrepaired DSBs, and p53, responding to the genomic stress of impaired HR (**Figure**

3.8A). p53 and pKAP1 staining were both concentrated in the VZ, very close to the ventricular surface. This is identical to the pattern seen in the *Ino80* cKO-E cortex, and suggested that these cells are likely in late S- or G2-phase as they are migrating to the ventricular surface to divide following genome replication. *Brca2* is a validated HR gene and I have demonstrated that *Ino80* cKO impairs HR, suggesting that location and constellation of these molecular markers may act as a reliable signature of HR-deficient cell division. Importantly, E13.5 *Brca2* cKO-E cortex demonstrated a mediolateral gradient of pKAP1 and p53 staining with intense staining in the medial neocortex, similarly to *Ino80* cKO-E (**Figure 3.8A**), suggesting that NPC mode of division is driving this phenotypic difference in *Brca2* cKO-E also.

Brca2 cKO-E cortex stains intensely for activated caspase, as many cells are undergoing apoptotic cell death. In a striking phenocopy of the *Ino80* cKO-E, apoptotic cells in *Brca2* cKO-E cortex were almost completely confined to the medial compartment whereas the lateral neocortex had very few apoptotic cells (**Figure 3.8B**). This pattern of cell death represents a gradient that is inverse to that of the TNG, and remarkably similar to the observed cell death in *Ino80* cKO-E. These observations demonstrate that medial, symmetrically dividing cells were more sensitive to HR impairment, via *Brca2* or *Ino80* deletion, than the asymmetrically dividing cells in the lateral neocortex.

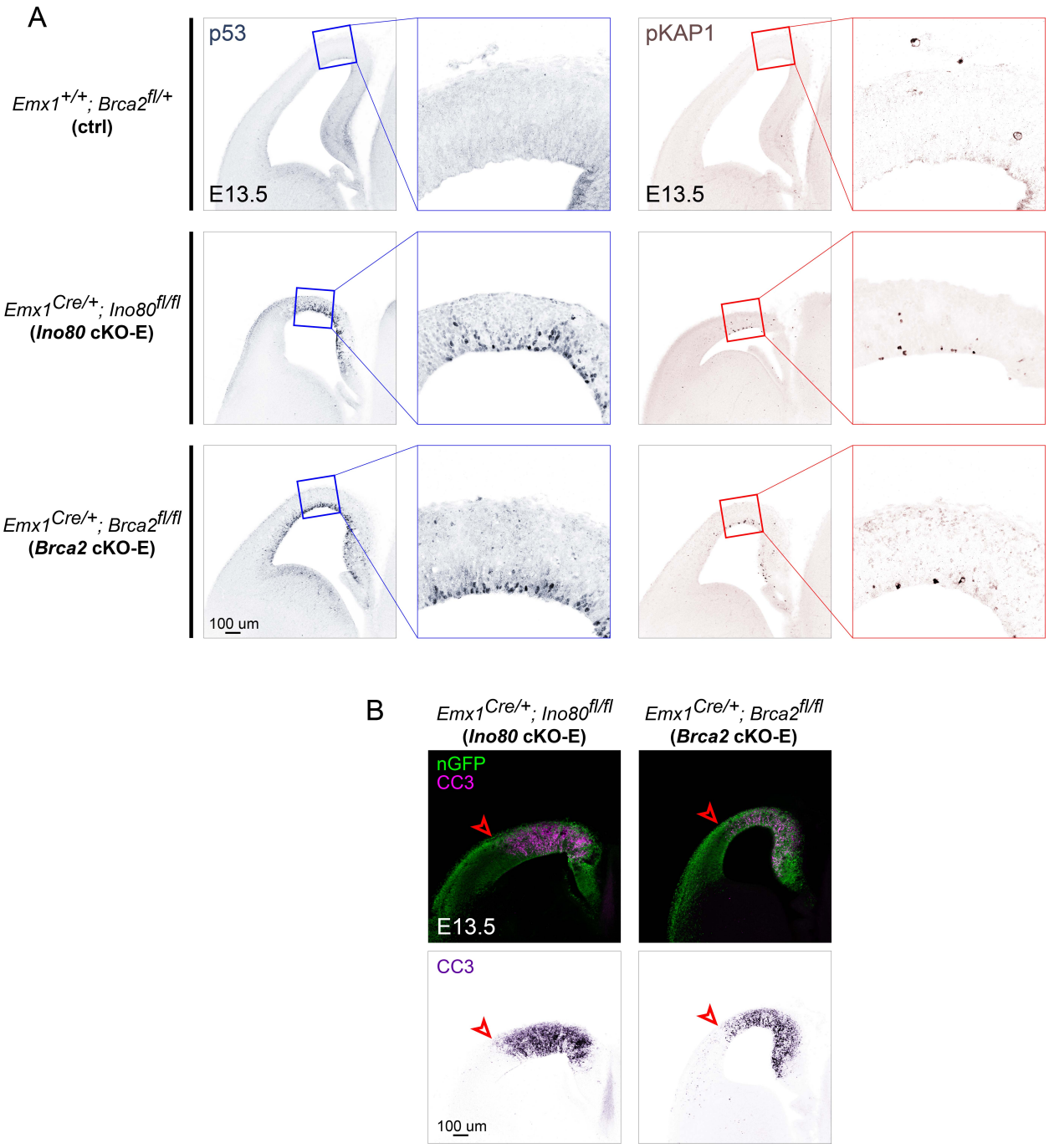

Figure 3.8: *Brca2* cKO-E embryonic cortex phenocopied *Ino80* cKO-E

(A) Immunostaining of pKAP1 and p53 in ctrl, Ino80 cKO-E, and Brca2 cKO-E E13.5 cortex. In both knockouts, p53-positive nuclei were enriched in the VZ near the ventricular surface. pKAP1 staining also demonstrated intensely stained nuclei near the ventricles, only present in the medial compartment.

(B) Apoptosis was confined to the medial compartment of the neocortex in E13.5 Ino80 cKO-E and Brca2 cKO-E.

Discussion

Cortical neurons are generated through a series of NPC divisions, first in a symmetric fashion to expand the pool of progenitors, and then in an asymmetric fashion where divisions give rise to the excitatory neurons that migrate into the cortex. Differences in molecular composition and cellular behavior of NPCs during these modes of division have been described, though understanding of the regulation and processes of division are incomplete. This includes scattered reports of differential sensitivity to cellular and genomic stress between 'early' and 'late' NPCs (Lee et al., 2012; Pulvers and Huttner, 2009). However, the mechanism of this sensitivity and delineation of what differentiates early and late NPCs remains poorly understood.

Here, we report that early, symmetrically dividing NPCs have a strict requirement for HR repair of DSBs – impaired HR leads to widespread apoptosis. In striking contrast, NPCs undergoing neurogenic asymmetric divisions are insensitive to impaired HR, indicating fundamental differences DSB repair and sensitivity to impaired repair between these modes of NPC division (**Figure 3.9**). Leveraging the spatial induction of neurogenesis in a stereotyped developmental wave across the cortex, we identified differential sensitivity of the medial and lateral compartments of the cortex following *Emx1*^{Cre}-mediated deletion of HR genes, *Ino80* and *Brca2*. The differential sensitivity of these compartments correlated with the border between symmetrically and asymmetrically dividing cells. We further used *Foxg1*^{Cre} and *Tg(hGFAP-Cre),* to more specifically delete *Ino80* during symmetric and asymmetric divisions, respectively, with dramatically different phenotypic outcome because of differential NPC sensitivity at the time of deletion.

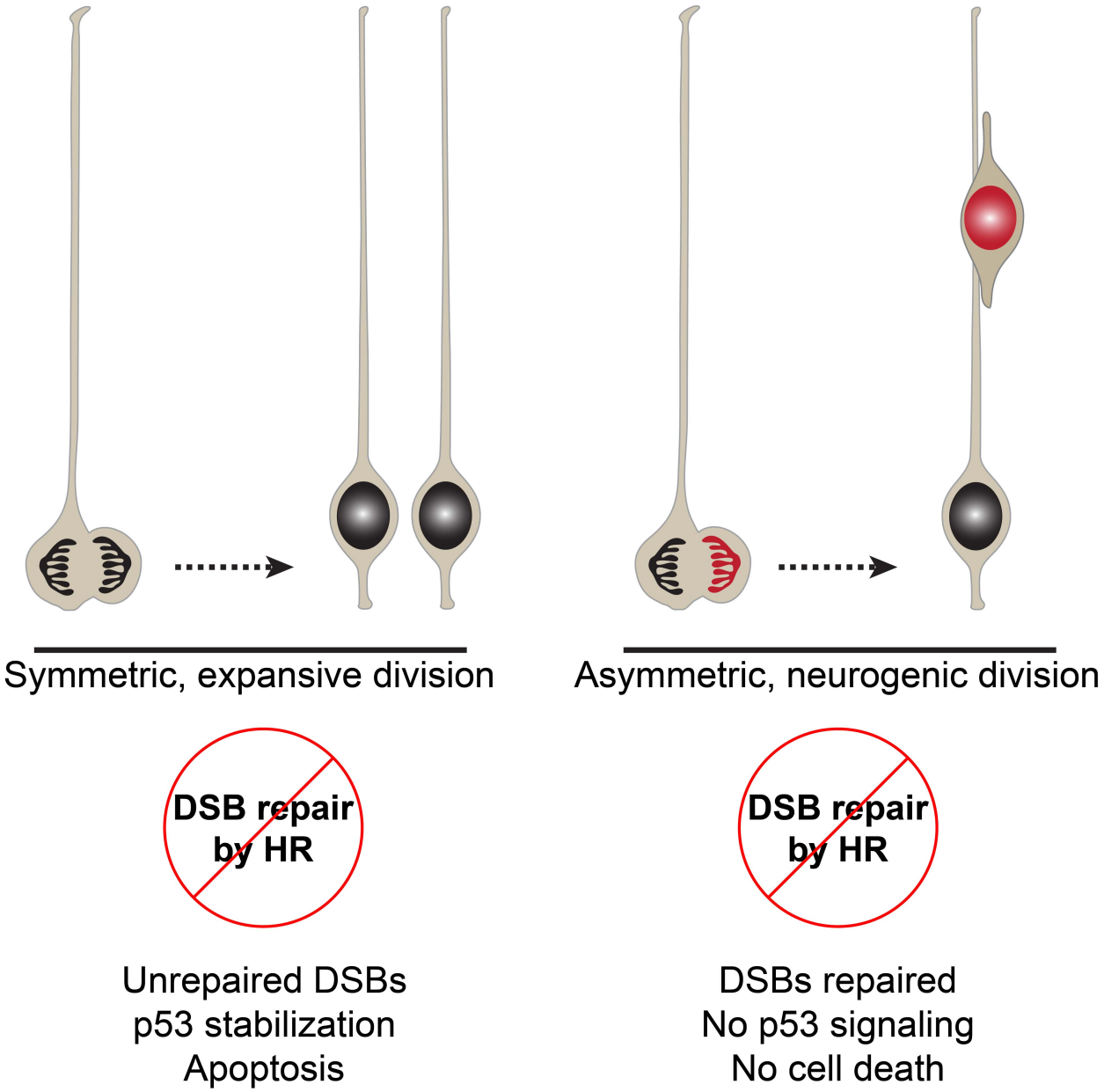

Figure 3.9: Symmetric and asymmetric divisions differ in requirement for HR

When HR is impaired, symmetric NPC divisions are not able to repair DSBs, with resulting stabilization of p53, leading to massive apoptosis. Asymmetric neurogenic NPC divisions, however, do not have this stringent requirement for HR and continue to proliferate without unrepaired DSBs, p53 signaling or cell death.

Regulation of chromatin in the local neighborhood of a DSB is necessary for proper nucleosome dynamics and processing of broken DNA ends. These aspects of chromatin regulating complexes remain incompletely understood, and virtually unexplored in brain development. Although the mechanism remains controversial, *Ino80*-deficiency likely impairs HR following improper nucleosome remodeling surrounding a DSB. BRCA2, on the other hand, catalyzes the RPA-to-RAD51 transition, and has no canonical function in nucleosome dynamics. Because of these fundamental differences in mechanism within the HR process, I investigated whether chromatin regulation of DSB processing displayed similar dynamics to BRCA2-mediated impairment in presynaptic filament formation. Using a conditional allele of *Brca2*, I observed a similar pattern of DNA damage and p53 response after $Emx1^{Cre}$-mediated deletion, supplying further evidence that *Ino80* is necessary for HR and generating a 'fingerprint' of molecular changes present in HR-impaired cortex. Strikingly, the same mediolateral gradient of cell death was observed in *Ino80* cKO-E and *Brca2* cKO-E cortex, indicating that the differential sensitivity between symmetric and asymmetric divisions was generalizable to multiple components of the HR pathway and not confined to chromatin-mediated processing of broken DNA ends.

The basis of neurogenic NPC insensitivity to impaired HR is not known. A number of potential molecular explanations could explain why neurogenic NPCs are not dependent on HR. First, neurogenic divisions may be less sensitive to unrepaired or persistent DSBs, perhaps through lower expression of p53 or an attenuation of signaling. This seems unlikely as p53 functions in cellular divisions throughout the body and developmental timeframe. Additionally, post-mitotic neurons utilize p53-dependent

mechanisms to respond to unrepaired DSBs and induce apoptosis, including cells deficient in DSB repair because of NHEJ-factor impairment. Another possibility is that these cells are using alternative methods of DSB repair, such as c-NHEJ or Alt-EJ. Although inherently mutagenic, these processes can repair DSBs to prevent cellular death, and may be used if the dividing cell is programmed to prioritize other outcomes over high-fidelity genome repair. As previously noted, cell cycle parameters differ between symmetric and asymmetric divisions, with dramatic S-phase shortening in neurogenic cell populations (Arai et al., 2011). This difference can be visualized in E12 control brains, due to the difference in number of EdU-positive cells in the medial, symmetrically dividing cells compared to the lateral, asymmetrically dividing population (**Figure 3.3**). Neurogenic cells spend a far smaller proportion of their cell cycle (~2 out of ~16 hours) in S-phase than symmetrically dividing NPCs (~8 out of ~22 hours) (Arai et al., 2011). Given a short pulse of EdU, fewer neurogenic cells will be in S-phase during this hour than symmetrically dividing cells. Not only is this difference in cell cycle interesting to note, it may indicate a potential reason why asymmetrically dividing cells do not rely on HR, which is a process requiring multiple hours to complete (Whelan et al., 2018). If a short cell cycle is paramount in these neurogenic divisions, the fidelity of genome repair may be relegated to a secondary tier of importance.

Conclusion

Here, I report that the requirement for HR differs by mode of division in cortical NPCs. Using a conditional allele of the chromatin remodeling gene *Ino80,* critical for HR in developing cortex, I show that HR is a stringent necessity for symmetric NPC divisions. Unexpectedly, HR was not required for neurogenic NPC divisions, indicating a

dramatic difference between the genome fidelity requirements of each cell. I validated the findings from the *Ino80* cKOs using a conditional allele of the HR gene *Brca2*. *Ino80* and *Brca2* cKO display striking developmental similarities, indicating that the differences found in symmetric and asymmetric divisions extend to multiple molecules and discrete steps in the process of HR.

Materials and Methods

Mice and mouse husbandry

All mice were maintained on a C57BL/6 background with standard 12 hour day:night cycle with *ad libitum* access to food and water. Copulation plugs were used to determine mating, with noon of the day with visualized plug designated as E0.5 for timed pregnancy identification. Transgenic mice are listed in **Table 3.1**. Genomic DNA was isolated from toe or tail clips and genotyping was performed using DreamTaq Green 2x Master Mix (Thermo Fisher) with oligos listed in **Table 3.2**. All procedures were approved by the University of Michigan IACUC.

Immunostaining

Brains were dissected and fixed in 4% PFA in PBS at 4°C with agitation overnight. Brains were embedded in 4% low-melting agarose and sectioned using a Leica Vibratome (VT1000S or VT1200S). Some antigens benefit from antigen retrieval in pH 6.1 citrate buffer (Dako, Agilent) at 70°C for 30 minutes (as noted in **Table 3.3**). Sections were then incubated for 1 hour at room temperature in blocking solution consisting of 5% Donkey Serum, 1% BSA, 0.1% glycine, 0.1% lysine and 0.3% Triton X-100. Primary antibodies (**Table 3.3**) were added to blocking solution and incubated with

free-floating sections overnight at 4°C with agitation. Sections were washed 3 X 5 minutes in PBS and incubated with fluorescently-linked secondary antibodies (**Table 3.4**) and DAPI, diluted in blocking solution, for 1 hour at RT. Fluorescently-linked primary antibodies were used for immunostaining with multiple primary antibodies raised in the same species. In these cases, fluorescently-linked primaries were diluted in blocking solution and incubated at RT for 1 hour after the secondary antibody incubation. Sections were affixed to slides and allowed to dry, before mounting with VECTASHIELD mounting media (Vector Laboratories). For sections with endogenous fluorescent reporters (nT-nG or EYFP), 100 mM HCl was added to VECTASHIELD to decrease the pH to roughly 6, which reduced the epifluorescence and allowed immunostaining in multiple fluorescent channels.

EdU/CldU Incorporation and Visualization

EdU or CldU was given by intraperitoneal injection at the indicated time before sacrifice at a final concentration of 5 ug per gram or 50 ug per gram, respectively. Following dissection, brains were fixed in 4% PFA in PBS overnight, embedded in agarose and sectioned using a vibratome (VT1000S or VT1200S) at 70 micron thickness. For EdU staining, sections were permeabilized by incubation for 30 minutes in 0.5% Triton X-100 in PBS followed by 3 X 5 minute washes in PBS. EdU staining solution was made fresh each time, containing 100 mM Tris, 4 mM $CuSO_4$, and 100 mM ascorbic acid diluted in 1X PBS. The fluorescently-labeled azide molecule was added last and the staining cocktail was immediately added to sections for a 30 minute incubation at room temperature (final concentrations of each fluorescent molecule: 4 mM AlexaFluor488-Azide, 10 mM Cy3-Azide, 16 mM AlexaFluor647-Azide). After

incubation, sections were washed 3 X 5 minutes in PBS. After EdU labeling, standard protocols were followed for immunostaining.

Imaging

Whole mount and early postnatal brain images were taken on an Olympus SZX16 dissecting scope with Olympus U-HGLGPS fluorescent source. Q-Capture Pro 7 software was used to operate a Q-Imaging Retiga 6000 camera. Confocal images were obtained using an Olympus Fluoview FV1000 confocal microscope utilizing Olympus FV10-ASW software.

Statistical Analysis

Statistical calculations were performed in GraphPad Prism (7 or 8). Values were compared using a two-tailed, unpaired student's *t*-test or one-way ANOVA with Tukey post-test. A p-value <0.05 was considered statistically significant.

Image Processing and Analysis

Images were exported as TIFF files and processed in Adobe Photoshop. Counts and measurements were performed in Photoshop or using ImageJ software.

Acknowledgements

I owe many thanks to the following people. Nitesh Mohan, Stephen Harvey, and Nikita Khan completed critical work like genotyping, sectioning, and immunostaining. Lisa Gallmon and Debra Fitzgerald from NCI assisted in the shipment of *Brca2* cryopreserved embryos. Thom Saunders, Galina Gavrilina, Corey Ziebell, and Anna LaForest from the University of Michigan Transgenic Animal Model Core helped to perform the cryorecovery of the *Brca2* conditional mouse line. Finally, all members of

the Kwan lab have provided thoughtful analysis and input about scientific questions, figure organization, and technical support.

Table 3.1: Mice used in this study.

Mouse	Description	ID Number	Citation
B6.129(C3)-*Ino80*$^{tm1.1Jland}$/J *Ino80*^{fl}	Floxed exons 2-4 of *Ino80*	JAX# 027920	(Qiu et al., 2016)
B6N.129S6-*Gt(ROSA)26Sor*$^{tm1(CAG-tdTomato*,-EGFP*)Ees}$/J *ROSA*$^{nT-nG}$	Cre-dependent switch from *nTdTomato* to *nEGFP*	JAX# 023537	(Prigge et al., 2013)
Brca2^{tm1Bm}/Nci *Brca2*^{fl}	Floxed exon 11 of *Brca2*	NCI# 01XB9	(Jonkers et al., 2001)
B6.129S2-*Emx1*$^{tm1(cre)Krj}$/J *Emx1*$^{IRES-Cre}$	Knock-in of *Cre* to *Emx1* locus driven by IRES	JAX# 005628	(Gorski et al., 2002)
B6.129P2(Cg)-*Foxg1*$^{tm1(cre)Skm}$/J *Foxg1*^{Cre}	Knock-in of *Cre* to *Foxg1* locus	JAX# 006084	(Hébert and McConnell, 2000)
FVB-*Tg(GFAP-cre)25Mes/J Tg(hGFAP-Cre)*	Transgenic line with *hGFAP* promoter driving *Cre*	JAX# 004600	(Zhuo et al., 2001)
B6.129P2-*Gt(ROSA)26Sor*$^{tm1(DTA)Lky}$/J *ROSA*^{DTA}	Cre-dependent expression of *DTA* at ROSA26 locus	JAX# 009669	(Voehringer et al., 2008)

Table 3.2: Oligos used for genotyping mice in this study.

Gene Target	Oligo Name	Sequence (5' - 3')	Notes
Cre	Cre-F	TCGATGCAACGAGTGATGAG	Detects all Cre lines tested 500 bp
	Cre-R	TTCGGCTATACGTAACAGGG	
Ino80^{fl}	Ino80-F	GCACTTCCTGGTTTTGCTGT	WT = 290 bp Floxed = 350 bp
	Ino80-R	CACTGACTGGCGTGTTCAGA	
Ino80^{fl}	Ino80-P1	CTGGATGTGAAGGGAGAAGG	WT = 416 bp Floxed = 482 bp (-) allele = 352 bp
	Ino80-P2	CATCTCTCCAGCCAGCACACT	
	Ino80-P3	TGCCACTCTACCTGCATCTG	
Brca2^{fl}	Brca2-F	GGCTGTCTTAGAACTTAGGCTG	WT = 298 bp Floxed = 376 bp
	Brca2-R	CTCCACACATACATCATGTGTC	

Table 3.3: Primary antibodies used in this study

Primary Antibody	Company and product number	Dilution	Notes
Chicken anti-MAP2	Novus Biologicals NB300-213	1:2000	
Rabbit anti-GFP	Thermo Fisher A-11122	1:250	
Chicken anti-GFP	Abcam ab13970	1:2000	
Rabbit anti-LHX2	EMD Millipore ABE1402	1:2000	
Rat anti-BCL11B	Abcam ab18465	1:500	
Mouse anti-TLE4	Santa Cruz Biotechnology sc-365406	1:250	
Rat anti-EOMES	Thermo Fisher 14-4875-80	1:500	
Rabbit anti-SOX2	Millipore/Chemicon AB5603	1:2000	
Goat anti-SOX2	Santa Cruz Biotechnology sc-17320	1:250	
Rabbit anti-CC3	Cell Signaling 9661S	1:500	
Rabbit anti-CC3-Alexa555	Cell Signaling 9604S	1:100	Alexa555-labeled
Rabbit anti-TRP53	Leica P53-CM5P-L	1:500	
Rabbit anti-pKAP1	Bethyl Laboratories A300-767A	1:200	
Rabbit anti-γH2AX	Cell Signaling 9718S	1:250	
Chicken anti-RBFOX3	EMD Millipore ABN91	1:2000	
Rabbit anti-Ngn2	Cell Signaling 13144S	1:250	Antigen Retrieval
Rabbit anti-SATB2	Abcam ab92446	1:500	

Table 3.4: Fluorescently-linked secondary antibodies used in this study.

Secondary Antibody	Company	Dilution
AlexaFluor 488 AffiniPure Donkey anti-Rabbit IgG (H+L)	Jackson ImmunoResearch Labs	1:250
AlexaFluor 488 AffiniPure Donkey anti-Rat IgG (H+L)	Jackson ImmunoResearch Labs	1:250
AlexaFluor 488 AffiniPure Donkey anti-Goat IgG (H+L)	Jackson ImmunoResearch Labs	1:250
AlexaFluor 594 AffiniPure Donkey anti-Mouse IgG (H+L)	Jackson ImmunoResearch Labs	1:250
Cy3 AffiniPure Donkey anti-Rabbit IgG (H+L)	Jackson ImmunoResearch Labs	1:250
Cy3 AffiniPure Donkey anti-Rat IgG (H+L)	Jackson ImmunoResearch Labs	1:250
AlexaFluor 647 AffiniPure Donkey anti-Goat IgG (H+L)	Jackson ImmunoResearch Labs	1:250
AlexaFluor 647 Affinipure Donkey anti-Rabbit IgG (H+L)	Jackson ImmunoResearch Labs	1:250
AlexaFluor 647 Affinipure Donkey anti-Rat IgG (H+L)	Jackson ImmunoResearch Labs	1:250
AlexaFluor 647 Affinipure Donkey anti-Chicken IgG (H+L)	Jackson ImmunoResearch Labs	1:250

Chapter 4: Discussion

Overview

INO80 mutations have been implicated in individuals with microcephaly, and therefore may play a role in human neurodevelopment. My dissertation research focused on elucidating the function of *Ino80* in the developing cortex, and efforts to understand the necessity of HR for DSB repair in cortical NPCs. In Chapter 2, I used conditional deletion of *Ino80* from developing cortex and found that deletion from NPCs led to massive apoptosis and loss of stem cells in the medial neocortical compartment, including the hippocampus. Further analyses identified impaired DSB repair as a likely cause of the cell death and I used a novel DSB repair assay to demonstrate that HDR was selectively decreased compared to NHEJ in *Ino80*-deficient cortex. Consistent with these findings, co-deletion of p53*,* encoded by the *Trp53* gene, and *Ino80* rescued the microcephaly phenotype due to failure to activate apoptosis in cells with DSBs. Transcriptomic changes in cKO-E and dKO-E cortex identified genes upregulated by p53 signaling and cell death. Genes persistently down in cKO-E and dKO-E cortex, however, revealed transcriptionally regulated targets of YY1, a transcription factor binding partner of INO80-C. These analyses enabled the disentanglement of the DSB repair and gene regulatory functions of INO80-C, specifically implicating impaired DSB repair and subsequent apoptosis as key cellular processes in observed microcephaly.

During my efforts to characterize INO80-C function in cortex, I unexpectedly found that HR was not required in all dividing NPCs. In Chapter 3, I showed that HR,

which is critical to the early symmetric divisions of the cortex, was not required for asymmetric neurogenic NPC divisions. This relationship was dissected using the spatiotemporal dynamics of developmental neurogenesis dynamics and multiple Cre driver lines to delete *Ino80* with temporal control. Conditional deletion of *Brca2* strikingly phenocopied *Ino80* cKO, with NPC mode of division dictating dramatically different requirements for HR.

In Chapter 4, I explore questions remaining from the preceding work and potential lines of inquiry for additional work.

INO80 in human disease

INO80 is a candidate gene for human microcephaly, with missense mutations identified in affected individuals within a consanguineous pedigree. My finding that *Ino80* is crucial for DSB repair by HR in the developing brain offers insights into the potential mechanism through which these mutations may be functioning. It should be noted, however, that there are differences in INO80-C disruption between the affected individuals and the mouse models utilized herein. GnomAD data showed very few healthy individuals with heterozygous LOF *INO80* mutations and no individuals, healthy or diseased, have been observed with homozygous LOF mutations, suggesting that such mutations would be incompatible with life. If the missense mutations are responsible for the microcephaly in this family, it is likely that they are hypomorphic alleles with decreased function. Given the fact that my studies deleted *Ino80* in the entire cortex, re-expression studies of the human variants may offer a suitable way to test the function of these potentially pathogenic mutant forms. In addition to mutations in *INO80*, the catalytic subunit of the INO80-C, there are 13 other canonical members of

the complex (Chen et al., 2011). Although not all are essential for functionality, in depth investigations to detail the importance of each component in HR have not been undertaken.

In addition to a critical role in HR, I showed that *Ino80* also participated in a gene regulatory capacity, as *Ino80*-deficiency led to robust transcriptome changes. However, it is unclear whether these have an effect on brain development that is not structurally obvious. It is possible that dysregulation of INO80:YY1-regulated genes may have a more subtle effect on neuronal function that would need to be investigated via behavioral or electrophysiological studies. This question is especially interesting in light of the recent finding that human YY1-haploinsufficiency has been identified in multiple individuals with intellectual disability. Most of these individuals do not exhibit microcephaly, consistent with a role of YY1 in transcriptional regulation, as opposed to genome stability (Gabriele et al., 2017). The *Ino80;Trp53* dKO-E and *Ino80* cKO-N mice are both models of *Ino80*-deficiency without structural abnormality and could provide useful tools of transcriptional dysregulation for further study.

Chromatin-mediated DSB repair in brain somatic mosaicism

Chromatin regulation of DSB repair is a topic that has not been widely investigated in the brain. Certainly, impaired DSB repair via mutations of well-characterized players in the HR and NHEJ pathways have been implicated in human neurodevelopmental disorders (**Table 1.1**) and modeled in various systems. And though multiple chromatin remodelers have been implicated in some form of DSB repair in other systems (**Figure 1.5B**), little is known about the contribution of this mechanism during brain development.

Recent evidence has identified somatic mosaicism in the brain. Some have argued that mosaicism could be beneficial as a way of making the brain genomically diverse (Singer et al., 2010), though others have found mosaic genetic variation in human disease (D'Gama et al., 2017; Jamuar et al., 2014; McConnell et al., 2017; Poduri et al., 2012). These interpretations are not mutually exclusive, but to fully understand the role of somatic mosaicism in brain development and function, efforts to catalog somatic mutations in neurotypical and disordered brains must be well informed.

Novel genetic approaches have identified somatic mosaicism in diseases like autism spectrum disorder, though sequencing and computational approaches are currently only able to identify mosaic SNVs with some accuracy (Freed and Pevsner, 2016; Krupp et al., 2017). It remains to be determined whether somatic structural variants play a role in pathogenesis of diseases such as autism. It is known, however, that germline mutations in chromatin regulating genes have consistently been identified as pathogenic in autism, demonstrating enrichment over other subsets of gene functions (Sanders et al., 2015). Two notable high confidence germline-mutated autism genes (*de novo* loss-of-function, FDR<0.01), *CHD2* (Luijsterburg et al., 2016) and *ARID1B* (Watanabe et al., 2014), have demonstrated roles in DSB repair. Future investigations of brain somatic mosaicism may benefit from investigating somatic structural variants as a result of germline-mutated DNA repair enzymes, including chromatin remodelers.

In this light, the *Ino80* cKO and *Ino80;Trp53* dKO mouse models may represent valuable resources to understand normal and pathological DSB repair in the developing brain. Neurotypical cortex has robust mechanisms, including p53, to surveil for genomic

lesions that may propagate in the brain or become tumorigenic in the future. The dKO mouse, however, demonstrates no apoptosis downstream of the unrepaired DSBs present in *Ino80*-deficient cortex. This model, therefore, presents an interesting paradigm of a brain with a potentially high burden of SV. Identifying somatic structural variants present at low frequency presents a problem that is challenging from a sequencing and computational perspective. These techniques will likely be more successful if developed first in a model system with a relative plethora of events before transitioning to the investigation of complex and valuable patient samples. A similar approach has been used recently to sequence tumors from NHEJ- or HR-deficient brain (Ratnaparkhe et al., 2018). However, the genomic events identified from these tumors represent clonal amplifications that likely conferred a proliferative advantage, and therefore, offer little insight into the non-tumorigenic, low-level somatic mosaicism that may be present in non-cancerous disease. Additionally, comparative analysis of the types and locations of SV in the cKO-E and dKO-E brains may offer valuable information. Identification of genes, regions of the genome, or SV types present in the dKO versus the cKO brain, could offer insights into how the brain actively guards against mutation using p53-mediated mechanisms and what gene disruptions prevent cells from surviving as a post-mitotic neuron.

c-NHEJ and Alt-EJ in neurogenesis

DNA damage, and DSBs in particular, are inevitable during genome replication. In human cells, it is estimated that each S-phase leads to 50 DSBs (Vilenchik and Knudson, 2003). DSBs are therefore likely to occur in asymmetric, neurogenic NPC

divisions. My finding that HR is not required for these divisions therefore raises questions about the nature of DSB repair during different modes of NPC division.

First, how is this neurogenic population of NPCs specifically protected from apoptosis following impaired HR? Molecularly, this could be driven by decreased p53 level or signaling. This seems unlikely, however, as our lab has observed p53-dependent apoptosis following *Tg(hGFAP-Cre)*-mediated deletion of *Casc5*, a gene important for appropriate chromosome segregation. Missegregation in neurogenic NPC divisions (E15.5) leads to DSBs during cytokinesis and robust p53 stabilization, signaling, and apoptotic induction (Shi L, Qalieh A, Lam MM, Keil JM and Kwan KY, In press, Nature Communications). The tolerance for impaired HR in asymmetric divisions, therefore, is unlikely to be based on p53.

Second, how are DSBs repaired if HR is compromised? Although evolution has formulated multiple ways to repair DSBs including c-NHEJ and Alt-EJ, the mechanisms they employ are not dependent on long sequences of high homology. The resection-independent c-NHEJ generates SNVs and small indels at sites of repair if the two original ends of a break are re-joined. However, since there is no homology involved, c-NHEJ can also form SV including CNVs and translocations if two free DNA ends that were not from the original break are ligated. Conversely, Alt-EJ relies on short stretches of homology (5-25 bp) for strand annealing following resection to ssDNA. If two original strands are re-ligated, there is an obligate loss of genetic information as resected ssDNA will bind and sequence near the resected ends outside of the homology will be lost. And similarly to c-NHEJ, Alt-EJ can also generate large SV or translocations by re-

joining ssDNA strands that were from initially distinct breaks. Both of these potential pathways are sub-optimal if genome fidelity is the ultimate objective.

HR in larger brains

Although the mouse is a tractable system for studying brain development, it cannot be used to precisely mimic the neurodevelopment of the larger, gyrenchephalic brains of primates. However, some general principles remain constant between mouse and human brain development. These include the early symmetric division of NPCs followed by a transition to asymmetric divisions, the presence of radially directed cortical columns, and largely similar molecular markers of major cell types. The dramatic expansion of the primate neocortex has been driven by a number of factors, one of which is an increase in the complexity and types of germinal zones present to generate neurons. Mouse cortex is built by aRG residing in the VZ and IPCs positioned in the SVZ. In addition to these cells, primate brains have other progenitors that are rarely present in mouse brain (Wang et al., 2011). Notably, the bRG, which extend a basal process to the dorsal, pial surface, but do not maintain a physical connection to the ventricular surface. These bRG make up a large portion of the germinal zone in the primate. These increasing complexities in developmental dynamics are thought to underlie the evolution of the primate cortex.

Our abilities to ask mechanistic questions in mouse brain allow great flexibility to understand NPC dynamics and investigate molecular mechanisms, but the relative simplicity of NPCs in the mouse brain can make extrapolation to the primate brain unreliable. In primate brains, the increasing number of progenitor cell types and modes of division do not make for simple categorization of a division as symmetric or

asymmetric. Rather, there are divisions of aRG that generate IPCs, bRG, and bIPs. These classes of NPCs that do not maintain ventricular contact continue to divide, both in symmetric and asymmetric fashions, with eventual production of neurons. I am not able to make claims about these developmental processes from my observations in mouse development, however, I will note similarities from developmental studies of primates that may offer insight.

As previously discussed, variations in cell cycle are particularly pronounced between types of NPCs and modes of division in the mouse cortex. Specifically, asymmetrically dividing, neurogenic NPCs have a much shorter cell cycle than symmetrically dividing NPCs (15 hours compared to 22 hours). This change is driven by a dramatically decreased time in S-phase, (2 hours compared to 8 hours). In gyrencephalic brains, the cell cycle is longer and fine dissection of these S-phase numbers is more difficult. However, a constant observation is that cell cycle lengths vary throughout cortical neurogenesis and that S-phase is a driver of those changes. In particular, the length of S-phase generally decreases as the cortex progresses into neurogenic divisions. This has been noted in ferret (Reillo and Borrell, 2012; Turrero García et al., 2016) and macaque (Betizeau et al., 2013; Kornack and Rakic, 1998). Gyrencephalic brains, and particularly the primate lineage have dramatically increased the number of bRG. Interestingly, studies of mouse (Arai et al., 2011), and macaque (Betizeau et al., 2013) both found decreased S-phase length in these neurogenic basal progenitors.

The length of S-phase has important implications for DSB repair. HR and NHEJ differ in the amount of time necessary for repair. As NHEJ requires less processing of

DNA ends and does not rely on searching for homology, it is a process estimated to be completed in ~30 minutes. HR, on the other hand, has more extensive processing, recruitment of important factors, and homology searching, and has been reported to take 7 hours or longer (Mao et al., 2008). It is unknown whether S-phase length affects the choice of DSB repair pathway. However, the total combined length of S- and G2-phase in mouse neurogenic NPCs is estimated to be <4 hours. As HR requires multiple hours to complete and each genome replication likely induces multiple DSBs, it seems likely that decreased S-phase length may necessitate the use of NHEJ rather than HR, as the required time differs by an order of magnitude. Given that S-phase length has been demonstrated to shorten in neurogenic NPCs across multiple species, future investigations into the use of HR in primate and human cortical neurogenesis are of interest.

Did evolution favor error-prone repair in neurogenesis?

Excitatory cortical neurons are only generated during gestation, lasting the lifetime of the organism, and therefore are a non-renewable resource. As a result, one could reasonably hypothesize that neurogenesis would be subject to requirements for high fidelity genome replication and repair. Since HR is thought to be the highest fidelity option for DSB repair, my findings that HR is not required in neuron-producing divisions raise intrigue.

The mammalian brain, and especially the primate lineage, exhibits a dramatic increase in the size of the neocortex compared to reptiles and birds. Many contributing factors for this expansion have been proposed, focused on increasing the number and subtype of NPCs in addition to the duration of the neurogenic period. One way to

increase neuronal number would be to decrease the length of each cell cycle, allowing more cell divisions to occur within the same gestational window. However, shorter cell cycles may have trade-offs such as lower-fidelity DNA damage repair that result in negative consequences. As stated previously, S-phase length is reduced in neurogenic NPCs in mice and primates. In mice, this reduction is drastic, and may not leave sufficient time for successful completion of HR to repair DSBs induced by genome replication. If these observations and hypotheses are true, this may represent an evolutionary trade-off: the cortex generates more neurons, but sacrifices genome fidelity within these neurons. Early indications of large CNVs and aneuploidy in human neurons support the idea that neuronal genomes are far from perfect (McConnell et al., 2013), and may in fact, contain structural variation that arose during NPC proliferation.

My findings in mice demonstrate that genome fidelity is still of high priority in symmetrical divisions as impaired HR leads to massive apoptosis in these NPCs. This is a critical distinction because mutations in symmetric NPC divisions would be exponentially amplified whereas mutations in asymmetric neurogenic NPC divisions are only subject to linear amplification in number. Any individual asymmetrically dividing progenitor will only give rise to, at most, dozens of post-mitotic neurons, therefore limiting the potential scope of mutated neuronal genomes. In fact, due to the columnar nature of brain development, best visualized by the radial unit hypothesis (**Figure 1.3**), mutations that occur during asymmetric divisions may be confined to a single vertical column. In contrast, somatic mutations in symmetrically dividing NPCs can be exponentially amplified and have the potential to be much more widespread.

Nucleosome dynamics in genome replication

Regulation of chromatin is important for DNA synthesis and genome replication. As the replication fork progresses, highly compacted DNA must be freed from its nucleosomal packaging to be copied by polymerase. This involves the liberation of H2A-H2B dimers and $(H3\text{-}H4)_2$ tetramers from the parental (pre-replication) strand and subsequent re-assembly on the two daughter strands post-synthesis (Groth et al., 2007). The INO80-C has been implicated in replication fork progression, specifically through an interaction with ubiquitinated H2A and the tumor suppressor BAP1 (Lee et al., 2014). It remains unknown whether INO80-C is removing nucleosomes ahead of the replication fork, replacing them post-synthesis, or performing another function promoting genome replication. It is possible that *Ino80* deficiency is disrupting the genome replication process in the brain and contributes to the S-phase breaks that were observed in NPCs. Qualitatively, I have not observed a difference in the amount of DNA damage, indicated via γH2AX foci, in S-phase NPCs, though these analyses are low resolution and I have not investigated this quantitatively. However, the *Brca2* cKO-E mouse is a useful comparison for this question. BRCA2 has no known function in chromatin-mediated replication fork progression, but rather functions to repair DSBs by HR following replication fork collapse. Therefore, *Brca2* deletion allows us to isolate the process of DSB repair by HR. Comparative analysis of *Ino80* cKO-E and *Brca2* cKO-E cortex shows remarkably similar developmental phenotypes. These results are consistent with the hypothesis that *Ino80* deficiency impairs HR of endogenous S-phase breaks, rather than an alternative hypothesis whereby *Ino80* deficiency is causing more S-phase breaks due to impaired nucleosome dynamics near the replication fork.

Zika virus infection in microcephaly

In recent years, a concerning link has been established between gestational Zika virus infection and microcephaly of infants from these births, now called congenital Zika syndrome (CZS). First identified in Northeast Brazil as a new strain of Zika virus swept across South America, thousands of babies born with microcephaly alarmed public health officials throughout Brazil and the world. Although the mechanisms underlying the neurodevelopmental defects are not fully elucidated, it is clear that following maternal infection, Zika virus particles cross the placenta and infect NPCs of the developing fetus leading to cell death through caspase-mediated apoptosis (Tang et al., 2016). Zika-infected NPCs exhibit chromosomal and centrosomal abnormalities (Souza et al., 2016), and targets of TP53 are transcriptionally upregulated (Ghouzzi et al., 2016), all markers of DNA damage and genome instability. These observations suggest that DNA damage may contribute to NPC death and therefore the pathogenesis of microcephaly in CZS. Interestingly, Zika infection during the first trimester leads to higher rates of microcephaly, ~15%, than infection during the second or third trimester, ~5% and 4%, respectively (CDC). Data on the severity of these infections is not currently available, but it is notable that infection during the first trimester when NPCs are undergoing symmetric, expansive divisions results in higher rates of neurological abnormality than infections that occur when NPC divisions are largely neurogenic. These observations suggest that earlier NPC divisions may be more susceptible to Zika infection, mirroring the sensitivity of symmetric NPC divisions in the context of impaired HR.

Future investigations

This work has addressed fundamental questions about chromatin remodeling, genome stability, and DNA damage repair during corticogenesis. These findings have also generated new questions that will be central to future investigations.

The first and most pressing question concerns the DSB repair processes used during neurogenic divisions. Although DSBs occur during neurogenic divisions as they do in all cell divisions, my data showed that high-fidelity repair via HR is not a requirement for neurogenic divisions. My investigations have only detailed DSB repair in neurogenic divisions when HR is impaired via *Ino80* or *Brca2* deletion. Other DSB repair options that might be used including c-NHEJ and Alt-EJ have lower fidelity and can lead to indels or large structural variation as a result. This suggests that neurogenic divisions may have a lower requirement for genome fidelity. However, the methods of DSB repair in HR-proficient, non-pathologic neurogenic divisions remain unknown. Are DSBs in neurogenic divisions generally repaired with error-prone methods? Or does the threshold for NPC apoptosis differ during these divisions, thereby allowing for less stringent repair? Use of the *Tg(hGFAP-Cre)* driver line to disrupt HR (*Ino80*, *Brca2*) in conjunction with genetic or pharmacologic inhibition of c-NHEJ or Alt-EJ pathways in asymmetrically dividing NPCs will yield insights into these questions.

Previous discussions have assumed that post-mitotic neurons carrying genomic structural variation would be permanent in the brain and could disrupt circuitry development and function. The brain, however, has an additional level of quality control for neurons that will become components of its circuitry. Neurodevelopment produces more neurons than will constitute the final, mature circuitry of the brain, with excess

neurons lost to apoptosis (Dekkers et al., 2013). In circuit development and refinement, neurotrophic factors strengthen the connections of a certain number of appropriately targeted axons. Axons that are in excess of this necessary number or that are inappropriately targeted do not receive these necessary neurotrophic signals and will undergo programmed cell death (Yamaguchi and Miura, 2015). This physiological process ensures that the required connections are made between connected areas and additionally serves as a filter to maintain only neurons that are connected and firing appropriately. A neuron carrying genomic mutations that prevent it from functioning properly may be subject to apoptotic processes, therefore negating the harmful effects of its damaged genome. Recent single neuron sequencing of neurotypical individuals supports this idea, finding that neurons with complex karyotypes are less prevalent as the brain develops and ages (Chronister et al., 2019). This suggests that neurons carrying structural variation may have lower fitness and could be lost from the brain as a result of processes that occur subsequent to neurogenesis.

A second open question concerns the effects on neural development and function of the dysregulated transcriptome following *Ino80* deletion. My analyses focused on the early generation, migration, and specification of cortical projection neurons. However, the transcriptional fidelity and functionality of these *Ino80*-deficient neurons in more mature brains remains to be elucidated. Patients with haploinsufficiency of *YY1*, the major known transcription factor binding partner of *INO80*, are characterized by intellectual disability without significant structural brain abnormalities. This suggests that transcriptional fidelity of *YY1* target genes, including *INO80*-dependent genes, may be necessary for normal functionality of these neurons.

To dissect this relationship, transcriptome and electrophysiology changes in post-mitotic neurons of postnatal brains would be informative. *Neurod6-Cre* deletion of *Ino80* (cKO-N) showed no obvious morphological changes, even though *Ino80* was deleted from early post-mitotic neurons. Additional use of *Tg(CamK2a-Cre)* to delete *Ino80*, in post-mitotic excitatory neurons of the cortex at ~P14, would enable deletion from neurons that have migrated, developed connections, and matured prior to *Ino80* deletion (Tsien et al., 1996).

Concluding remarks

My dissertation research dissected the roles of INO80-C in cortical development, distinguishing gene regulatory and genome stability functionalities. Importantly, I demonstrated that chromatin-mediated DSB repair is a critically important mechanism for appropriate cortex development and that *Ino80* participates in HR in NPCs. The microcephaly phenotype resulting from *Ino80* deletion was completely rescued by *Trp53* co-deletion, indicating that unrepaired DNA damage in *Ino80* cKO-E mice led to the observed apoptosis. Through this work I developed a novel DSB repair assay based solely on plasmid transfection, which is therefore extremely versatile for use *in vitro* or *in vivo*. My transcriptomic analysis of cKO-E and dKO-E mice yielded valuable insights into potential binding partners for INO80-mediated transcriptional changes. To my knowledge, this is the first transcriptome-wide expression study of *Ino80* that attempted to circumvent the analytic issues from cell death and p53-signaling related to genomic instability in an *Ino80*-deficient context.

I additionally investigated the novel finding that DSB repair via HR was variably necessary in NPCs, depending on the mode of division. Unexpectedly, symmetric NPC divisions required HR whereas asymmetric, neurogenic NPC divisions were largely unaffected by *Ino80* or *Brca2* deletion. This finding raises many questions for future work to understand basic mechanisms of genome repair during neurogenic divisions and has important implications for acquisition of somatic mutations during different modes of NPC division.

References

Alatwi, H.E., and Downs, J.A. (2015). Removal of H2A.Z by INO80 promotes homologous recombination. EMBO Rep *16*, 986-994.

Alazami, A.M., Patel, N., Shamseldin, H.E., Anazi, S., Al-Dosari, M.S., Alzahrani, F., Hijazi, H., Alshammari, M., Aldahmesh, M.A., Salih, M.A.*, et al.* (2015). Accelerating novel candidate gene discovery in neurogenetic disorders via whole-exome sequencing of prescreened multiplex consanguineous families. Cell Rep *10*, 148-161.

Albert, M., Kalebic, N., Florio, M., Lakshmanaperumal, N., Haffner, C., Brandl, H., Henry, I., and Huttner, W.B. (2017). Epigenome profiling and editing of neocortical progenitor cells during development. EMBO J *36*, 2642-2658.

Alter, B.P., Rosenberg, P.S., and Brody, L.C. (2007). Clinical and molecular features associated with biallelic mutations in FANCD1/BRCA2. J Med Genet *44*, 1-9.

Ameziane, N., May, P., Haitjema, A., van de Vrugt, H.J., van Rossum-Fikkert, S.E., Ristic, D., Williams, G.J., Balk, J., Rockx, D., Li, H.*, et al.* (2015). A novel Fanconi anaemia subtype associated with a dominant-negative mutation in RAD51. Nat Commun *6*, 8829.

Anders, S., Pyl, P.T., and Huber, W. (2015). HTSeq--a Python framework to work with high-throughput sequencing data. Bioinformatics *31*, 166-169.

Anthony, T.E., Klein, C., Fishell, G., and Heintz, N. (2004). Radial glia serve as neuronal progenitors in all regions of the central nervous system. Neuron *41*, 881-890.

Arai, Y., Pulvers, J.N., Haffner, C., Schilling, B., Nüsslein, I., Calegari, F., and Huttner, W.B. (2011). Neural stem and progenitor cells shorten S-phase on commitment to neuron production. Nat Commun *2*, 154.

Arlt, M.F., Ozdemir, A.C., Birkeland, S.R., Wilson, T.E., and Glover, T.W. (2011). Hydroxyurea induces de novo copy number variants in human cells. Proc Natl Acad Sci U S A *108*, 17360-17365.

Arlt, M.F., Rajendran, S., Birkeland, S.R., Wilson, T.E., and Glover, T.W. (2012). De novo CNV formation in mouse embryonic stem cells occurs in the absence of Xrcc4-dependent nonhomologous end joining. PLoS Genet *8*, e1002981.

Ashwell, K. (1990). Microglia and cell death in the developing mouse cerebellum. Brain Res Dev Brain Res *55*, 219-230.

Banin, S., Moyal, L., Shieh, S., Taya, Y., Anderson, C.W., Chessa, L., Smorodinsky, N.I., Prives, C., Reiss, Y., Shiloh, Y.*, et al.* (1998). Enhanced phosphorylation of p53 by ATM in response to DNA damage. Science *281*, 1674-1677.

Barlow, C., Hirotsune, S., Paylor, R., Liyanage, M., Eckhaus, M., Collins, F., Shiloh, Y., Crawley, J.N., Ried, T., Tagle, D.*, et al.* (1996). Atm-deficient mice: a paradigm of ataxia telangiectasia. Cell *86*, 159-171.

Bertrand, N., Castro, D.S., and Guillemot, F. (2002). Proneural genes and the specification of neural cell types. Nat Rev Neurosci *3*, 517-530.

Betizeau, M., Cortay, V., Patti, D., Pfister, S., Gautier, E., Bellemin-Ménard, A., Afanassieff, M., Huissoud, C., Douglas, R.J., Kennedy, H.*, et al.* (2013). Precursor diversity and complexity of lineage relationships in the outer subventricular zone of the primate. Neuron *80*, 442-457.

Blackburn, D., Sargsyan, S., Monk, P.N., and Shaw, P.J. (2009). Astrocyte function and role in motor neuron disease: a future therapeutic target? Glia *57*, 1251-1264.

Bryant, H.E., Schultz, N., Thomas, H.D., Parker, K.M., Flower, D., Lopez, E., Kyle, S., Meuth, M., Curtin, N.J., and Helleday, T. (2005). Specific killing of BRCA2-deficient tumours with inhibitors of poly(ADP-ribose) polymerase. Nature *434*, 913-917.

Buck, D., Malivert, L., de Chasseval, R., Barraud, A., Fondanèche, M.C., Sanal, O., Plebani, A., Stéphan, J.L., Hufnagel, M., le Deist, F.*, et al.* (2006). Cernunnos, a novel nonhomologous end-joining factor, is mutated in human immunodeficiency with microcephaly. Cell *124*, 287-299.

Bultje, R.S., Castaneda-Castellanos, D.R., Jan, L.Y., Jan, Y.N., Kriegstein, A.R., and Shi, S.H. (2009). Mammalian Par3 regulates progenitor cell asymmetric division via notch signaling in the developing neocortex. Neuron *63*, 189-202.

Butt, S.J., Fuccillo, M., Nery, S., Noctor, S., Kriegstein, A., Corbin, J.G., and Fishell, G. (2005). The temporal and spatial origins of cortical interneurons predict their physiological subtype. Neuron *48*, 591-604.

Cai, Y., Jin, J., Yao, T., Gottschalk, A.J., Swanson, S.K., Wu, S., Shi, Y., Washburn, M.P., Florens, L., Conaway, R.C.*, et al.* (2007). YY1 functions with INO80 to activate transcription. Nat Struct Mol Biol *14*, 872-874.

Ceccaldi, R., Liu, J.C., Amunugama, R., Hajdu, I., Primack, B., Petalcorin, M.I., O'Connor, K.W., Konstantinopoulos, P.A., Elledge, S.J., Boulton, S.J.*, et al.* (2015). Homologous-recombination-deficient tumours are dependent on Polθ-mediated repair. Nature *518*, 258-262.

Ceccaldi, R., Rondinelli, B., and D'Andrea, A.D. (2016). Repair Pathway Choices and Consequences at the Double-Strand Break. Trends Cell Biol *26*, 52-64.

Chambers, A.L., and Downs, J.A. (2012). The RSC and INO80 chromatin-remodeling complexes in DNA double-strand break repair. Prog Mol Biol Transl Sci *110*, 229-261.

Chen, L., Cai, Y., Jin, J., Florens, L., Swanson, S.K., Washburn, M.P., Conaway, J.W., and Conaway, R.C. (2011). Subunit organization of the human INO80 chromatin remodeling complex: an evolutionarily conserved core complex catalyzes ATP-dependent nucleosome remodeling. J Biol Chem *286*, 11283-11289.

Chen, P.L., Chen, C.F., Chen, Y., Xiao, J., Sharp, Z.D., and Lee, W.H. (1998). The BRC repeats in BRCA2 are critical for RAD51 binding and resistance to methyl methanesulfonate treatment. Proc Natl Acad Sci U S A *95*, 5287-5292.

Cheng, Q., and Chen, J. (2010). Mechanism of p53 stabilization by ATM after DNA damage. Cell Cycle *9*, 472-478.

Chenn, A., and McConnell, S.K. (1995). Cleavage orientation and the asymmetric inheritance of Notch1 immunoreactivity in mammalian neurogenesis. Cell *82*, 631-641.

Chizhikov, V.V., Lindgren, A.G., Currle, D.S., Rose, M.F., Monuki, E.S., and Millen, K.J. (2006). The roof plate regulates cerebellar cell-type specification and proliferation. Development *133*, 2793-2804.

Chou, S.J., Perez-Garcia, C.G., Kroll, T.T., and O'Leary, D.D. (2009). Lhx2 specifies regional fate in Emx1 lineage of telencephalic progenitors generating cerebral cortex. Nat Neurosci *12*, 1381-1389.

Chronister, W.D., Burbulis, I.E., Wierman, M.B., Wolpert, M.J., Haakenson, M.F., Smith, A.C.B., Kleinman, J.E., Hyde, T.M., Weinberger, D.R., Bekiranov, S.*, et al.* (2019). Neurons with Complex Karyotypes Are Rare in Aged Human Neocortex. Cell Rep *26*, 825-835.e827.

Clouaire, T., Rocher, V., Lashgari, A., Arnould, C., Aguirrebengoa, M., Biernacka, A., Skrzypczak, M., Aymard, F., Fongang, B., Dojer, N.*, et al.* (2018). Comprehensive Mapping of Histone Modifications at DNA Double-Strand Breaks Deciphers Repair Pathway Chromatin Signatures. Mol Cell *72*, 250-262.e256.

Costelloe, T., Louge, R., Tomimatsu, N., Mukherjee, B., Martini, E., Khadaroo, B., Dubois, K., Wiegant, W.W., Thierry, A., Burma, S.*, et al.* (2012). The yeast Fun30 and human SMARCAD1 chromatin remodellers promote DNA end resection. Nature *489*, 581-584.

Couëdel, C., Mills, K.D., Barchi, M., Shen, L., Olshen, A., Johnson, R.D., Nussenzweig, A., Essers, J., Kanaar, R., Li, G.C.*, et al.* (2004). Collaboration of homologous recombination and nonhomologous end-joining factors for the survival and integrity of mice and cells. Genes Dev *18*, 1293-1304.

Cárdenas, A., Villalba, A., de Juan Romero, C., Picó, E., Kyrousi, C., Tzika, A.C., Tessier-Lavigne, M., Ma, L., Drukker, M., Cappello, S.*, et al.* (2018). Evolution of

Cortical Neurogenesis in Amniotes Controlled by Robo Signaling Levels. Cell *174*, 590-606.e521.

D'Gama, A.M., Woodworth, M.B., Hossain, A.A., Bizzotto, S., Hatem, N.E., LaCoursiere, C.M., Najm, I., Ying, Z., Yang, E., Barkovich, A.J.*, et al.* (2017). Somatic Mutations Activating the mTOR Pathway in Dorsal Telencephalic Progenitors Cause a Continuum of Cortical Dysplasias. Cell Rep *21*, 3754-3766.

Dang, L., Yoon, K., Wang, M., and Gaiano, N. (2006). Notch3 signaling promotes radial glial/progenitor character in the mammalian telencephalon. Dev Neurosci *28*, 58-69.

Davis, A.J., and Chen, D.J. (2013). DNA double strand break repair via non-homologous end-joining. Transl Cancer Res *2*, 130-143.

De Rubeis, S., He, X., Goldberg, A.P., Poultney, C.S., Samocha, K., Ercument Cicek, A., Kou, Y., Liu, L., Fromer, M., Walker, S.*, et al.* (2014). Synaptic, transcriptional and chromatin genes disrupted in autism. Nature *515*, 209-215.

DeFelipe, J., López-Cruz, P.L., Benavides-Piccione, R., Bielza, C., Larrañaga, P., Anderson, S., Burkhalter, A., Cauli, B., Fairén, A., Feldmeyer, D.*, et al.* (2013). New insights into the classification and nomenclature of cortical GABAergic interneurons. Nat Rev Neurosci *14*, 202-216.

Dekkers, M.P., Nikoletopoulou, V., and Barde, Y.A. (2013). Cell biology in neuroscience: Death of developing neurons: new insights and implications for connectivity. J Cell Biol *203*, 385-393.

Dobin, A., Davis, C.A., Schlesinger, F., Drenkow, J., Zaleski, C., Jha, S., Batut, P., Chaisson, M., and Gingeras, T.R. (2013). STAR: ultrafast universal RNA-seq aligner. Bioinformatics *29*, 15-21.

Domchek, S.M., Tang, J., Stopfer, J., Lilli, D.R., Hamel, N., Tischkowitz, M., Monteiro, A.N., Messick, T.E., Powers, J., Yonker, A.*, et al.* (2013). Biallelic deleterious BRCA1 mutations in a woman with early-onset ovarian cancer. Cancer Discov *3*, 399-405.

Dwyer, N.D., Chen, B., Chou, S.J., Hippenmeyer, S., Nguyen, L., and Ghashghaei, H.T. (2016). Neural Stem Cells to Cerebral Cortex: Emerging Mechanisms Regulating Progenitor Behavior and Productivity. J Neurosci *36*, 11394-11401.

Ebbert, R., Birkmann, A., and Schüller, H.J. (1999). The product of the SNF2/SWI2 paralogue INO80 of Saccharomyces cerevisiae required for efficient expression of various yeast structural genes is part of a high-molecular-weight protein complex. Mol Microbiol *32*, 741-751.

Fenech, M., Kirsch-Volders, M., Natarajan, A.T., Surralles, J., Crott, J.W., Parry, J., Norppa, H., Eastmond, D.A., Tucker, J.D., and Thomas, P. (2011). Molecular mechanisms of micronucleus, nucleoplasmic bridge and nuclear bud formation in mammalian and human cells. Mutagenesis *26*, 125-132.

Fenlon, L.R., Liu, S., Gobius, I., Kurniawan, N.D., Murphy, S., Moldrich, R.X., and Richards, L.J. (2015). Formation of functional areas in the cerebral cortex is disrupted in a mouse model of autism spectrum disorder. Neural Dev *10*, 10.

Fischl, B., and Dale, A.M. (2000). Measuring the thickness of the human cerebral cortex from magnetic resonance images. Proc Natl Acad Sci U S A *97*, 11050-11055.

Frank, K.M., Sharpless, N.E., Gao, Y., Sekiguchi, J.M., Ferguson, D.O., Zhu, C., Manis, J.P., Horner, J., DePinho, R.A., and Alt, F.W. (2000). DNA ligase IV deficiency in mice leads to defective neurogenesis and embryonic lethality via the p53 pathway. Mol Cell *5*, 993-1002.

Frappart, P.O., Lee, Y., Lamont, J., and McKinnon, P.J. (2007). BRCA2 is required for neurogenesis and suppression of medulloblastoma. EMBO J *26*, 2732-2742.

Freed, D., and Pevsner, J. (2016). The Contribution of Mosaic Variants to Autism Spectrum Disorder. PLoS Genet *12*, e1006245.

Fritsch, O., Benvenuto, G., Bowler, C., Molinier, J., and Hohn, B. (2004). The INO80 protein controls homologous recombination in Arabidopsis thaliana. Mol Cell *16*, 479-485.

Gabriele, M., Lopez Tobon, A., D'Agostino, G., and Testa, G. (2018). The chromatin basis of neurodevelopmental disorders: Rethinking dysfunction along the molecular and temporal axes. Prog Neuropsychopharmacol Biol Psychiatry *84*, 306-327.

Gabriele, M., Vulto-van Silfhout, A.T., Germain, P.L., Vitriolo, A., Kumar, R., Douglas, E., Haan, E., Kosaki, K., Takenouchi, T., Rauch, A.*, et al.* (2017). YY1 Haploinsufficiency Causes an Intellectual Disability Syndrome Featuring Transcriptional and Chromatin Dysfunction. Am J Hum Genet *100*, 907-925.

Gallegos, D.A., Chan, U., Chen, L.F., and West, A.E. (2018). Chromatin Regulation of Neuronal Maturation and Plasticity. Trends Neurosci *41*, 311-324.

Gao, Y., Ferguson, D.O., Xie, W., Manis, J.P., Sekiguchi, J., Frank, K.M., Chaudhuri, J., Horner, J., DePinho, R.A., and Alt, F.W. (2000). Interplay of p53 and DNA-repair protein XRCC4 in tumorigenesis, genomic stability and development. Nature *404*, 897-900.

Gao, Y., Sun, Y., Frank, K.M., Dikkes, P., Fujiwara, Y., Seidl, K.J., Sekiguchi, J.M., Rathbun, G.A., Swat, W., Wang, J.*, et al.* (1998). A critical role for DNA end-joining proteins in both lymphogenesis and neurogenesis. Cell *95*, 891-902.

Ghouzzi, V.E., Bianchi, F.T., Molineris, I., Mounce, B.C., Berto, G.E., Rak, M., Lebon, S., Aubry, L., Tocco, C., Gai, M.*, et al.* (2016). ZIKA virus elicits P53 activation and genotoxic stress in human neural progenitors similar to mutations involved in severe forms of genetic microcephaly. Cell Death Dis *7*, e2440.

Glasser, M.F., Coalson, T.S., Robinson, E.C., Hacker, C.D., Harwell, J., Yacoub, E., Ugurbil, K., Andersson, J., Beckmann, C.F., Jenkinson, M.*, et al.* (2016). A multi-modal parcellation of human cerebral cortex. Nature *536*, 171-178.

Goebbels, S., Bormuth, I., Bode, U., Hermanson, O., Schwab, M.H., and Nave, K.A. (2006). Genetic targeting of principal neurons in neocortex and hippocampus of NEX-Cre mice. Genesis *44*, 611-621.

Goodarzi, A.A., Noon, A.T., Deckbar, D., Ziv, Y., Shiloh, Y., Löbrich, M., and Jeggo, P.A. (2008). ATM signaling facilitates repair of DNA double-strand breaks associated with heterochromatin. Mol Cell *31*, 167-177.

Gorski, J.A., Talley, T., Qiu, M., Puelles, L., Rubenstein, J.L., and Jones, K.R. (2002). Cortical excitatory neurons and glia, but not GABAergic neurons, are produced in the Emx1-expressing lineage. J Neurosci *22*, 6309-6314.

Groth, A., Rocha, W., Verreault, A., and Almouzni, G. (2007). Chromatin challenges during DNA replication and repair. Cell *128*, 721-733.

Guo, T., Feng, Y.L., Xiao, J.J., Liu, Q., Sun, X.N., Xiang, J.F., Kong, N., Liu, S.C., Chen, G.Q., Wang, Y.*, et al.* (2018). Harnessing accurate non-homologous end joining for efficient precise deletion in CRISPR/Cas9-mediated genome editing. Genome Biol *19*, 170.

Hansen, D.V., Lui, J.H., Parker, P.R., and Kriegstein, A.R. (2010). Neurogenic radial glia in the outer subventricular zone of human neocortex. Nature *464*, 554-561.

Harhaj, N.S., and Antonetti, D.A. (2004). Regulation of tight junctions and loss of barrier function in pathophysiology. Int J Biochem Cell Biol *36*, 1206-1237.

Haydar, T.F., Ang, E., and Rakic, P. (2003). Mitotic spindle rotation and mode of cell division in the developing telencephalon. Proc Natl Acad Sci U S A *100*, 2890-2895.

Hendry, S.H., Schwark, H.D., Jones, E.G., and Yan, J. (1987). Numbers and proportions of GABA-immunoreactive neurons in different areas of monkey cerebral cortex. J Neurosci *7*, 1503-1519.

Hicks, S.P., and D'Amato, C.J. (1968). Cell migrations to the isocortex in the rat. Anat Rec *160*, 619-634.

Hong, S., Beja-Glasser, V.F., Nfonoyim, B.M., Frouin, A., Li, S., Ramakrishnan, S., Merry, K.M., Shi, Q., Rosenthal, A., Barres, B.A.*, et al.* (2016). Complement and microglia mediate early synapse loss in Alzheimer mouse models. Science *352*, 712-716.

Hubel, D.H., and Wiesel, T.N. (1969). Anatomical demonstration of columns in the monkey striate cortex. Nature *221*, 747-750.

Hur, S.K., Park, E.J., Han, J.E., Kim, Y.A., Kim, J.D., Kang, D., and Kwon, J. (2010). Roles of human INO80 chromatin remodeling enzyme in DNA replication and chromosome segregation suppress genome instability. Cell Mol Life Sci *67*, 2283-2296.

Hébert, J.M., and McConnell, S.K. (2000). Targeting of cre to the Foxg1 (BF-1) locus mediates loxP recombination in the telencephalon and other developing head structures. Dev Biol *222*, 296-306.

Iacopetti, P., Michelini, M., Stuckmann, I., Oback, B., Aaku-Saraste, E., and Huttner, W.B. (1999). Expression of the antiproliferative gene TIS21 at the onset of neurogenesis identifies single neuroepithelial cells that switch from proliferative to neuron-generating division. Proc Natl Acad Sci U S A *96*, 4639-4644.

Iwase, S., and Martin, D.M. (2018). Chromatin in nervous system development and disease. Mol Cell Neurosci *87*, 1-3.

Jackson, A.P., Eastwood, H., Bell, S.M., Adu, J., Toomes, C., Carr, I.M., Roberts, E., Hampshire, D.J., Crow, Y.J., Mighell, A.J.*, et al.* (2002). Identification of microcephalin, a protein implicated in determining the size of the human brain. Am J Hum Genet *71*, 136-142.

Jamuar, S.S., Lam, A.T., Kircher, M., D'Gama, A.M., Wang, J., Barry, B.J., Zhang, X., Hill, R.S., Partlow, J.N., Rozzo, A.*, et al.* (2014). Somatic mutations in cerebral cortical malformations. N Engl J Med *371*, 733-743.

Jonkers, J., Meuwissen, R., van der Gulden, H., Peterse, H., van der Valk, M., and Berns, A. (2001). Synergistic tumor suppressor activity of BRCA2 and p53 in a conditional mouse model for breast cancer. Nat Genet *29*, 418-425.

Kageyama, R., Ohtsuka, T., and Kobayashi, T. (2007). The Hes gene family: repressors and oscillators that orchestrate embryogenesis. Development *134*, 1243-1251.

Kastenhuber, E.R., and Lowe, S.W. (2017). Putting p53 in Context. Cell *170*, 1062-1078.

Keil, R.L., and McWilliams, A.D. (1993). A gene with specific and global effects on recombination of sequences from tandemly repeated genes in Saccharomyces cerevisiae. Genetics *135*, 711-718.

Klopf, E., Paskova, L., Solé, C., Mas, G., Petryshyn, A., Posas, F., Wintersberger, U., Ammerer, G., and Schüller, C. (2009). Cooperation between the INO80 complex and histone chaperones determines adaptation of stress gene transcription in the yeast Saccharomyces cerevisiae. Mol Cell Biol *29*, 4994-5007.

Komatsu, K. (2016). NBS1 and multiple regulations of DNA damage response. J Radiat Res *57 Suppl 1*, i11-i17.

Kornack, D.R., and Rakic, P. (1998). Changes in cell-cycle kinetics during the development and evolution of primate neocortex. Proc Natl Acad Sci U S A *95*, 1242-1246.

Krupp, D.R., Barnard, R.A., Duffourd, Y., Evans, S.A., Mulqueen, R.M., Bernier, R., Rivière, J.B., Fombonne, E., and O'Roak, B.J. (2017). Exonic Mosaic Mutations Contribute Risk for Autism Spectrum Disorder. Am J Hum Genet *101*, 369-390.

Kwan, K.Y., Sestan, N., and Anton, E.S. (2012). Transcriptional co-regulation of neuronal migration and laminar identity in the neocortex. Development *139*, 1535-1546.

Lademann, C.A., Renkawitz, J., Pfander, B., and Jentsch, S. (2017). The INO80 Complex Removes H2A.Z to Promote Presynaptic Filament Formation during Homologous Recombination. Cell Rep *19*, 1294-1303.

Lee, H.S., Lee, S.A., Hur, S.K., Seo, J.W., and Kwon, J. (2014). Stabilization and targeting of INO80 to replication forks by BAP1 during normal DNA synthesis. Nat Commun *5*, 5128.

Lee, Y., Katyal, S., Downing, S.M., Zhao, J., Russell, H.R., and McKinnon, P.J. (2012). Neurogenesis requires TopBP1 to prevent catastrophic replicative DNA damage in early progenitors. Nat Neurosci *15*, 819-826.

Lek, M., Karczewski, K.J., Minikel, E.V., Samocha, K.E., Banks, E., Fennell, T., O'Donnell-Luria, A.H., Ware, J.S., Hill, A.J., Cummings, B.B.*, et al.* (2016). Analysis of protein-coding genetic variation in 60,706 humans. Nature *536*, 285-291.

Liang, H., Hippenmeyer, S., and Ghashghaei, H.T. (2012). A Nestin-cre transgenic mouse is insufficient for recombination in early embryonic neural progenitors. Biol Open *1*, 1200-1203.

Lieber, M.R. (2010). The mechanism of double-strand DNA break repair by the nonhomologous DNA end-joining pathway. Annu Rev Biochem *79*, 181-211.

Lim, D.S., and Hasty, P. (1996). A mutation in mouse rad51 results in an early embryonic lethal that is suppressed by a mutation in p53. Mol Cell Biol *16*, 7133-7143.

Lim, D.S., Vogel, H., Willerford, D.M., Sands, A.T., Platt, K.A., and Hasty, P. (2000). Analysis of ku80-mutant mice and cells with deficient levels of p53. Mol Cell Biol *20*, 3772-3780.

Luijsterburg, M.S., de Krijger, I., Wiegant, W.W., Shah, R.G., Smeenk, G., de Groot, A.J.L., Pines, A., Vertegaal, A.C.O., Jacobs, J.J.L., Shah, G.M.*, et al.* (2016). PARP1 Links CHD2-Mediated Chromatin Expansion and H3.3 Deposition to DNA Repair by Non-homologous End-Joining. Mol Cell *61*, 547-562.

Mallamaci, A., Mercurio, S., Muzio, L., Cecchi, C., Pardini, C.L., Gruss, P., and Boncinelli, E. (2000). The lack of Emx2 causes impairment of Reelin signaling and

defects of neuronal migration in the developing cerebral cortex. J Neurosci *20*, 1109-1118.

Mao, H., McMahon, J.J., Tsai, Y.H., Wang, Z., and Silver, D.L. (2016). Haploinsufficiency for Core Exon Junction Complex Components Disrupts Embryonic Neurogenesis and Causes p53-Mediated Microcephaly. PLoS Genet *12*, e1006282.

Mao, Z., Bozzella, M., Seluanov, A., and Gorbunova, V. (2008). Comparison of nonhomologous end joining and homologous recombination in human cells. DNA Repair (Amst) *7*, 1765-1771.

Marino, S., Vooijs, M., van Der Gulden, H., Jonkers, J., and Berns, A. (2000). Induction of medulloblastomas in p53-null mutant mice by somatic inactivation of Rb in the external granular layer cells of the cerebellum. Genes Dev *14*, 994-1004.

Maréchal, A., and Zou, L. (2013). DNA damage sensing by the ATM and ATR kinases. Cold Spring Harb Perspect Biol *5*.

Mason, H.A., Rakowiecki, S.M., Raftopoulou, M., Nery, S., Huang, Y., Gridley, T., and Fishell, G. (2005). Notch signaling coordinates the patterning of striatal compartments. Development *132*, 4247-4258.

McConnell, M.J., Lindberg, M.R., Brennand, K.J., Piper, J.C., Voet, T., Cowing-Zitron, C., Shumilina, S., Lasken, R.S., Vermeesch, J.R., Hall, I.M.*, et al.* (2013). Mosaic copy number variation in human neurons. Science *342*, 632-637.

McConnell, M.J., Moran, J.V., Abyzov, A., Akbarian, S., Bae, T., Cortes-Ciriano, I., Erwin, J.A., Fasching, L., Flasch, D.A., Freed, D.*, et al.* (2017). Intersection of diverse neuronal genomes and neuropsychiatric disease: The Brain Somatic Mosaicism Network. Science *356*.

McKinley, K.L., and Cheeseman, I.M. (2017). Large-Scale Analysis of CRISPR/Cas9 Cell-Cycle Knockouts Reveals the Diversity of p53-Dependent Responses to Cell-Cycle Defects. Dev Cell *40*, 405-420.e402.

McKinnon, P.J. (2013). Maintaining genome stability in the nervous system. Nat Neurosci *16*, 1523-1529.

McSherry, G.M., and Smart, I.H. (1986). Cell production gradients in the developing ferret isocortex. J Anat *144*, 1-14.

Mendenhall, E.M., Koche, R.P., Truong, T., Zhou, V.W., Issac, B., Chi, A.S., Ku, M., and Bernstein, B.E. (2010). GC-rich sequence elements recruit PRC2 in mammalian ES cells. PLoS Genet *6*, e1001244.

Mokrani-Benhelli, H., Gaillard, L., Biasutto, P., Le Guen, T., Touzot, F., Vasquez, N., Komatsu, J., Conseiller, E., Pïcard, C., Gluckman, E.*, et al.* (2013). Primary

microcephaly, impaired DNA replication, and genomic instability caused by compound heterozygous ATR mutations. Hum Mutat *34*, 374-384.

Monuki, E.S., Porter, F.D., and Walsh, C.A. (2001). Patterning of the dorsal telencephalon and cerebral cortex by a roof plate-Lhx2 pathway. Neuron *32*, 591-604.

Mountcastle, V.B. (1997). The columnar organization of the neocortex. Brain *120 (Pt 4)*, 701-722.

Mountcastle, V.B., Davies, P.W., and Berman, A.L. (1957). Response properties of neurons of cat's somatic sensory cortex to peripheral stimuli. J Neurophysiol *20*, 374-407.

Moynahan, M.E., and Jasin, M. (2010). Mitotic homologous recombination maintains genomic stability and suppresses tumorigenesis. Nat Rev Mol Cell Biol *11*, 196-207.

Neumann, H., Kotter, M.R., and Franklin, R.J. (2009). Debris clearance by microglia: an essential link between degeneration and regeneration. Brain *132*, 288-295.

O'Driscoll, M., Cerosaletti, K.M., Girard, P.M., Dai, Y., Stumm, M., Kysela, B., Hirsch, B., Gennery, A., Palmer, S.E., Seidel, J.*, et al.* (2001). DNA ligase IV mutations identified in patients exhibiting developmental delay and immunodeficiency. Mol Cell *8*, 1175-1185.

Orii, K.E., Lee, Y., Kondo, N., and McKinnon, P.J. (2006). Selective utilization of nonhomologous end-joining and homologous recombination DNA repair pathways during nervous system development. Proc Natl Acad Sci U S A *103*, 10017-10022.

Papamichos-Chronakis, M., Watanabe, S., Rando, O.J., and Peterson, C.L. (2011). Global regulation of H2A.Z localization by the INO80 chromatin-remodeling enzyme is essential for genome integrity. Cell *144*, 200-213.

Paul, L.K., Brown, W.S., Adolphs, R., Tyszka, J.M., Richards, L.J., Mukherjee, P., and Sherr, E.H. (2007). Agenesis of the corpus callosum: genetic, developmental and functional aspects of connectivity. Nat Rev Neurosci *8*, 287-299.

Pellegrini, L., Yu, D.S., Lo, T., Anand, S., Lee, M., Blundell, T.L., and Venkitaraman, A.R. (2002). Insights into DNA recombination from the structure of a RAD51-BRCA2 complex. Nature *420*, 287-293.

Pelvig, D.P., Pakkenberg, H., Stark, A.K., and Pakkenberg, B. (2008). Neocortical glial cell numbers in human brains. Neurobiol Aging *29*, 1754-1762.

Poduri, A., Evrony, G.D., Cai, X., Elhosary, P.C., Beroukhim, R., Lehtinen, M.K., Hills, L.B., Heinzen, E.L., Hill, A., Hill, R.S.*, et al.* (2012). Somatic activation of AKT3 causes hemispheric developmental brain malformations. Neuron *74*, 41-48.

Pontious, A., Kowalczyk, T., Englund, C., and Hevner, R.F. (2008). Role of intermediate progenitor cells in cerebral cortex development. Dev Neurosci *30*, 24-32.

Prigge, J.R., Wiley, J.A., Talago, E.A., Young, E.M., Johns, L.L., Kundert, J.A., Sonsteng, K.M., Halford, W.P., Capecchi, M.R., and Schmidt, E.E. (2013). Nuclear double-fluorescent reporter for in vivo and ex vivo analyses of biological transitions in mouse nuclei. Mamm Genome.

Pulvers, J.N., and Huttner, W.B. (2009). Brca1 is required for embryonic development of the mouse cerebral cortex to normal size by preventing apoptosis of early neural progenitors. Development *136*, 1859-1868.

Qiu, Z., Elsayed, Z., Peterkin, V., Alkatib, S., Bennett, D., and Landry, J.W. (2016). Ino80 is essential for proximal-distal axis asymmetry in part by regulating Bmp4 expression. BMC Biol *14*, 18.

Qvist, P., Huertas, P., Jimeno, S., Nyegaard, M., Hassan, M.J., Jackson, S.P., and Børglum, A.D. (2011). CtIP Mutations Cause Seckel and Jawad Syndromes. PLoS Genet *7*, e1002310.

Rakic, P. (1972). Mode of cell migration to the superficial layers of fetal monkey neocortex. J Comp Neurol *145*, 61-83.

Rakic, P. (1988). Specification of cerebral cortical areas. Science *241*, 170-176.

Rakic, P. (1995). A small step for the cell, a giant leap for mankind: a hypothesis of neocortical expansion during evolution. Trends Neurosci *18*, 383-388.

Ran, F.A., Hsu, P.D., Wright, J., Agarwala, V., Scott, D.A., and Zhang, F. (2013). Genome engineering using the CRISPR-Cas9 system. Nat Protoc *8*, 2281-2308.

Rash, B.G., Lim, H.D., Breunig, J.J., and Vaccarino, F.M. (2011). FGF signaling expands embryonic cortical surface area by regulating Notch-dependent neurogenesis. J Neurosci *31*, 15604-15617.

Ratnaparkhe, M., Wong, J.K.L., Wei, P.C., Hlevnjak, M., Kolb, T., Simovic, M., Haag, D., Paul, Y., Devens, F., Northcott, P.*, et al.* (2018). Defective DNA damage repair leads to frequent catastrophic genomic events in murine and human tumors. Nat Commun *9*, 4760.

Reillo, I., and Borrell, V. (2012). Germinal zones in the developing cerebral cortex of ferret: ontogeny, cell cycle kinetics, and diversity of progenitors. Cereb Cortex *22*, 2039-2054.

Robinson, M.D., McCarthy, D.J., and Smyth, G.K. (2010). edgeR: a Bioconductor package for differential expression analysis of digital gene expression data. Bioinformatics *26*, 139-140.

Rodgers, K., and McVey, M. (2016). Error-Prone Repair of DNA Double-Strand Breaks. J Cell Physiol *231*, 15-24.

Routh, A., Head, S.R., Ordoukhanian, P., and Johnson, J.E. (2015). ClickSeq: Fragmentation-Free Next-Generation Sequencing via Click Ligation of Adaptors to Stochastically Terminated 3'-Azido cDNAs. J Mol Biol *427*, 2610-2616.

Sanders, S.J., He, X., Willsey, A.J., Ercan-Sencicek, A.G., Samocha, K.E., Cicek, A.E., Murtha, M.T., Bal, V.H., Bishop, S.L., Dong, S.*, et al.* (2015). Insights into Autism Spectrum Disorder Genomic Architecture and Biology from 71 Risk Loci. Neuron *87*, 1215-1233.

Savic, V., Yin, B., Maas, N.L., Bredemeyer, A.L., Carpenter, A.C., Helmink, B.A., Yang-lott, K.S., Sleckman, B.P., and Bassing, C.H. (2009). Formation of dynamic gamma-H2AX domains along broken DNA strands is distinctly regulated by ATM and MDC1 and dependent upon H2AX densities in chromatin. Mol Cell *34*, 298-310.

Schnack, H.G., van Haren, N.E., Brouwer, R.M., Evans, A., Durston, S., Boomsma, D.I., Kahn, R.S., and Hulshoff Pol, H.E. (2015). Changes in thickness and surface area of the human cortex and their relationship with intelligence. Cereb Cortex *25*, 1608-1617.

Sekiguchi, J., Ferguson, D.O., Chen, H.T., Yang, E.M., Earle, J., Frank, K., Whitlow, S., Gu, Y., Xu, Y., Nussenzweig, A.*, et al.* (2001). Genetic interactions between ATM and the nonhomologous end-joining factors in genomic stability and development. Proc Natl Acad Sci U S A *98*, 3243-3248.

Shen, X., Mizuguchi, G., Hamiche, A., and Wu, C. (2000). A chromatin remodelling complex involved in transcription and DNA processing. Nature *406*, 541-544.

Shetty, A.S., Godbole, G., Maheshwari, U., Padmanabhan, H., Chaudhary, R., Muralidharan, B., Hou, P.S., Monuki, E.S., Kuo, H.C., Rema, V.*, et al.* (2013). Lhx2 regulates a cortex-specific mechanism for barrel formation. Proc Natl Acad Sci U S A *110*, E4913-4921.

Singer, T., McConnell, M.J., Marchetto, M.C., Coufal, N.G., and Gage, F.H. (2010). LINE-1 retrotransposons: mediators of somatic variation in neuronal genomes? Trends Neurosci *33*, 345-354.

Smith, T., Heger, A., and Sudbery, I. (2017). UMI-tools: modeling sequencing errors in Unique Molecular Identifiers to improve quantification accuracy. Genome Res *27*, 491-499.

Sokpor, G., Castro-Hernandez, R., Rosenbusch, J., Staiger, J.F., and Tuoc, T. (2018). ATP-Dependent Chromatin Remodeling During Cortical Neurogenesis. Front Neurosci *12*, 226.

Sokpor, G., Xie, Y., Rosenbusch, J., and Tuoc, T. (2017). Chromatin Remodeling BAF (SWI/SNF) Complexes in Neural Development and Disorders. Front Mol Neurosci *10*, 243.

Souza, B.S., Sampaio, G.L., Pereira, C.S., Campos, G.S., Sardi, S.I., Freitas, L.A., Figueira, C.P., Paredes, B.D., Nonaka, C.K., Azevedo, C.M.*, et al.* (2016). Zika virus infection induces mitosis abnormalities and apoptotic cell death of human neural progenitor cells. Sci Rep *6*, 39775.

Srinivas, S., Watanabe, T., Lin, C.S., William, C.M., Tanabe, Y., Jessell, T.M., and Costantini, F. (2001). Cre reporter strains produced by targeted insertion of EYFP and ECFP into the ROSA26 locus. BMC Dev Biol *1*, 4.

Stoeckli, E.T. (2018). Understanding axon guidance: are we nearly there yet? Development *145*.

Subramanian, V., Fields, P.A., and Boyer, L.A. (2015). H2A.Z: a molecular rheostat for transcriptional control. F1000Prime Rep *7*, 01.

Sy, S.M., Huen, M.S., and Chen, J. (2009). PALB2 is an integral component of the BRCA complex required for homologous recombination repair. Proc Natl Acad Sci U S A *106*, 7155-7160.

Takahashi, T., Goto, T., Miyama, S., Nowakowski, R.S., and Caviness, V.S. (1999). Sequence of neuron origin and neocortical laminar fate: relation to cell cycle of origin in the developing murine cerebral wall. J Neurosci *19*, 10357-10371.

Tang, H., Hammack, C., Ogden, S.C., Wen, Z., Qian, X., Li, Y., Yao, B., Shin, J., Zhang, F., Lee, E.M.*, et al.* (2016). Zika Virus Infects Human Cortical Neural Progenitors and Attenuates Their Growth. Cell Stem Cell *18*, 587-590.

Toki, T., Yoshida, K., Wang, R., Nakamura, S., Maekawa, T., Goi, K., Katoh, M.C., Mizuno, S., Sugiyama, F., Kanezaki, R.*, et al.* (2018). De Novo Mutations Activating Germline TP53 in an Inherited Bone-Marrow-Failure Syndrome. Am J Hum Genet *103*, 440-447.

Tsien, J.Z., Chen, D.F., Gerber, D., Tom, C., Mercer, E.H., Anderson, D.J., Mayford, M., Kandel, E.R., and Tonegawa, S. (1996). Subregion- and cell type-restricted gene knockout in mouse brain. Cell *87*, 1317-1326.

Turrero García, M., Chang, Y., Arai, Y., and Huttner, W.B. (2016). S-phase duration is the main target of cell cycle regulation in neural progenitors of developing ferret neocortex. J Comp Neurol *524*, 456-470.

Vallianatos, C.N., and Iwase, S. (2015). Disrupted intricacy of histone H3K4 methylation in neurodevelopmental disorders. Epigenomics *7*, 503-519.

van Attikum, H., Fritsch, O., Hohn, B., and Gasser, S.M. (2004). Recruitment of the INO80 complex by H2A phosphorylation links ATP-dependent chromatin remodeling with DNA double-strand break repair. Cell *119*, 777-788.

Vilenchik, M.M., and Knudson, A.G. (2003). Endogenous DNA double-strand breaks: production, fidelity of repair, and induction of cancer. Proc Natl Acad Sci U S A *100*, 12871-12876.

Voehringer, D., Liang, H.E., and Locksley, R.M. (2008). Homeostasis and effector function of lymphopenia-induced "memory-like" T cells in constitutively T cell-depleted mice. J Immunol *180*, 4742-4753.

Walker, J.R., Corpina, R.A., and Goldberg, J. (2001). Structure of the Ku heterodimer bound to DNA and its implications for double-strand break repair. Nature *412*, 607-614.

Wang, X., Tsai, J.W., LaMonica, B., and Kriegstein, A.R. (2011). A new subtype of progenitor cell in the mouse embryonic neocortex. Nat Neurosci *14*, 555-561.

Watanabe, R., Ui, A., Kanno, S., Ogiwara, H., Nagase, T., Kohno, T., and Yasui, A. (2014). SWI/SNF factors required for cellular resistance to DNA damage include ARID1A and ARID1B and show interdependent protein stability. Cancer Res *74*, 2465-2475.

Wei, P.C., Chang, A.N., Kao, J., Du, Z., Meyers, R.M., Alt, F.W., and Schwer, B. (2016). Long Neural Genes Harbor Recurrent DNA Break Clusters in Neural Stem/Progenitor Cells. Cell *164*, 644-655.

Weinstock, D.M., Nakanishi, K., Helgadottir, H.R., and Jasin, M. (2006). Assaying double-strand break repair pathway choice in mammalian cells using a targeted endonuclease or the RAG recombinase. Methods Enzymol *409*, 524-540.

Whelan, D.R., Lee, W.T.C., Yin, Y., Ofri, D.M., Bermudez-Hernandez, K., Keegan, S., Fenyo, D., and Rothenberg, E. (2018). Spatiotemporal dynamics of homologous recombination repair at single collapsed replication forks. Nat Commun *9*, 3882.

White, D., Rafalska-Metcalf, I.U., Ivanov, A.V., Corsinotti, A., Peng, H., Lee, S.C., Trono, D., Janicki, S.M., and Rauscher, F.J. (2012). The ATM substrate KAP1 controls DNA repair in heterochromatin: regulation by HP1 proteins and serine 473/824 phosphorylation. Mol Cancer Res *10*, 401-414.

Wilson, T.E., Arlt, M.F., Park, S.H., Rajendran, S., Paulsen, M., Ljungman, M., and Glover, T.W. (2015). Large transcription units unify copy number variants and common fragile sites arising under replication stress. Genome Res *25*, 189-200.

Wong, A.K., Pero, R., Ormonde, P.A., Tavtigian, S.V., and Bartel, P.L. (1997). RAD51 interacts with the evolutionarily conserved BRC motifs in the human breast cancer susceptibility gene brca2. J Biol Chem *272*, 31941-31944.

Yamaguchi, Y., and Miura, M. (2015). Programmed cell death in neurodevelopment. Dev Cell *32*, 478-490.

Yang, X., Klein, R., Tian, X., Cheng, H.T., Kopan, R., and Shen, J. (2004). Notch activation induces apoptosis in neural progenitor cells through a p53-dependent pathway. Dev Biol *269*, 81-94.

Yao, W., King, D.A., Beckwith, S.L., Gowans, G.J., Yen, K., Zhou, C., and Morrison, A.J. (2016). The INO80 Complex Requires the Arp5-Ies6 Subcomplex for Chromatin Remodeling and Metabolic Regulation. Mol Cell Biol *36*, 979-991.

Yao, X., Wang, X., Hu, X., Liu, Z., Liu, J., Zhou, H., Shen, X., Wei, Y., Huang, Z., Ying, W*., et al.* (2017). Homology-mediated end joining-based targeted integration using CRISPR/Cas9. Cell Res *27*, 801-814.

Zhao, W., Steinfeld, J.B., Liang, F., Chen, X., Maranon, D.G., Jian Ma, C., Kwon, Y., Rao, T., Wang, W., Sheng, C*., et al.* (2017). BRCA1-BARD1 promotes RAD51-mediated homologous DNA pairing. Nature *550*, 360-365.

Zhong, W., Feder, J.N., Jiang, M.M., Jan, L.Y., and Jan, Y.N. (1996). Asymmetric localization of a mammalian numb homolog during mouse cortical neurogenesis. Neuron *17*, 43-53.

Zhuo, L., Theis, M., Alvarez-Maya, I., Brenner, M., Willecke, K., and Messing, A. (2001). hGFAP-cre transgenic mice for manipulation of glial and neuronal function in vivo. Genesis *31*, 85-94.

Zilfou, J.T., and Lowe, S.W. (2009). Tumor suppressive functions of p53. Cold Spring Harb Perspect Biol *1*, a001883.

Ziv, Y., Bielopolski, D., Galanty, Y., Lukas, C., Taya, Y., Schultz, D.C., Lukas, J., Bekker-Jensen, S., Bartek, J., and Shiloh, Y. (2006). Chromatin relaxation in response to DNA double-strand breaks is modulated by a novel ATM- and KAP-1 dependent pathway. Nat Cell Biol *8*, 870-876.

Zovkic, I.B., Paulukaitis, B.S., Day, J.J., Etikala, D.M., and Sweatt, J.D. (2014). Histone H2A.Z subunit exchange controls consolidation of recent and remote memory. Nature *515*, 582-586.